THESE DE DOCTORAT

Présenté par

David KLEIN

En vu de l'obtention du diplôme de

Docteur

de l'université Paul Verlaine de Metz et de la Freie Universität de Berlin

dans le cadre d'une cotutelle

_____

Characterization and improvement of silicon solar cells: Enhanced light acceptance and better separation and extraction of charge-carriers.

_____

Soutenue le vendredi 27 février 2009 devant la commission d'examen:

Marinus KUNST   Directeur de recherche, HZB
             Président du jury

Jocelyn HANSSEN   Professeur à l'Université de Metz
                                                                        Co-directeur de thèse

William BREWER   Professeur à la FreieUniversität de Berlin   **Co-directeur de thèse**

Aotmane EN NACIRI   Maitre de conférences

                      Examinateur

I

Frank WÜNSCH   Dr. HDR,

Helmholtz-Zentrum Berlin   **Examinateur**

Paul FUMAGALLI   Professeur à la FreieUniversität de

Berlin   **Rapporteur**

Omar Ariel FOJÓN   Professeur à l'Universidad de Rosario

                                   Rapporteur

Cette thèse a été préparée au Helmholtz-Zentrum Berlin (HZB)

Abstract

This work studies Silicon nitride and its electrical passivation and anti-reflection properties on n-type and p-type mono crystalline silicon for its use as light entrance window of an inverted a-Si:H/c-Si heterocontact solar cell in the frame of the development of low cost, high efficiency solar cells. Comparative investigation on silicon dioxide and amorphous silicon coatings were performed.

Silicon nitride is deposited by plasma enhanced chemical vapour deposition and was investigated by various measurement methods. The modifications induced by variation of the precursor gas mixture (Silane, Ammoniac and Nitrogen) on the composition were measured by Elastic Recoil Detection Analysis (ERDA). Correlation between the composition and the optical and electrical properties were studied (Fourier Transform InfraRed (FTIR) spectroscopy, XPS, …) and simulated. Evolution of the thickness and refractive indices were measured by ellipsometry. Measurements of the reflection, absorption and transmission were performed with spectroscopy. Time resolved microwaves conductivity (TRMC) was used as a non-destructive method to determine the electrical passivation effect due to silicon nitride. Optimum deposition parameters were found in order to obtain the best electrical passivation (Surface recombination velocity <20 cm.s^{-1}) and the minimum reflection (0.03% of reflection for $\lambda=560$ nm). Reproducibility of the deposition method and behaviour of the layers for different pre-treatment and under annealing were also investigated.

Zusammenfassung

Die vorliegende Arbeit untersucht die elektrische Passivierung und die Anti-reflexionseigenschaften von Siliciumnitriden (SiN_x) auf n-type und p-type monokristallinem Silicium als Lichteintrittsfenster für invertierte a-Si:H/c-Si Heterokontakt Solarzellen. Zum Vergleich der Passivierungseigenschaften werden auf dem gleichen Substrat Siliciumoxid oder hydrogenisiertes amorphes Silicium deponiert.

Amorphe Siliciumnitridschichten wurden mit plasmaunterstützter Gasphasenabscheidung (PECVD, Plasma Enhanced Chemical Vapour Deposition) bei Substrattemperaturen von 300°C oder 350°C auf vorbehandelten Oberflächen monokristalliner Siliciumproben deponiert. So wurde die Komposition der Schichten in Abhängigkeit von der Zusammensetzung des Gasgemisches (Silan, Ammoniak, Stickstoff) während der Abscheidung mit hilfe von ERDA (Elastic Recoil Detection Analysis) ermittelt. Korrelationen zwischen der Schichtkomposition und den optischen und elektrischen Eigenschaften wurden ermittelt (Fourier Transform InfraRed (FTIR) spectroscopy, XPS, …) und durch Simulationsrechnungen unterstützt. Schichtdicke und Brechungsindex wurden mit Ellipsometrie gemessen. Reflexion, Transmission und Absorption der SiN_x schichten mit optische Spektroskopie bestimmt. Time Resolved Microwaves Conductivity (TRMC) wurde als nicht destruktive Messmethode zur Charakterisierung der elektrischen Passivierung benutzt. Es wurden optimale Parameter für gut elektrische Passivierung (Oberflächenrekombinationsgeschwindigkeit < 20 cm^{-1}) und minimal Reflexion (0.003% für λ=560nm) gefunden. Abscheidung und Eigenschaftsreproduzierbarkeit der Schichten wurden für verschiedene Abscheidungsbedingungen untersucht.

Contents

1. Introduction

World wide the energy needs are continuously increasing. The different energy sources thus far in use are not able to address the problems created by a further increase of the already enormous energy consumption. The environmental problems (pollution, greenhouse effect …) and the limited stock of classical energy sources such as oil, gas and coal [I.1] have led to a search for alternative energy stocks. Nuclear energy appears to be a poor solution in view of the radioactivity generated and the problem of the storage of the radioactive wastes. Furthermore, the reserves of nuclear fuel are estimated to last only until 2100 [I.1]. The ITER project, which is based on nuclear fusion (less radioactivity and using hydrogen instead of uranium as fuel) seems to be an interesting solution but its success is uncertain and a potential application is expected only in a distant future.

The best solution will be the use of renewable energy, using wind, sun … these energies are present everywhere on the earth and are unlimited in principle. Direct solar energy is particularly interesting because every point on the earth is more or less illuminated and the time during which this light can be used to produce electricity is corresponds to the maximal electrical demand. The cost of solar cells for converting the solar energy into electrical energy is a critical point. The price of the cells must be as low as possible; On the other hand, the efficiency must be as high as possible. A good efficiency is obtained by:

- An optimization of the light coupling (anti-reflective and non-absorbing front coating, texturing of the illuminated surface, …)

- An optimal separation of the photo-generated excess charge-carriers.

- Reduced losses of excess charge-carriers before their collection by the external circuit. (limited recombination either in the volume or at the surface)

This work focuses on the different coatings used in the fabrication of silicon solar cells, especially in view of the "inverted a-Si:H/c-Si heterocontact solar cell". The main part of the experiments concentrated on the use of silicon nitride. Due to its numerous useful properties (insulating, hardness…), silicon nitride is used in many domains (microelectronic, mechanical protection of surfaces …). In the solar energy domain, especially for silicon solar cells, silicon nitride is used for chemical and electrical passivation [I.2]. Its refractive index is

also well adapted for anti-reflective front coatings on silicon. Some comparison will be made with silicon dioxide and amorphous silicon. Silicon nitride has more advantages than the silicon oxide used up to now for solar energy applications. Even though silicon oxide more effectively suppresses surface states, the electrical passivation induced by the silicon nitride is superior (due to its higher field effect). Furthermore, the refractive index of silicon oxide is not adequate to form a good anti-reflective coating on silicon.

This work is divided in three parts:

- Chapter 2 will deal with the theoretical backgrounds needed in this work. An overview of the charge-carriers generation and kinetics will be given. General considerations of the interactions between light and matter, semiconductors and passivation will be presented.

- Chapter 3 explains the different methods used during this work in order to analyze the composition of a layer as well as its optical and electrical properties.

- Chapter 4 will present the results of the measurements and their interpretations and explanations.

- The thesis closes with a summary of the main conclusions and outlook for future work.

2. Theory

The mechanisms taking place in a photovoltaic cell are multiple and often difficult to understand. This first chapter will introduce the different concepts and theories used for silicon solar cell conception. The principle of solar cell (and silicon solar cell in this case) is based on the generation of excess charge-carriers (electron-hole pairs) in a semiconductor with a band gap adapted to the solar spectrum, i.e. the maximisation of the light absorbed in the semiconductor and converted in electron-hole pairs. After the generation of the excess charge-carriers, they have to be separate at an interface (for example a p-n junction) to avoid recombination. The third process is the collection of the excess charge-carriers in the external circuit.
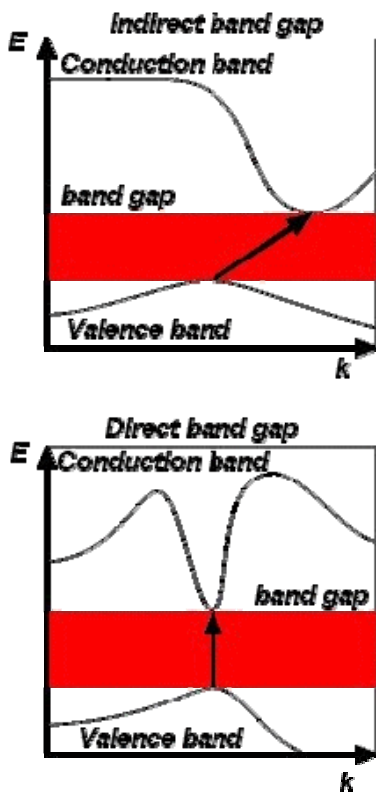
In contrast to other solar cells, excess electron-hole pairs attain the separating interface by diffusion in silicon solar cells.

2.1. Semiconductors

The physics behind the photovoltaic effect is directly related to the properties of the compounds used for the cells, the semiconductor. They can be defined as insulators with a low band gap and their conductivity increases as the temperature increases. The resistivity of semiconductors is generally included between 10^{-5} and 10^6 Ω.cm.

These properties come from the structure of the matter itself. An atom is composed, of a nucleus and electron shells. This means that electrons can only stay on certain energy levels. For an insulator or a semi-conductor, the energy structure of an atom is composed by a valence band where the electrons of low energy contribute to the cohesion of the crystal, and, the conduction band with electrons able to move from one atom to the other. Between both bands there is a band gap, where no energy levels, except those due to defaults, are available. If an electron in the valence band gets an amount of energy higher than the band gap (induced by a photon, a thermal excitation etc…) then it can be excited into the conduction band. At room temperature the conduction band of semiconductors is not empty. Indeed, due to thermal excitation some electrons are (without any other excitations) in the conduction band.

There are two kinds of semiconductors, those with a direct band gap such as gallium arsenide or those with an indirect band gap such as silicon or germanium. This is described by the diagram of the Energy E vs k, the wave vector (Fig.1). This diagram will define, in the wave vector (k) space, the extremum of the valence and conduction bands. It will show where the density of charge-carriers (holes for the valence band and electrons for the conduction band) are the highest. A semiconductor has a direct band gap when the maximum of the valence band and the minimum of the conduction band are both at the same value of the k vector. More details about semiconductors can be found here [II.18].

Fig. 1 : Scheme of the band's structure of a semiconductor. The upper picture shows an indirect band gap semiconductor, where the minimum of the conduction band and the maximum of the valence band are not at the same wave vector value contrary to the direct band gap semiconductors.

2.1.1. *Silicon*

This work focuses on the silicon solar cells. Silicon is a well known semiconductor, with a band gap of 1.12 eV at 300° K and a refractive index around 4.15 for a 530 nm radiation [II.1]. More details about its properties are given in the appendix 1 *Physical properties*. Silicon is, after oxygen, the second most abundant element on earth (25.7 % of its mass). This makes it a good candidate for cheap solar cells. The silicon does not exist in a pure form, it is always associated with other elements (oxygen…) which is why it has to be purified first, the solar industry quality is nowadays 99.9999%, and to obtain such purity several steps (chemical purification, floating zone …) are needed. All of these processes make silicon wafers expensive.

Silicon is an indirect band gap semiconductor, its absorption is lower than the one of other semiconductors with a direct band gap but its abundance and its relative low price (compared to some other semiconductors used in the fabrication of solar cells) makes it an interesting base material.

2.1.2. *Interaction between light and matter*

The photovoltaic effect is directly based on the interaction between the light and the matter. In this section, only the interactions relevant for this work will be introduced in order to understand the phenomenon leading to the photovoltaic effect and to give an overview about what happens in measurements such as ellipsometry.

The light can be described as an electro-magnetic wave, the electric field and the magnetic field oscillate perpendicularly to each other and to the direction of propagation. An electromagnetic wave can be defined by one of its fields (it is related to the other field by the Maxwell's equations). We are not dealing with magnetic material, thus in the following only the electric field is used. The general equation for a monochromatic, plane wave is:

$$\vec{E}(\vec{r},t) = \vec{E}_0 . e^{i(\omega t - \vec{k}.\vec{r} + \varphi)}$$

(1)

Where E_0 is the amplitude, ω the pulsation, $\vec{k}$ the wave vector, $\vec{r}$ the position vector and φ the phase.

A photon can interact in 2 different ways with the matter. It can be either scattered or absorbed (i.e. elastic or inelastic scattering)

In the first case the electromagnetic wave is modified, the consequences are optical effects like interferences, diffraction, polarization, … We will focus especially on the polarization of the light in order to explain the principle of ellipsometry [II.2, 3] which is a large part of the measurements done in this work. Following Maxwell's equations, there are three kinds of polarizations for a monochromatic light wave depending on the E field projection on the x and y plane (perpendicular to the direction of propagation).
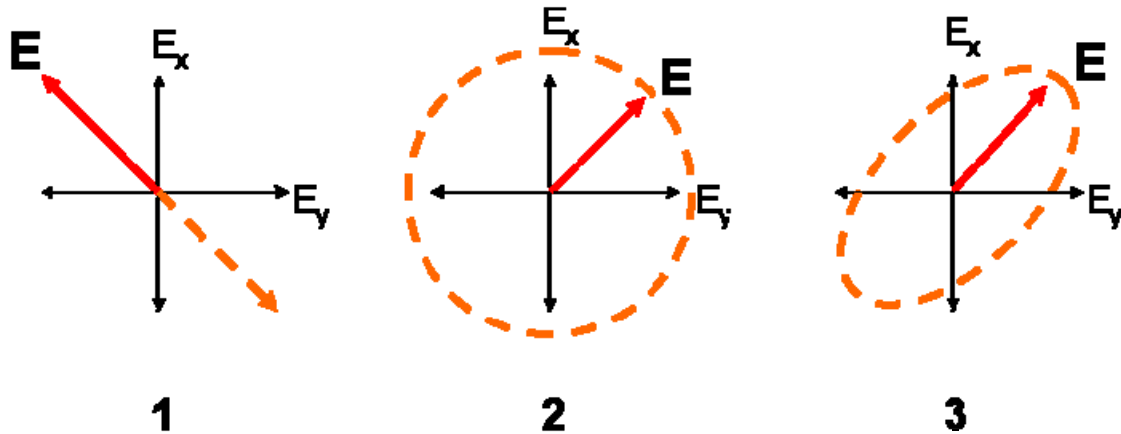
Fig. 2: Three different polarization state of a monochromatic wave. The electromagnetic field E is projected on the x y plan giving Ex and Ey. Scheme 1) Projected linearly polarized light. 2) Projected circularly polarized light. 3) Projected ellipticaly polarized light.

Analysis of the modifications induced by a sample on the state of polarization of an electromagnetic wave can give the optical parameters of the sample itself. This principle is used for the ellipsometric measurement.

The electric field can be decomposed in two components, one parallel to the plan of incidence called $E_{i.p}$ the other one perpendicular to this plane of incidence called $E_{i.s}$. The amplitude and the phase of the incoming electro-magnetic wave will be modified at the interface and in the layer (by the difference of media). The optical nature of the sample will define by how much.
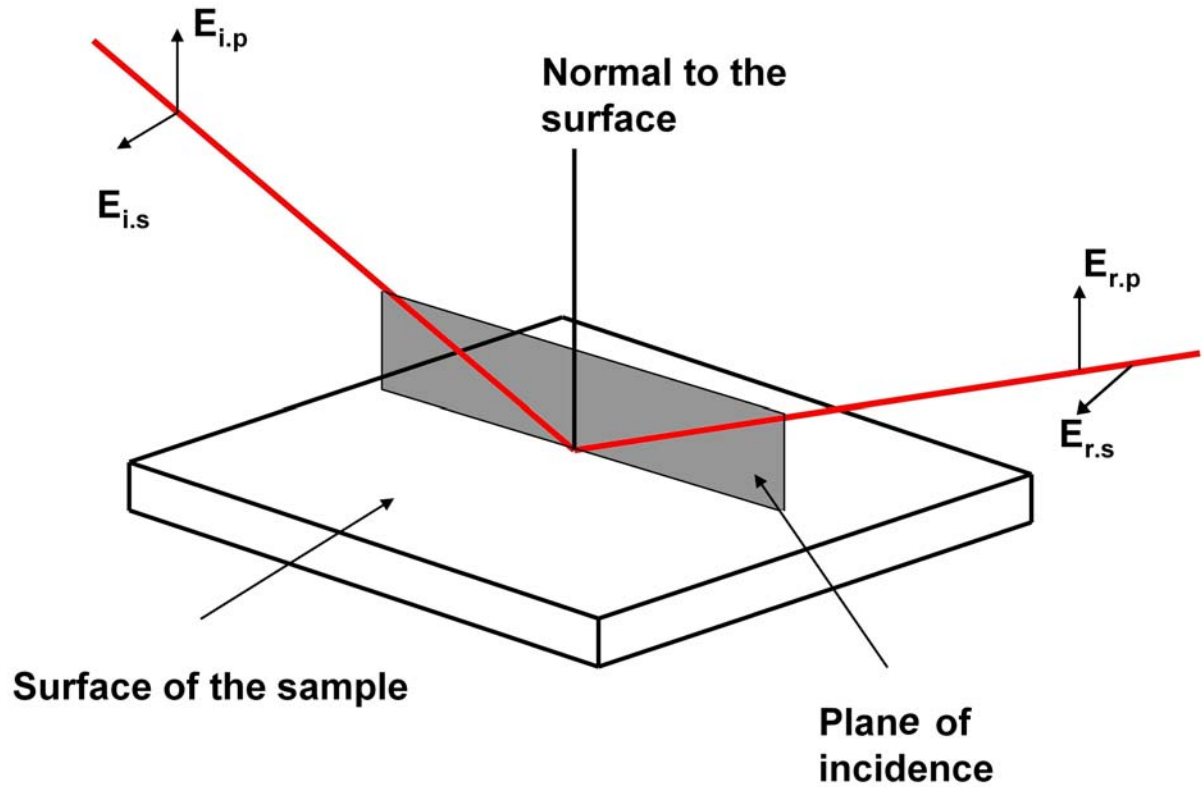
Fig. 3: Reflection of a polarized light on a sample. The incident components of the electric field are noticed $E_{II.p}$ and $E_{II.s}$. The reflected one are $E_{r.p}$ and $E_{r.s}$. The plan of incidence corresponds to the plan containing the normal to the surface and the incident beam.

The change of the phase is called Δ , if δ_p is the phase change for the p component after the reflection and δ_s the phase change for the s component then $\Delta = \delta_p - \delta_s$. The modifications of the amplitude of each component of the reflected field are called $|r_p|$ and $|r_s|$.

With:

$$r_p = \frac{E_{r.p}}{E_{i.p}} = |r_p|e^{i\delta_p} \tag{2}$$

$$r_s = \frac{E_{r.s}}{E_{i.s}} = |r_s|e^{i\delta_s} \tag{3}$$

With those elements we can define a complex reflection coefficient ρ .
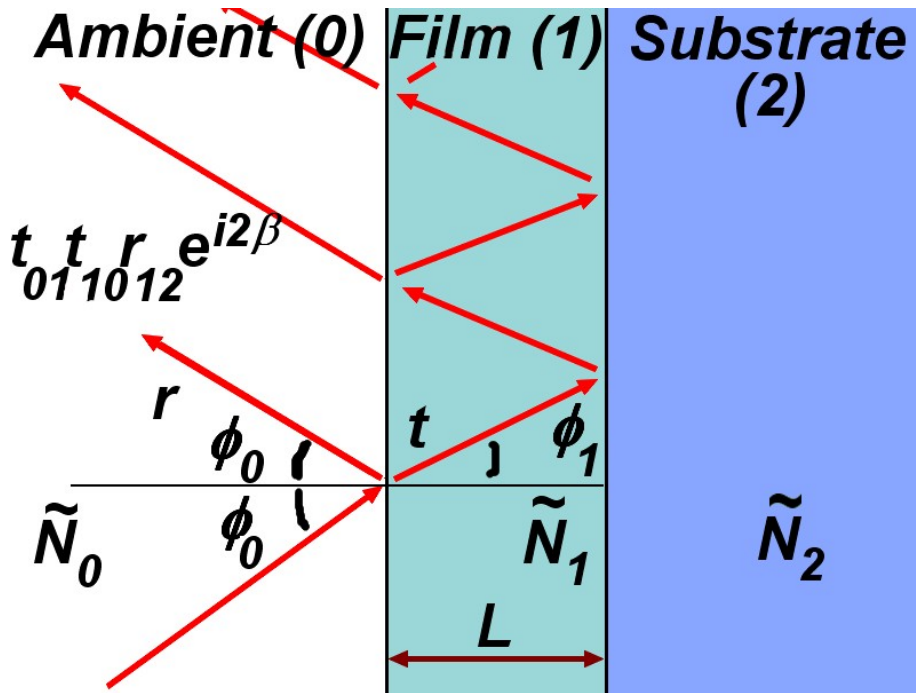
$$\rho = \frac{r_p}{r_s} \tag{4}$$

With the definition of r_p and r_s (Eq. 2, 3)

$$\rho = \frac{E_{r.p} E_{i.s}}{E_{i.p} E_{r.s}} = \frac{|r_p| e^{i\delta_p}}{|r_s| e^{i\delta_s}} = \tan(\Psi).e^{i\Delta} \tag{5}$$

Then:

$$\tan(\Psi) = \frac{|r_p|}{|r_s|} \tag{6}$$

In order to understand the relation between the measurement of Ψ and Δ and the characterization of a layer we can correlate r_p and r_s with the properties of this layer.

Fig. 4: Scheme of a reflected beam (under an incident angle ϕ_0) on a substrate covered with a layer (with a thickness L). $\tilde{N}_j$ are the complex refractive index and r and t the Fresnel reflection and transmission coefficients.

The simple case of a film on a substrate is shown in Fig.4 where L represents the thickness and $\tilde{N}$ the complex refractive index ($\tilde{N}=n+ik$). $\tilde{N}$ is composed by n, the refractive

index of the medium, which is defined by c, the speed of light in vacuum, divided by v, the speed of light in the medium, (n=c/v). Its imaginary part, k, is related to α the absorption coefficient of the medium for a certain wavelength λ. ($k = \dfrac{\alpha\lambda}{4\pi}$).

We notice here that with these optical parameters, the dielectric function ε of the medium can also be expressed.

$\varepsilon=\varepsilon_1 + i\varepsilon_2$ (ε_1 the real part and ε_2 the imaginary part of the dielectric function)

$\tilde{N}^2= \varepsilon\mu$ (but in this case (non magnetic material) μ_r is very close to 1 in optical frequency)

$\varepsilon = \tilde{N}^2 = (n+ik)^2$

$\varepsilon_1 = n^2 - k^2$

$\varepsilon_2 = 2nk$

Using the Fresnel equations, r_s and r_p can be written:

$$r_s = \frac{\tilde{N}_0 \cos\phi_0 - \tilde{N}_1 \cos\phi_1}{\tilde{N}_0 \cos\phi_0 + \tilde{N}_1 \cos\phi_1} \qquad (7)$$

$$r_p = \frac{\tilde{N}_1 \cos\phi_0 - \tilde{N}_0 \cos\phi_1}{\tilde{N}_1 \cos\phi_0 + \tilde{N}_0 \cos\phi_1} \qquad (8)$$

The reflection coefficient ρ can then be expressed as a function of all the parameters.

$$\rho = \rho(\tilde{N}_0, \tilde{N}_1, \tilde{N}_2, ..., L, ...\phi_0, \lambda) \qquad (9)$$

Several terms in the equations like ϕ_0 the angle of incidence or λ the wavelength are already known. The only parameters determinable by an ellipsometric measurement are Ψ and Δ. This means that only two unknown parameters can be worked out. For complex systems a simulation using a model of the optical system used is necessary. In such systems the values of the parameters measured by the ellipsometer (ψ and Δ) are calculated and the different parameters are fitted until the calculated values give a result as near as possible to the measured one. In order to improve the accuracy of the approximation, measurements have to be made on a large wavelength scale.

In the case of absorption, the matter is modified. These effects will be used in photo-electric devices (Solar cell) for example. They are based on the energy of the incoming photon.

Regarding the photo-electric devices, three interactions are important:

- The absorption, a photon can be absorbed, i.e. it will give its energy to an electron of the valence band and this one will be excited into the conduction band.

- The emission, a photon is emitted when an electron fall from the conduction band to the valence band.

- The stimulated emission, an incident photon will perturb an electron of the conduction band, this electron will fall to the valence band and emit a photon with the same phase, direction, polarization and frequency than the incoming one. The incoming photon will not be destroyed during this process.

If a photon with an energy higher than the band gap hits an electron in the valence band of the semiconductor, the photon will give its energy to the electron which will be excited into the conduction band. This means that it will have an electron in the conduction band (which can move inside the crystal) and a hole in the valence band (which can also move inside the crystal).
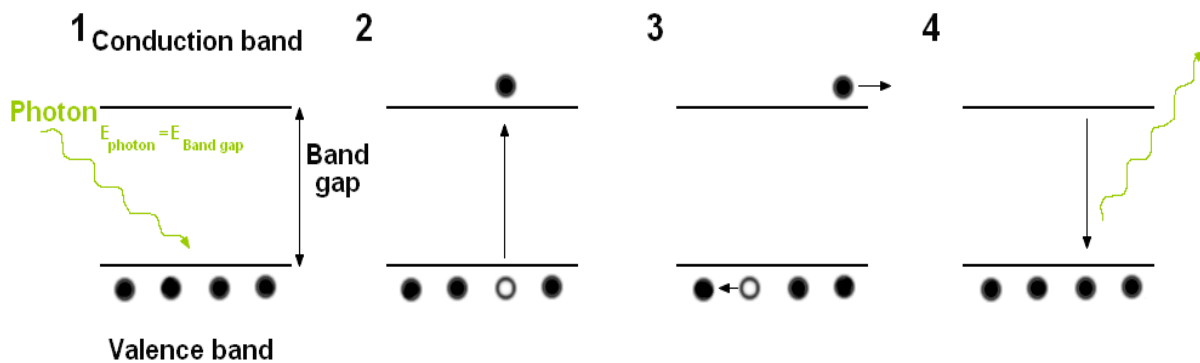
Fig. 5 : Scheme of a band structure in a direct semi conductor. After receiving enough energy from a photon, an electron (black spot) moves to the conduction band and lets an empty place (white spot) called hole in the valence band.

If nothing is done, the electron will lose energy (by emitting a photon or by transferring kinetic energy to the system) and go back into the valence band (recombination). The probability of recombination increases if there is energy level in the band gap due to defects. This is why it is important to have a very pure material (99.9999%). More

information about the losses will be given in the section *2.6.3 losses* of the *solar cell* sub-chapter.

The number of charge-carriers generated under illumination can be described by a generation function G(x,t) which can be expressed as the product of a time dependent function f(t) representing the temporal profile of the excitation and a spatial dependent function g(x) reflecting the spatial profile of the generation given by Beers´ law:

$$G(x,t)=f(t)g(x) \tag{10}$$

An equal concentration of mobile electrons ($\Delta n_0(t)$) and holes ($\Delta p_0(t)$) are generated if the energy of the incoming light is higher than the band gap. As the quantum efficiency for generation can assumed to be unity for semiconductors, g(x) and so the density of electron-hole pairs generated by monochromatic excitation light of wavelength λ, absorption coefficient α_λ and photon density I_λ is given by:

$$\Delta n_0(t)= \Delta p_0(t)=(1-R)f(t)I_\lambda\alpha_\lambda e^{-\alpha x} \tag{11}$$

Where (1-R) takes reflection of the incoming light into account.

For the measurement of the temporal evolution of the photoinduced excess charge-carriers techniques such as Time Resolved Microwave Conductivity used to determine lifetime. The mode of generation of charge-carriers is essential for the meaning of the results. This is why several modes of optical excitation characterized by different shapes for f(t) can be distinguished:

1. Stationary (steady state) excitation. Measurements under stationary excitation will be called Steady State PhotoConductance (SSPC) measurements.

2. Pulsed excitation. Transient measurement under pulsed excitation will be called Time Resolved PhotoConductance (TRPC) measurements.

3. Quasi steady state excitation. These measurements will be called Quasi-Steady-State Photoconductance (QSSPC) measurements [II.4].

4. Harmonically modulated excitation. These measurements will be called HMPC measurements [II.5].

All excitation modes can be used under bias illumination: a constant illumination but with much higher intensity as the modulation light is simultaneously applied.

Further explanations about the kinetics of the generated excess charge-carriers will be discussed in the section *2.3. Charge-carriers kinetic*

To avoid the phenomenon of recombination, besides using very pure silicon, the charge-carriers (i.e. the electrons and the holes) have to be separated. If the semiconductor is then connected to an external circuit, the generated "excess" charge-carriers can contribute to the supply of an electric load. The typical way to reach that goal in the silicon solar cell is to use a "p-n" junction.

2.2. Junctions

A junction is prepared when two materials with different properties are brought together to establish a junction in the semiconductor device sense (physisorption or chemisorption are necessary). In the case of the p-n junction, the base material is always the silicon (in the case of this work), only its doping is changing, forming a so called homojunction. First of all we have to introduce the notion of dopant. Let us take, for example, a crystalline lattice of silicon (column IV in the periodic table of the elements) and replace some of the silicon atoms with phosphorus atoms. The Phosphor (column V) has 5 valence electrons and 4 of these will bond to the surrounding silicon to form the crystalline lattice. The 5th electron, due to the thermal excitation, will be donated into the conduction band. Consequently, the Phosphor will have an extra positive charge. Phosphor is called a "donor" because it gives one electron to the conduction band and this then leads to a n-type doped silicon. The same principle is applied to atoms (such as boron) which have one less electron. The atom of Boron will take an electron of a neighboring Si-Si bond (an electron of the valence band) to build its own bonding with the 4 atoms of silicon around it. Because of the strong bonding energy this electron will no longer be able to move (contrary to the hole generated) and thus it will give a negative ion. Such atoms are called "acceptors" and the result is p-type doped silicon.

A p-n junction is realized when 2 semiconductors, a p type and an n-type one are in contact. In the case of silicon solar cells, both semiconductors are silicon and the dopants used are usually Phosphor and Boron. The concentration of acceptors will be called N_a and the concentration of donor N_d. The density of electrons will be named n and p the density of holes. The excess of electrons (resp. holes) will be given as Δn (resp. Δp).
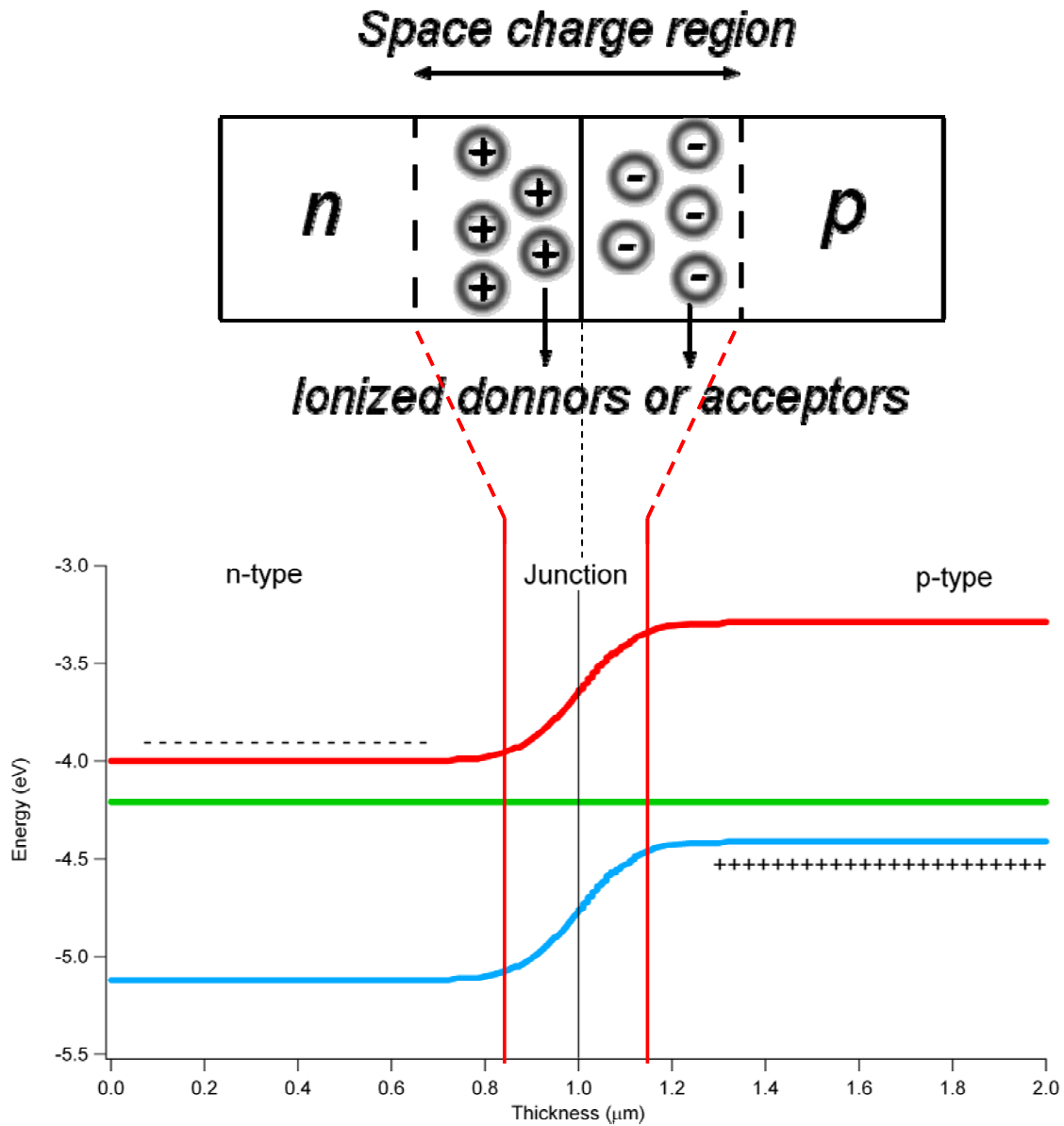
fig. 6 : On the upper part, the scheme of a p-n junction. The space charge region has a width between 0, 1 and 1 μm. On the lower part, the band diagram resulting of the junction between 2 pieces of silicon. One p doped (right side of the junction) and one n doped (left side of the junction). The junction itself take place at the thickness 1. This graph was obtained with the software AFORS HET. The blue line is the energy of the valence band, the red one the energy of the conduction band and the green one is the Fermi level.

When a p and an n type piece of silicon are brought together, the excess of electrons in the n semiconductor will diffuse to the p region and recombine with the holes. The holes in excess in the p region will follow the opposite direction. At the interface, a region will be created where donors and acceptors are no longer neutralized.

The recombination of free charge-carriers on both sides of the junction and thus the resulting ionized donors and acceptors will generate a space charge. Therefore, at the

metallurgical interface, an electric field $\vec{E}$ will act against the diffusion of the majority carriers and when this field is equal to the diffusion force due to the free charge-carriers concentration gradients, the thermodynamic equilibrium is then obtained.

When a photon (with an energy higher than the band gap) hits the semiconductor, it will generate an electron-hole pair. Three cases are possible: The pair is generated in the p type region, in the space charge region or in the n type region. As previously mentioned, an electric field in the space charge region prevents the majority charge-carriers from crossing this region, but not the minority carriers. This means that the electron-hole pairs will diffuse in p and n type, when they attain the space charge region, the minority charge-carriers will be injected into the region where they are the majority carriers. In the space charge region, because of the electric field, electron-hole pairs will be separated, the holes will be injected into the p region and the electrons into the n region.
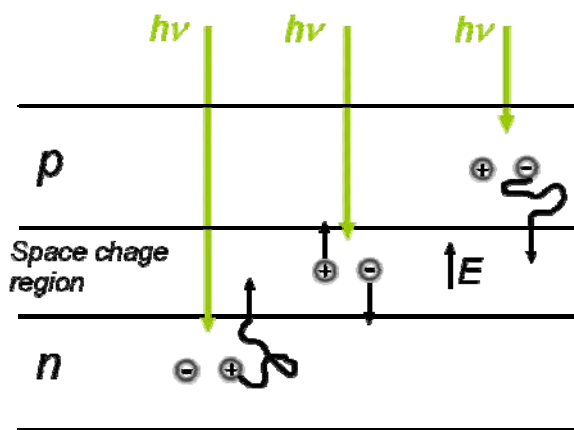
Fig. 7 : When a photon generates charge carriers in the silicon, the holes and electrons produced will be separate as shown on this picture.

In a silicon solar cell, the p-n junction plays an important role. One of the biggest challenges is not to generate electron-hole pairs under illumination, but to separate them completely in order to use ideally all of them to drive a load.

2.3. Charge-carrier kinetics

As seen previously, the excitation (under illumination) of a semiconductor leads to a generation of excess charge-carriers. These charge-carriers are not static inside the semiconductor and in this section we will speak about their kinetics. Before discussing about the kinetics of the charge-carriers let us assume that the system is one-dimensional where the thickness d is the only relevant parameter (x-direction) and the system is homogeneous in the y/z direction. The system is also assumed to be homogeneous in the x-direction with the exception of an infinitely thin range at both surfaces characterized by a different structure (in particular defect density). Only electrons at the bottom of the conduction band and holes at the top of the valence band are mobile charge-carriers and contribute to the (photo)conductance in c-Si. Excess charge-carrier dynamics is described with the drift diffusion model [II.6]. This model is generally used for semiconductor device simulation and is sufficiently sophisticated for our purposes if degeneration is avoided or taken into account in a restricted range. Furthermore, it is assumed that no applied field is present. To obtain an overview of the kinetics we used the photoconductance ΔP. This value is obtained by the following equation (12). It is composed by Δn, the excess electron concentration with a mobility μ_n at the bottom of the conduction band and Δp, the excess hole concentration with a mobility μ_p at the top of the valence band:

$$\Delta P = \int_0^d (\Delta n(x)\mu_n e + \Delta p(x)\mu_p e)dx \tag{12}$$

Eq.(12) shows that ΔP reflects the number of excess charge-carriers weighted by the mobilities. For the different excitation modes (seen in sub-chapter *2.1.2 Interaction light - matter*) there is a dependence of ΔP and the excess charge-carrier concentrations on time t since the start of the excitation (for pulsed excitation) or modulation frequency ω (for harmonically modulated measurements). For all excitation modes ΔP can be measured as a function of the excitation density.

Two kinds of information can be obtained from ΔP:

-The mobility of excess charge-carriers if their number is known.

-The kinetics of excess charge-carriers.

An effective lifetime τ_{eff} (of the excess charge-carriers) can be determined from the experimental $\Delta P(t)$ transient. This leads to following definitions for the different excitation modes (*2.1.2 Interaction light - matter)*:

-For stationary excitation:

$$\tau_{eff}^{ss} = \frac{\Delta P^{ss}}{\Delta N_0 (\mu_n + \mu_p) e} \tag{13}$$

where ΔP^{ss} refers to the photoconductance under stationary illumination and ΔN_0 to the number of holes (which is equal to the number of electrons under the excitation conditions defined above) generated by the illumination.

-For pulsed excitation:

$$\frac{1}{\left(\tau_{eff}^{tr}(t)\right)} = -\frac{1}{\Delta P(t)} \frac{\partial \Delta P(t)}{\partial t} \tag{14}$$

Where the time t refers to the time passed since the start of the illumination. Short laser pulses (10ns FWHM) are frequently used and in many cases the duration of the illumination can be neglected relative to the time constants of the relevant kinetic processes (δ-function excitation)

-For quasi-steady-state illumination

Here the sample is illuminated by a relatively long light pulse (in the ms range). In many cases the decay time of the illumination is much longer than all kinetic processes of interest. Then τ_{eff}^{qss} is defined as for stationary illumination (Eq.13) but a more general definition can be used [II.7].

-For harmonic modulation [II.5, 8]:

$$\Delta P(\omega) = \frac{\Delta P(\omega = 0)}{\sqrt{1 + (\omega \tau_{eff}^{hm})^2}} \tag{15}$$

Where $\Delta P(\omega)$ refers to the modulus of the photoconductance induced by harmonically modulated illumination at modulation (angular) frequency ω. These effective lifetimes refer to the time passed by excess charge-carriers in the conductive state (at the bottom of conduction band for electrons and the top of the valence band for holes) before being immobilized (due to trapping or recombination). These lifetimes can be a function of time (for transient measurements induced by pulsed excitation), excess carrier densities and profiles. Because

these parameters are different for the excitation modes, also τ_{eff} determined is in general different.

Within the model used here τ_{eff} is due to 3 decay processes, if trapping is neglected:

-        Recombination in the volume characterized by τ_v

-        Recombination at the front surface (illuminated surface) characterized by τ_s^{fr}

-        Recombination at the back surface characterized by τ_s^{ba}

The effective lifetime can be considered as a parallel combination of these recombination times:

$$\frac{1}{\tau_{eff}} = \frac{1}{\tau_v} + \frac{1}{\tau_s^{ba}} + \frac{1}{\tau_s^{fr}} \tag{16}$$

Eq.16 is not particularly useful because the contribution of the different decay processes to τ_{eff} is not clear before a more detailed study of kinetics is done. However, in the present model τ_s^{fr} and τ_s^{ba} depend on the thickness d of the sample (Eq. 34, 36) whereas τ_v does not. The contribution of surface recombination to the total decay can be enhanced by the use of light with a high absorption coefficient, i.e. surface excitation and minimized by the use of light with a low absorption coefficient, i.e. volume excitation. The surface recombination will be treated more in detail in the following sub chapter *2.4 Passivation*.

If the surface recombination can be neglected, the effective lifetime depends only on τ_v. In this case if τ_v is constant (i.e. depends neither on the injection level nor on time) all excitation modes yield the same effective lifetime identical to τ_v.

After this general introduction, the following text will deal with the charge-carrier kinetics in the case of a transient measurement (TRPC), i.e. pulsed excitation generation. The conversion to the other generation modes is trivial or, when important, indicated.

Under the conditions given above the concentration of excess charge-carriers is described by the 2 continuity equations, one for electrons and one for holes, and the Poisson equation relating these 2 equations, if no external field is applied. The continuity equation for the excess electrons is given by:

$$\frac{\partial \Delta n(x,t)}{\partial t} = \frac{1}{q}\frac{\partial j_n(x,t)}{\partial x} - R_n(x,t) + G(x,t), \tag{17}$$

and for excess holes:

$$\frac{\partial \Delta p(x,t)}{\partial t} = -\frac{1}{q}\frac{\partial j_p(x,t)}{\partial x} - R_p(x,t) + G(x,t)_{.}$$ (18)

With the following expressions for the currents j_n and j_p:

$$j_n(x,t) = q\mu_n n(x,t)E(x,t) + qD_n \frac{\partial n(x,t)}{\partial x},$$ (19)

and $$j_p(x,t) = q\mu_p p(x,t)E(x,t) - qD_p \frac{\partial p(x,t)}{\partial x},$$ (20)

this yields:

$$\frac{\partial \Delta n(x,t)}{\partial t} = \mu_n \frac{\partial\big(\Delta n(x,t)E(x,t)\big)}{\partial x} + D_n\left(\frac{\partial^2 \Delta n(x,t)}{\partial x^2}\right) - R_n(x,t) + G(x,t)$$ (21)

and

$$\frac{\partial \Delta p(x,t)}{\partial t} = -\mu_p \frac{\partial\big(\Delta p(x,t)E(x,t)\big)}{\partial x} + D_p\left(\frac{\partial^2 \Delta p(x,t)}{\partial x^2}\right) - R_p(x,t) + G(x,t),$$ (22)

with D_n (D_p) the diffusion constant of electrons (holes), $n(x,t)(p(x,t))$ the total concentration of electrons (holes), $\Delta n(x,t)(\Delta p(x,t))$ the concentration of excess electrons (excess holes) , μ_n (μ_p) the mobility of electrons (holes), R_n (R_p) the decay function of electrons (holes), E the (internal electric field built up by the differing transport velocity of electrons and holes) and G the generation function (equal for electrons and holes).

The decay function R represents all the processes leading to immobilization (i.e. trapping, recombination) of the corresponding species. As mentioned above, the generation function G(x,t) (which represents the generation of excess charge-carriers) is identical for electrons and holes. These two equations are connected by the Poisson equation:

$$\Delta E(x,t) = \frac{q}{\varepsilon_0 \varepsilon_r}\big(-n(x,t) + p(x,t) + N_a - N_d\big)$$ (23)

With q the unity charge, $\varepsilon_0\varepsilon_r$ the dielectric constant and $N_a(N_d)$ the concentration of ionized donors (acceptors).

Most important for our purpose is the decay function R: in the general case it involves the 3 decay mechanisms relevant in Si [II.4, 9, 10]:

-        Recombination (and trapping) via defects

- Bimolecular radiative recombination

- Auger recombination

The Auger recombination and the bimolecular recombination will not be discussed here as they occur at high injection which is not relevant to our case. However, more information about them can be found here [II.11, 12] The recombination via defects (or Shockley-Read-Hall (SRH) recombination) reflects the interaction between mobile charge-carriers in the bands and lattice defects [II.13, 14].

A lifetime τ_n (τ_p) for electrons (holes) can be introduced by the definitions:

$$R_n(t) = \Delta n/ \tau_n \tag{24}$$

and

$$R_p(t) = \Delta p/ \tau_p \tag{25}$$

It is clear that in the general case τ_n and τ_p depend on all the parameters of the system, i.e. time t, coordinate x and the local densities $\Delta n(x.t)$ and $\Delta p(x,t)$. In the case of SRH recombination the lifetimes depend also on the density of recombination centres and the corresponding cross sections.

For the solution of the Eqs.21-23 the appropriate boundary conditions must be chosen for n, p and E at every surface [II.15, 16].

The model for excess charge-carrier kinetics described by Eqs.21-23 and the boundary conditions will be called the extended kinetic model. For evaluation of PhotoConductance data with the extended kinetic model the solution of Eq.(21,22), i.e. $\Delta n(x,t)$, $\Delta p(x,t)$ must be integrated over the thickness of the sample as ΔP refers to the integral number of excess charge-carriers (Eq.12).

The complexity of the extended kinetic model limits its usefulness. Applications seem to be limited to determination of the parameters that yield the best fit of experimental data to the model [II.15, 16].

The theory can be greatly simplified if quasi-neutrality is assumed:

Space charge is neutralized with a characteristic time, the dielectric relaxation time, given by $\dfrac{\varepsilon_0\varepsilon_r}{\sigma}$, that can be assumed to be infinitely short relative to the relevant time scale of the measurements. This yields $\Delta n(t) = \Delta p(t)$ and under some generally acceptable approximations the model of ambipolar diffusion. Now Eqs.21-23 are reduced to one

ambipolar diffusion equation. In this model excess charge-carriers diffuse as electron hole pairs and so neutrality is maintained. More details on this model can be found in textbooks [II.17-II.19].

Transport in a (quasi)neutral region can be described by the ambipolar diffusion equation:

$$\frac{\partial \Delta n(x,t)}{\partial t} = D \left(\frac{\partial^2 \Delta n(x,t)}{\partial x^2} \right) - R_n(x,t) + G(x,t) ,$$ (26)

where D refers to the ambipolar diffusion constant:

$$D = \frac{(n+p)D_n D_p}{nD_n + pD_p} .$$ (27)

Under low injection conditions ($\Delta n = \Delta p \ll n + p$) D reduces to the minority carrier diffusion constant. This has lead to the convention to associate Eq.27 to the minority carriers

In this model the number of boundary conditions is reduced to two: one condition at every surface given by application of the continuity equation to both surfaces:

$$\left| D \frac{\partial \Delta n(x,t)}{\partial x} \right|_0 = R_s^{fr}(t)$$ (28)

and

$$\left| D \frac{\partial \Delta n(x,t)}{\partial x} \right|_d = R_s^{ba}(t)$$

(29),

with R_s^{fr} the surface recombination rate at the front side (at x=0) and R_s^{ba} the surface recombination rate at the back side (x=d).

The conventional approximation is that the recombination processes are first order, i.e. proportional to the excess minority carrier concentration $\Delta n(x,t)$, this gives:

$$R_n(x,t) = \frac{\Delta n(x,t)}{\tau_v}$$ (30)

with τ_v the (minority) volume lifetime and for the surfaces:

$$R_s^{fr} = S_{fr} \Delta n(x=0,t)$$ (31)

and

$$R_s^{ba} = S_{ba}\Delta n(x=d,t) \tag{32}$$

Where S_{fr} and S_{ba} are the surface recombination velocities (in cms^{-1}) at the front and the back side, respectively.

The standard description of PC measurements is with Eq.(26) ,boundary conditions Eqs.28-29 and also the approximations of Eqs.(30-32) . This will be called the simple kinetic model. It explains satisfactorily many experimental results for c-Si and somewhat less satisfactorily for mc-Si.

Analytical results for the simple model have been determined for δ-pulse with the time profile of the laser pulse (g(x)) as an initial condition [II.20]. For evaluation of PC data with the simple kinetic model the solution of Eq.(26), i.e. Δn(x,t), must be integrated over the thickness of the sample as ΔP refers to the integral number of excess charge-carriers (Eq.12).

Although it is recommendable to solve Eq.26 numerically where also the time profile of the excitation can additionally be taken into account [II.20], an interesting conclusion can be drawn from the analytical solution [II.21]. Indeed, the decay of the excess charge-carrier distribution occurs via modes with different decay times. These modes correspond to the Fourier components of the initial distribution of excess charge-carriers as determined by the distribution generated by the excitation light (Eq.11). The mode with the longest decay time is called the principal mode.

This is particularly interesting for TRPC measurements where the final decay (within the simple model represented by an exponential decay) is from this quasi stationary principal mode. It is intuitively clear that the surface decay time, τ_s, of this principal mode depends on the surface decay rate and the velocity of the supply of excess charge-carriers by diffusion. The two extreme cases are given for TRPC measurements by [II.22, 23]:

$$- \qquad \text{For S very large} \quad \frac{1}{\tau_s} = \frac{D\pi^2}{d^2} \tag{33}$$

and so

$$\frac{1}{\tau} = \frac{1}{\tau_v} + \frac{D\pi^2}{d^2} \tag{34}$$

Where τ refers to the total decay time of the principal mode.

The distribution of excess charge-carriers corresponding to this decay time is half a sinus-wave with the excess charge concentration effectively zeros at the surfaces. This case can be

called diffusion controlled surface recombination because $1/\tau_s$ is determined by the supply of excess (minority) carriers to the surfaces. Here the surface recombination rate is at its maximum level.

$\quad$ – $\qquad$ For S small $\dfrac{1}{\tau_s} = \dfrac{2S}{d}$ $\hfill$ (35)

and so

$$\frac{1}{\tau} = \frac{1}{\tau_v} + \frac{2S}{d} \hfill (36)$$

The distribution of excess charge-carriers corresponding to this case is a uniform distribution. This case can be called rate limited surface recombination because $1/\tau_s$ is determined by the surface decay rate and the supply of excess charge-carriers to the surfaces is sufficiently fast enough to flatten the distribution at any time. A problem of the analytical solution of Eq.26 is that the faster decaying modes must be considered together for an interpretation of the decay behaviour and the excess charge-carrier distribution. Consequently, interpretation of the initial decay is more convenient by a numerical solution.

2.4. Passivation

The passivation, of a solar cell can have different meanings: chemical passivation and electrical passivation. The first one should protect the cell from impurities providing a coating able to prevent degradations from the environment. The second one have to reduces losses due to recombination (in the bulk or at the surface) [II.24, 25]. This work focuses on the electrical passivation only.

Thanks to the progression of technology used to make crystalline silicon, very pure silicon (99.9999% for the standard solar quality and even 99.99999999% for the electronic quality) is now available. This means that for a cell several hundred micrometers thick, we are able to neglect the recombination in the bulk because the charge-carriers generated in the silicon have the time to attain the surface before they recombine. This is why the surface passivation has an important place in the conception of high efficiency silicon solar cells. This work will focus specifically on the silicon nitride whilst additionally comparing it with the amorphous silicon and the silicon oxide which passivate the surface of a silicon wafer.

The recombination is generally due to energy states within the band gap (for example, due to a defects). At the surface two other phenomena, an intrinsic and an extrinsic one, are creating localized states in the band gap. The first one is due to the end of the lattice where the atoms at the interface are not bonding with theirs neighbours like the ones in the bulk. They are only bonding in a half plane and are thus called dangling bonds. This electronic configuration will modify the band diagram and generate energy states in the band gap. The second phenomena is due to impurities (other atoms from those which make up the semiconductor, like oxygen) which are present at the surface. Those atoms will modify the electronic structure (introduce energy states in the band gap) and they will also create distortions in the lattice which will give recombination centres.

To minimize the recombination at the surface and thus the surface recombination velocity, there are several possible solutions. A surface field can be generated in order to push back into the bulk one type of charge-carriers (and thus reduce the possibility of recombination). Another possibility would be the deposition of a layer on the top of the semiconductor to suppress the dangling bonds.

One of the first surface passivation techniques was the growth of a thermal oxide layer on the silicon substrate. The oxide is formed at high temperatures (around 1000°C) and during the process the silicon oxide layer grows into the silicon substrate. This will move the

interface silicon-oxide / silicon into the bulk of the substrate. By chemically bonding to silicon atoms, the oxygen atoms will suppress (or significantly reduce) the dangling bonds and hence reduce the recombination at the surface. The production of those oxide layers is highly reproducible and a good passivation is obtained. With a refractive index of 1.5 (lying between the silicon's one ($n_{Si}=4$) and the air's one ($n_{Air}=1$)), the silicon oxide can also act as an anti-reflection coating.

However the silicon oxide layer has also some disadvantages.

- The cost of energy used to build this film.

- The possible contamination by diffusion of impurities during the process.

- The degradation of lower quality Si-wafer.

For these reasons it is preferable to work with coatings made at lower temperature.

The amorphous hydrogenated silicon nitride (designated by SiN_x in this work) seems to be a good alternative to silicon oxide as a passivation and anti-reflection coating for silicon solar cells. We will study SiN_x deposited as described in the sub chapter *4.1 Deposition's methods*. The low temperature deposition minimized the contamination and varying parameters allowed us to form different silicon nitrides (by the composition, density …). Another possibility for a good passivation is the amorphous silicon which is also deposited at low temperature but its high refractive index and its high absorption make its use as a front coating less useful.

2.5. Anti-reflection coatings

The silicon solar cells are based on a silicon substrate (mono-crystalline, multi-crystalline, etc…). To maximize the generation of excess charge-carriers, the number of photons which can be absorbed must also be maximized. The silicon has a band gap of 1.12 eV and following the Lambert-Beer's law mostly all photons with an energy higher than the band gap will generate charge-carriers. The conversion between energy and wavelength is described by the following formula:

$$E_{Joule} = \frac{c*h}{\lambda_{meter}} \qquad \text{or for practical use:} \qquad E_{eV} = \frac{1.24}{\lambda_{\mu m}} \qquad (37)$$

Where E is the energy of the photon (in Joule or eV), c the speed of light, h the Planck's constant and λ the wavelength (in meter or micro meter).

As shown on the transmission spectrum of a p type piece of silicon every photon with a wavelength under 1100 nm is absorbed (or reflected)
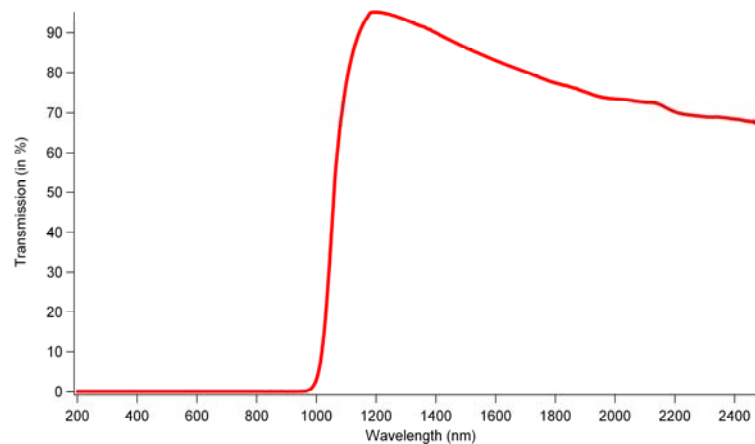
Fig. 8 : Transmission of a p type, 500 µm thick silicon substrate as a function of the wavelength. With a band gap of 1.12 eV and following the Beer-Lambert law, mostly all photons with a wavelength under 1100 nm are absorbed. The graph shows only the photons passing through the sample (related with the incident beam)

A non negligible optical loss process with silicon (in silicon solar cells) is its high reflection [II.26], especially in the visible range of the light, where the maximum of the sun light intensity takes place (around 500 nm). This effect is due to its high refractive index, around 4.32 for a radiation of 500 nm [II.1]. Under a perpendicular incidence, the intensity of the light which is reflected at the interface between 2 different media, is given by the

26

reflection coefficient R expressed by the following formula (deduced from the Fresnel equations). The coefficient R also has a component on the plan parallel to the plan of incidence (R_p) and another one perpendicular to this plan of incidence (R_s).

Considering Eq. 7, 8 (*2.1.2 Interaction light – matter*) the total reflection coefficient R is defined by:
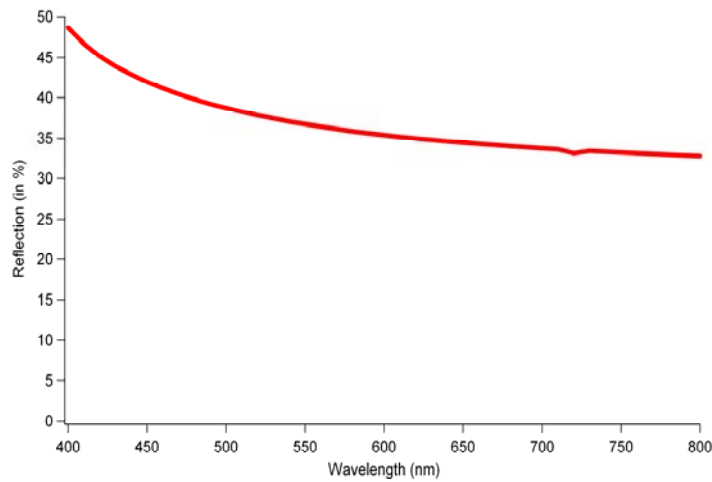
$$R = \frac{R_p + R_s}{2} \tag{38}$$

With:

$$R_p = \left| r_p \right|^2 \tag{39}$$

$$R_s = \left| r_s \right|^2 \tag{40}$$

Thus, for a normal incidence of the beam ($\phi_0 = 0°$) and a non absorbing layer (k=0):

$$R = R_p = R_s = \left(\frac{n_1 - n_2}{n_1 + n_2} \right)^2 \tag{41}$$

Where n_1 and n_2 are the refractive indices of the 2 media at the interface.

Fig. 9 : Reflection of a silicon substrate as a function of the wavelength between 400nm and 800 nm. The maximum of the sun light intensity is located around 500 nm, which shows clearly the need of an anti-reflection coating to reduce the losses.

At the interface between air ($n_1=1$) and silicon ($n_2=4.32$ for $\lambda=500$nm) the reflection should be around 0.39. It means that 39% of the incoming light with a wavelength of 500 nm will be reflected. An anti-reflection coating (ARC) is therefore necessary to reduce these huge losses due to reflection.

The anti-reflection effect can be performed thanks to the deposition of a thin layer between the 2 media (air and silicon in this case).
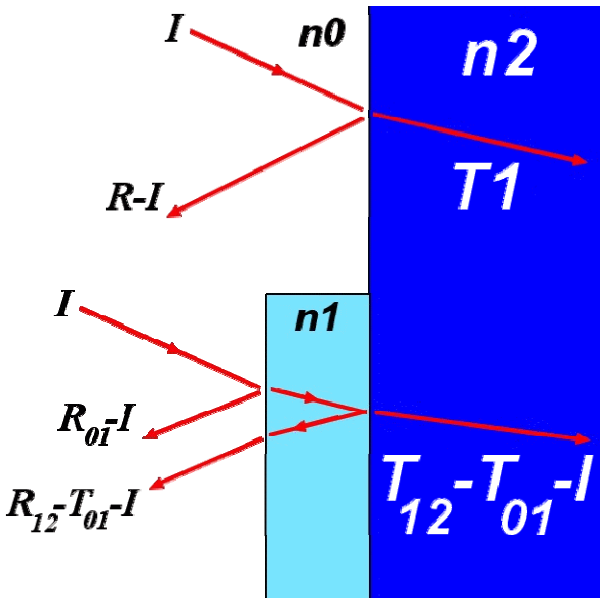

Fig. 10: Scheme of the simple reflection of a beam of light at the interface between 2 media with different refractive index. The light blue square represents an anti-reflection coating with a refractive index n_1 such as $n_0 < n_1 < n_2$

The best refractive index n_1 for an anti-reflection coating between the 2 media with respectively a refractive index n_0 and n_2 can be deduced from the formula:

$$n_1 = \sqrt{n_0 n_2} \ .$$ (42)

An anti-reflection coating uses the interference properties to reduce the reflection. Indeed, if for a perpendicular incidence, the film has a thickness equal to the quarter of the wavelength in the film (this wavelength is defined on p. 30). The reflected beam and the incident one will be exactly opposite in phase. If both intensities are equal, both beams will interfere destructively one with each other. This will suppress the reflection for the selected wavelength.
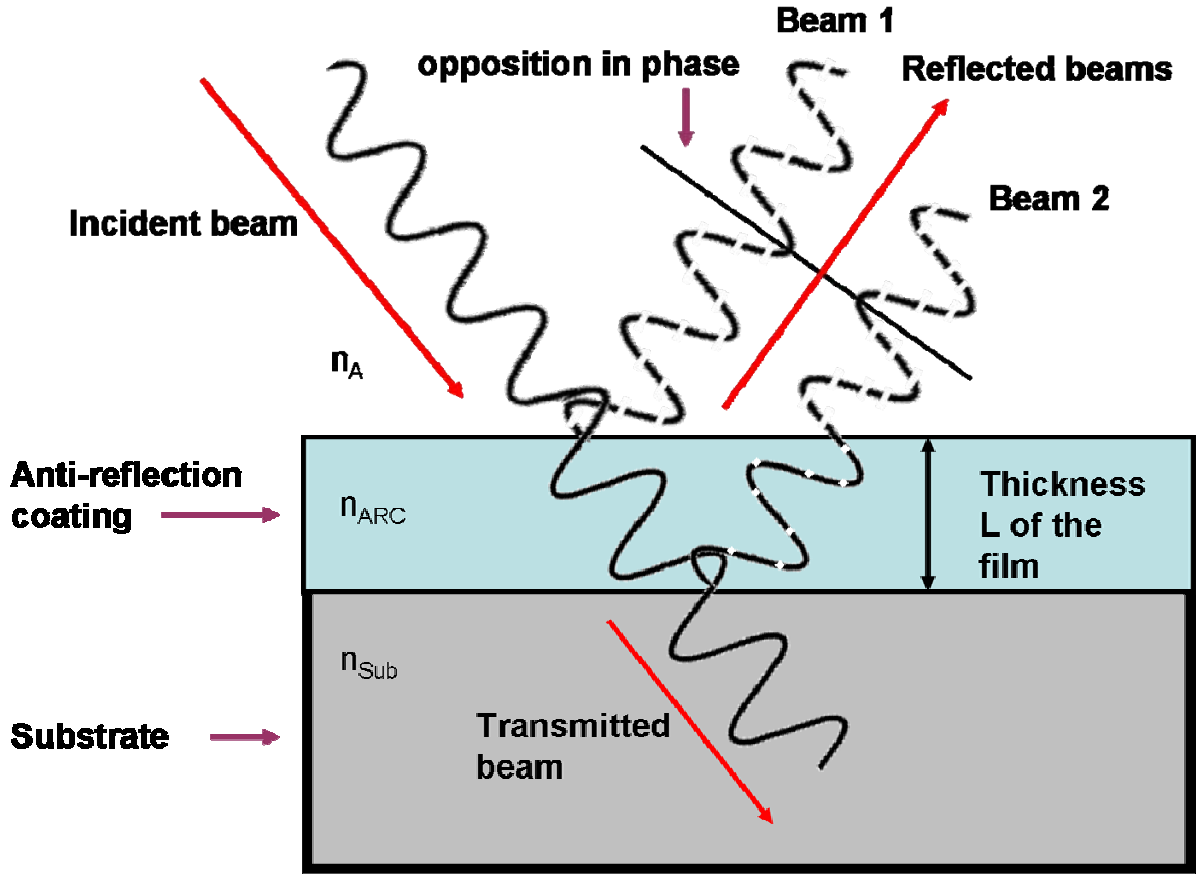
Fig. 11: Scheme of the destructing interference process (the proportions are not respected). The beams reflected at the interface Air-Anti reflection coating (beam 1) and the reflection at the interface anti reflection coating – substrate are opposite in phase. This leads to a destructive interference and all the energy of the incoming beam is transmitted into the substrate. For simplicity, no refraction of the transmitted beam is shown.

The amplitude of the reflection coefficients at both interfaces are:

$$r_{A-ARC} = \frac{n_A - n_{ARC}}{n_A + n_{ARC}} \tag{43}$$

$$r_{ARC-Sub} = \frac{n_{ARC} - n_{Sub}}{n_{ARC} + n_{Sub}} \tag{44}$$

The complex reflection coefficient between the ambient and the substrate is:

$$r_{A-Sub} = \frac{r_{A-ARC} + r_{ARC-Sub}e^{-i\varphi}}{1 + r_{A-ARC}r_{ARC-Sub}} \tag{45}$$

Where φ is the phase shift introduced by the Anti-reflection coating.

$$\varphi = \frac{2\pi\delta}{\lambda}$$ with δ the path difference ($\delta=2n_{Sub}.d_{Sub}/\cos\phi_1$, ϕ_1 the angle of the transmitted beam with the normal after the interface Ambient-ARC)

A wavelength changes when it goes from one medium to another. This means that in order to calculate the appropriate thickness of the anti-reflection coating, the refractive index must be taken into account. The optimum thickness for destructive interferences can be determined by the formula $\lambda_0/(4*n)$ with λ_0 the wavelength in vacuum and n the refractive index of the medium. In the case of silicon nitride the perfect thickness to suppress the reflection at the wavelength of 532, for example, is 532/(4*1.9)=70 nm.

To calculate the anti-reflection, a software taking the multiples reflections and the absorption of the layers into account was programmed. More details are given in the section *3.1.3 Simulation program*.

2.6. Solar cells

Crystalline Silicon solar cells are the most common type of solar cells, they represent more than 90% of the photovoltaic market. They can be found in different form:

- The mono-crystalline silicon solar cell is the most efficient (22.3% for HIT cells and up to 24.7% for the best p-n junction solar cell [II.27]). But these record cells are manufactured with a very expensive process.

- The multi-crystalline silicon solar cell is the standard for commercial application, it is cheaper compared to mono-crystalline cells but the efficiency is lower (between 15.3% to maximum 20.3%).

- We can also find multi-crystalline silicon solar cells based on silicon ribbon [II.28] sheet which also have a lower efficiency than the mono-crystalline cells but the fabrication process does not need to saw ingots and therefore the waste of silicon is reduced.

This work will focus on the standard crystalline silicon solar cell, based on a crystalline silicon substrate with electric contacts on the front and back side. Firstly we will examine the conventional silicon solar cell with its different aspects. Following on from this we will look at the concept of the inverted solar cell and the advantages of the new geometry used will be shown.

In a semi conductor, like silicon, and without any excitation (T=0K), all the electrons are in the valance band. If we excite the atoms in a crystal with light for example, some photons can transfer their energy to the electrons of the valence band which will be excited into the conduction band (if the energy is higher than the band gap). The generated electrons and the holes have to be separate to contribute to a photovoltage. This separation takes place in the space charge region of a p-n junction.
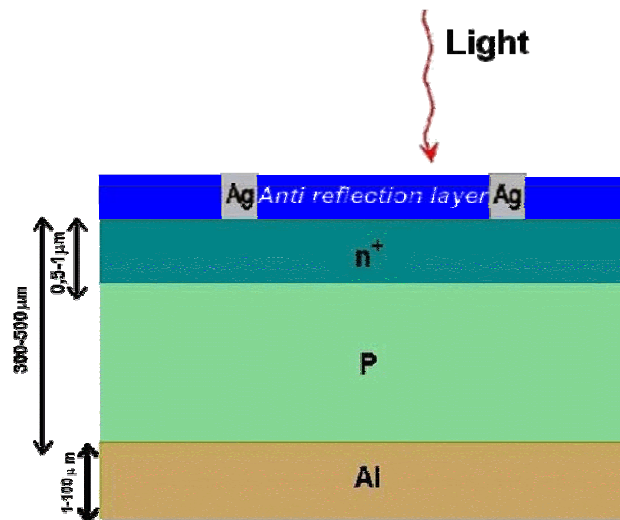

Fig. 12 : Scheme of a typical silicon solar cell. The substrate is a p-type silicon. The n-type region is created by thermal diffusion of dopands (phosphorus).

An n layer is created on a p type silicon substrate by thermal diffusion. A front and a back contact (generally metal is deposited on the surface) for the collection of excess charge-carriers into the external circuit are created. On the front surface a texturing can be performed and an anti-reflection coating can be deposited in order to enhance the light coupling into the absorbing layer.

2.6.2.<u>Losses</u>

Silicon solar cells do not convert all the energy of the incoming light into electricity. The best silicon solar cells (made in a laboratory) are able to reach 24.7% of efficiency [II.27] (without any focusing system). The limitation of the efficiency is due to the losses of energy. The losses have several origins [II.26], they can be optical, energetic or structural. In the Fig.13 you can see a scheme of the optical and energy losses.
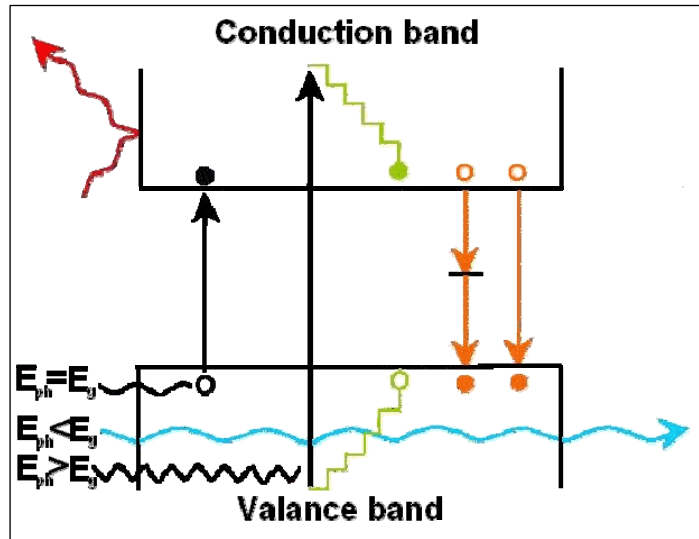
Fig. 13 : Energy losses (i.e. difference between the incoming energy of the incident light and the energy finally turned into electric energy) occurring in a semi conductor when it is illuminated.

The optical losses can have two reasons. One occurs from photons which are reflected at the cell surface (red line), it concerns around 35% of the photons with a wavelength of 500 nm coming onto crystalline silicon without any anti-reflection coating. Other losses come from photons which will pass through the cell without being absorbed, indeed, photons with energy lower than the band gap of the silicon will not have enough energy to excite an electron of the valence band into the conduction band. If we take the case of silicon with a band gap of E=1.12 eV the associated wavelength is $\lambda = \dfrac{1,24}{E} = \dfrac{1,24}{1,12} = 1,107\,\mu m$ it means that photons with a wavelength higher than 1100 nm will mostly not be absorbed (blue line on the Fig.13).

The energy losses come from the interaction of the incoming photons and the matter. In fact, the photons emitted by the sun have different energies. The solar cells use the light coming from the sun, either in space or on earth. In both cases the spectrum of the incoming light covers a very large wavelength range, as shown in Fig.14.
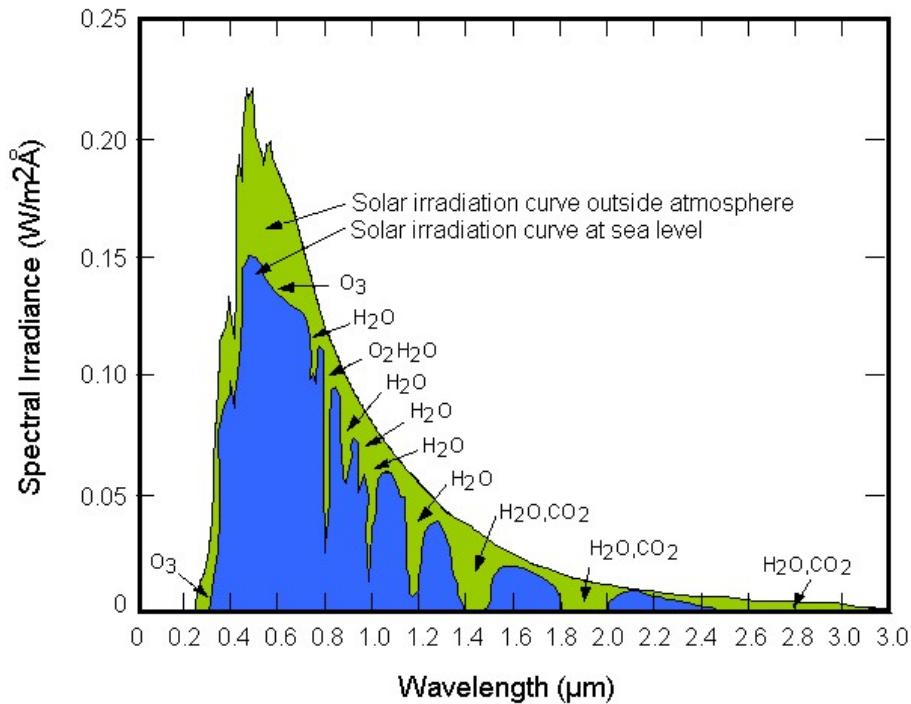
Fig. 14 : Spectrum of the irradiance [II.29] of the sun light. The difference between the irradiance outside atmosphere and at the sea level is due to the absorption (by CO2, H2O etc…) in the atmosphere.

The photons with energies higher than the band gap can create electron-hole pairs, but it is necessary to take into account several possible cases:

-   The photon can give the energy of the band gap to the electron. In this case the electron-hole pair generated can sometime recombine (directly or though defects) before they can be injected into the external circuit (orange line).

-   Another loss of energy due to these high energy photons can be the thermalisation. In this case, the photon gives more energy to the electron than the band gap. The electron (hole) pair generated will have to lose some energy to reach the lower (higher) part of the conduction (valance) band (green line).

-   Another source of losses comes from the thickness of the cell. Even if the energy of the incoming photon is high enough, they can pass through the cell without being absorbed. These losses can be reduced by a back surface reflection for example.

These losses are taking into account the processes acting on the generated charge-carriers. Indeed, excess charge-carriers can be trapped or they can recombine. This is due to the presence of defects in the bulk or at the surface. Defects induce sub-energy levels in the

forbidden band gap, hence, it is more probable for charge-carrier pairs to recombine. Defects in the bulk can be due to a stacking fault in the lattice or impurities present in the silicon (related to the kind of silicon used). Amorphous silicon only contains defects because of its amorphous composition. The multi-crystalline silicon consists of large grained crystallites (the defects take place between the grains of silicon). The silicon with lowest defect density is the mono-crystalline one, but even in the best quality crystals impurities can be found or some stacking faults in the crystalline lattice can occur.

The engineering process, such as the shadowing of the cell by the front contact, can cause other additional losses.

One problem of cells based on thermal diffusion of the p-n junction is that it requires a lot of energy because the wafer must be heated up to 1000 degrees Celsius. It costs a lot of energy/money and the risk to include impurities by this method is also higher. A deposition made at low temperature would be favourable to reduce costs. A part of the problem was solved by the deposition of doped amorphous silicon in order to have a p-n junction at low temperature, but the absorption in this dead layer is still a problem. All the excess charge-carriers generated in this area are lost due to their poor lifetime in this high defect region. This is also the case of the photons in the blue range of the solar spectrum for example (α_{400}=95200 cm^{-1}) which are an important part of the sun light.

To pass through these problems, another kind of solar cell is proposed, still based on crystalline silicon but using another geometry, the "inverted a-Si:H/c-Si heterocontact solar cell" [II.30].

In this kind of cell the p-n junction is placed on the back side. The junction is made by deposition at low temperature (250°C) of a p a-Si:H on a n c-Si substrate by Plasma Enhance Chemical Vapour Deposition (PECVD), this avoids the problem of the high temperature process. Absorption due to the hetero junction is then drastically reduced.
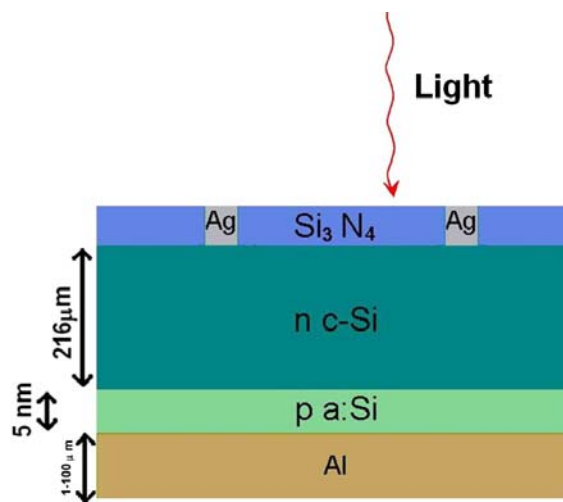
Fig. 15 : Scheme of an inverted silicon solar cell. The bulk is a n-type piece of silicon. The junction is made by deposition of a p-type amorphous silicon.

3. Methods

The studied layers (silicon nitride, amorphous silicon and silicon oxide) have different characteristics and properties. A modification inside the layer can modify its characteristics and behaviour, which is why a good investigation of the coatings by different aspects is necessary. Consequently, several methods were used to analyze these coatings. This chapter will describe the measurement methods used, explain their principles and show the kind of information we can obtain. The analysis of the data and their interconnection with each other will be presented in chapter *4. Coatings on silicon substrates*. The characterization of the different material properties can be divided in 3 parts:

1. The optical characterization: to determine the optical parameters or the anti reflection properties of the layer.

2. The electrical characterization: used to obtain the passivation properties (surface and bulk) of the layer and the fixed charge in the film.

3. The structural characterization: to know the composition and the structure of the coating.

3.1. Optical characterization

This sub-chapter will give an introduction to the different experiments used to analyze the optical properties of the layers.

3.1.1 _Ellipsometry_

Ellipsometric measurements allow us to obtain the optical properties of a layer (refractive index, absorption) and also its thickness. The ellipsometric measurements were performed at the University of Metz (France), by doctor En Naciri. Some other measurements with a monochromatic ellipsometer were made at the H.M.I. The ellipsometer used at the University of Metz uses a spectral source which allows us, compared to monochromatic ellipsometer, to have the refractive index (but also the other optical parameters) over a wide range of wavelengths.

Ellipsometry is an optical technique using the vectorial nature of an electromagnetic field. The reflection on the sample will induce modification of the polarization of an incoming (polarized) light. As shown in the sub-chapter _2.1.2 Interaction light-matter_
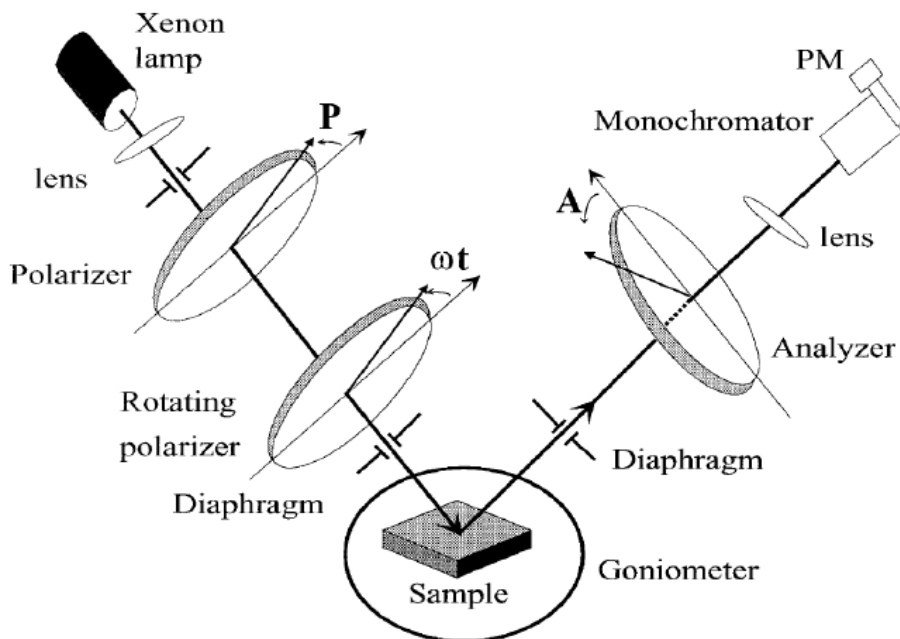
Fig. 16 : Scheme of the PRPSE ellipsometer used at the University of Metz to do the ellipsometric measurements. The Xeon lamp is the light source and PM the photomultiplier which will count the photons of each wavelength coming onto it. The first polarizer is fixed, it polarizes linearly the incoming light and suppresses the residual polarization of the source.

The ellipsometer used for our measurements is a Polarizer Rotating Polarizer Spectroscopic Ellipsometer (PRPSE) [III.1, .2]. In this ellipsometer, a Xeon lamp with a spectral range of 0.3 – 2 μm is used as the light source. The incident beam will then pass through a first fixed polarizer which gives the light a linear polarization and suppresses the residual polarizations of the source (the positioning precision of the polarizer is 0.09°) then the beam is modulated by a rotating polarizer. After the reflection on the sample placed on a goniometer, the beam passes through an analyzer and by using a lens it is focused onto a detection device composed of a monochromator and a photomultiplier. Diaphragms with a 1.5 mm diameter are used, their diameters and spacing will determine the divergence of the beam which is, in this case, reduced to 0.028°.

This measurement gives the ellipsometric parameters Ψ and $\cos(\Delta)$ for wavelengths between 400nm and 800 nm. The incident angle of 70° is fixed. Using both parameters, it is possible to know the thickness and the optical properties of our layer(s). A simulation program, called Deltapsy2, will calculate, using a model based on a theoretical configuration (number of layers, type of materials …) the parameters $\tan(\Psi)$ and $\cos(\Delta)$. The parameters of the model will be modified until they fit with the measurement. The measurement is not invasive or destructive. No special treatment of the samples is necessary.

These measurements are very useful because a good anti-reflection is directly related to the refractive index and the thickness of the different layers deposited on the silicon substrate. It is already well known that the amorphous hydrogenate silicon nitride has a refractive index around 1.9 at a wavelength of 530 nm, but this index can vary between 1.7 until more than 3 (at the same wavelength) for different compositions (i.e. different Si/N ratio).

The monochromatic ellipsometer was used to have a fast overview of the refractive index (for one wavelength) but also to determine the deposition rate under different conditions of deposition. The deposition rate of the layer is a very important parameter in order to control the thickness of the deposited coating. The deposition rate varies for the different parameters of deposition used during the process such as the gas mixtures or the temperature.

3.1.2 Spectroscopy

A spectrometer was used in order to get the basic but useful optical data of a layer: the reflection, the absorption and the transmission.

By using a photo-multiplier, the intensity of the light reflected (transmitted) by (through) a sample is analysed.
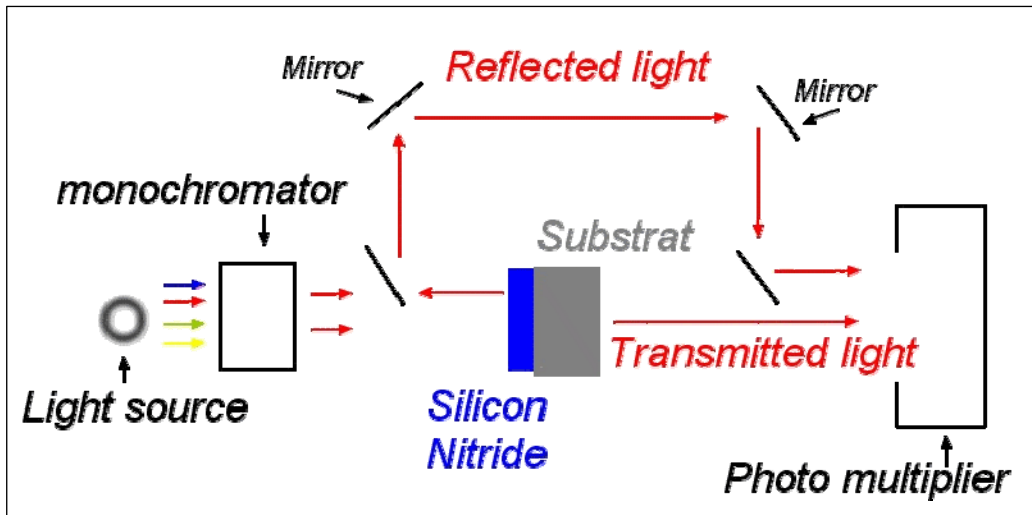
Fig. 17 : Principle of the spectrometer. The monochromator selects the wavelength coming from the tungsten lamp. After reflection or transmission the light is analysed by a computer program recording the signal coming out of the photo-multiplier

The source of the light is a tungsten lamp. A monochromator selects a wavelength. After reflection on the sample (for the reflection measurements) the light is sent via mirrors onto the photo-multiplier. For transmission measurements the light passes through the sample and goes directly onto the photo multiplier. There, the optical signal will be converted in an electric signal, amplified and sent to a computer. A LOCK IN amplifier and a computer software then analyses the signal of the sample and the reference signal. The references are either a piece of glass with an aluminium coating for the reflection or a piece of glass (quartz SiO_2) without any coating for the transmission. At the end, a reflection (or transmission) curve of the reflected (or transmitted) light in function of the wavelength is obtained. The range of the wavelength of this spectrometer is included between 400nm and 1200 nm.

The absorption A can not be directly measured but it can be obtained by the formula:

R+T+A=1

Where R is the reflection, T the transmission.

One aim of this work was the maximization of the absorption of incoming light by a silicon substrate (for solar cell applications). To reach that goal, a good knowledge of the reflection, transmission and absorption of the coatings establish was fundamental. The silicon nitride is used as the front coating. Its role is to enhance the anti-reflection and to reduce the surface recombination, thus, the absorption inside this layer must be as low as possible

3.1.3 *Simulation program*

To help us to predict the behaviour of an anti-reflecting layer and to avoid wasting time for useless depositions, it would be useful for us to predict the behaviour of an anti reflection layer. To reach that goal, we programmed a software program called Norbert. It is based on optical equations using resultant waves [III,3 p.59]. Using this program we are able to:

- ✓ Simulate the reflection of a multi layer silicon nitride coating on a silicon wafer, but more generally the reflection of every multi layer system.

- ✓ Check if the measurements made by ERDA or Ellipsometry fit well with the experiments.

- ✓ Have an idea of the thickness if we know the refractive index and inversely.

- ✓ Fit the curves obtained by spectroscopy measurements to have an idea of the thickness / refractive index.

- ✓ Use the ellipsometrical measurements to find the best system of layers to optimize the anti-reflection.
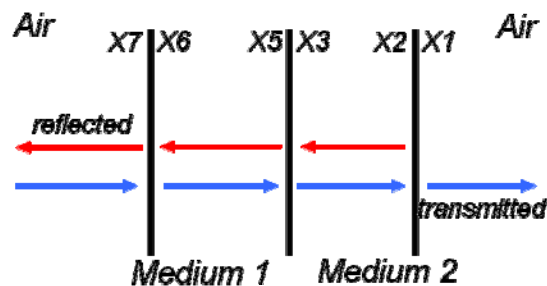
Fig. 18 : Representation of the resulting waves concept. In every point Xn we will consider the global reflection and the transmission

The program is based on a method using resultant waves. This means that at every interface we will calculate the resulting transmission and reflection as show in Fig.18.

One solution to solve the problem is to use the vector sums of the waves and apply the appropriate boundary conditions (at each surface) [III.3, 4, 5]. Consider the simplest case, one non absorbing layer with a thickness d_1 and a refractive index n_1 surrounded by 2 infinite mediums with a refractive index n_0 and n_2. In the first medium, the amplitude of the incoming electric vector will be noted E_0^+ and the reflected one at the first interface will be E_0^-. Using the same notation in the layer, the resultants of all waves going from the first interface to the second one will be noted E_1^+ and the one going in the opposite way E_1^-. The last medium is supposed to be infinite, which is why there will be only outgoing waves, noted E_2^+.
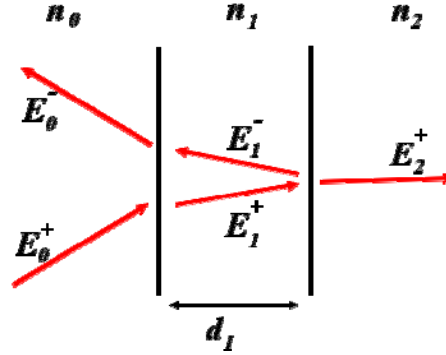
Fig. 19: Scheme of the simple case representing one layer surrounded by 2 media with refractive index n_0 and n_2

Let us consider a two films system (thickness d_1 and d_2) with the Fresnel coefficients r1, r2, r3 and the light going from the medium n_0 to the n_2 one. We start to compute the amplitude and phase of the reflected light from the lower film. (δ_i is the change in phase for the beam traversing the layer and $\delta_i = \dfrac{2\pi}{\lambda} n_i d_i \cos(\varphi_i)$, A the amplitude and Δ the phase)

$$A_2 e^{i\Delta_2} = \frac{r_2 + r_3 e^{-i\delta_2}}{1 + r_2 r_3 e^{-i\delta_2}}$$

(46)

This ($A_2 e^{i\Delta 2}$) is the Fresnel coefficient we obtain from the layer d_2, which we will use to calculate the one at the first layer d_1:

$$A_1 e^{i\Delta_1} = \frac{r_1 + A_2 e^{i\Delta_2} e^{-2i\delta_1}}{1 + r_1 A_2 e^{i\Delta_2} e^{-2i\delta_1}}$$

(47)

42

The reflection is then given by $(A_1e^{i\Delta 1})(A_1e^{i\Delta 1})^*$ where $(A_1e^{i\Delta 1})^*$ is the complex conjugate.

To gain confidence in the simulations performed with this program, a comparison was made with real measurements. The three pictures, Fig.20, 21 and 22 show simulations compared with real reflection measurements for different coatings (different thicknesses, refractive indices, absorptions). The simulations are the red lines and the measurements the black ones.
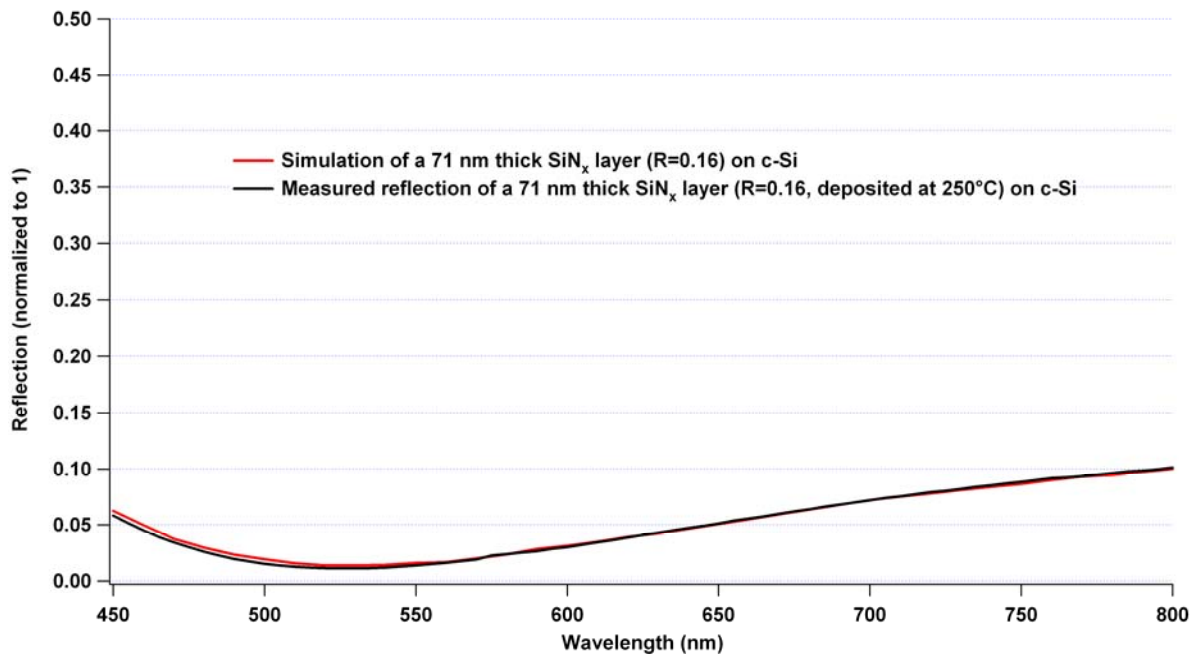

Fig. 20: Simulation (red line) and measure (black line) of the reflection of a crystalline silicon substrate covered with SiN$_x$. The silicon nitride is in this case 71 nm thick and was deposited at 250°C (R=0.16, n$_{630}$=1.808)
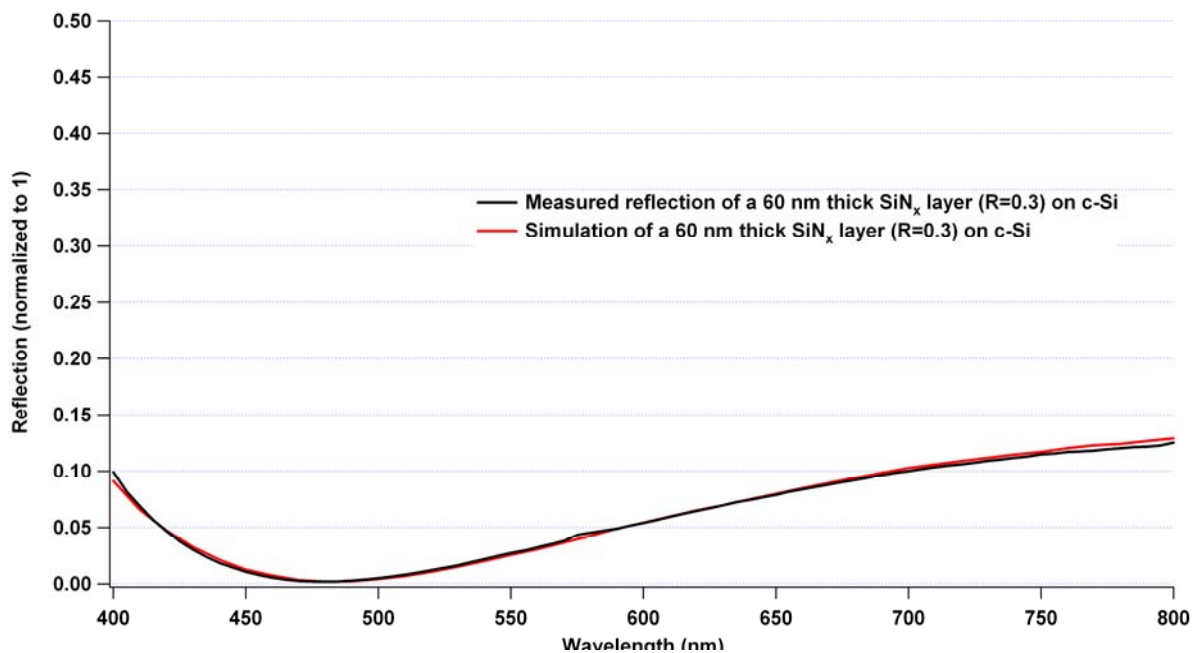
Fig. 21: Simulation (red line) and measure (black line) of the reflection of a crystalline silicon substrate covered with SiN$_x$. The silicon nitride is in this case 60 nm thick and was deposited under standard condition (R=0.3, n$_{630}$=1.912)
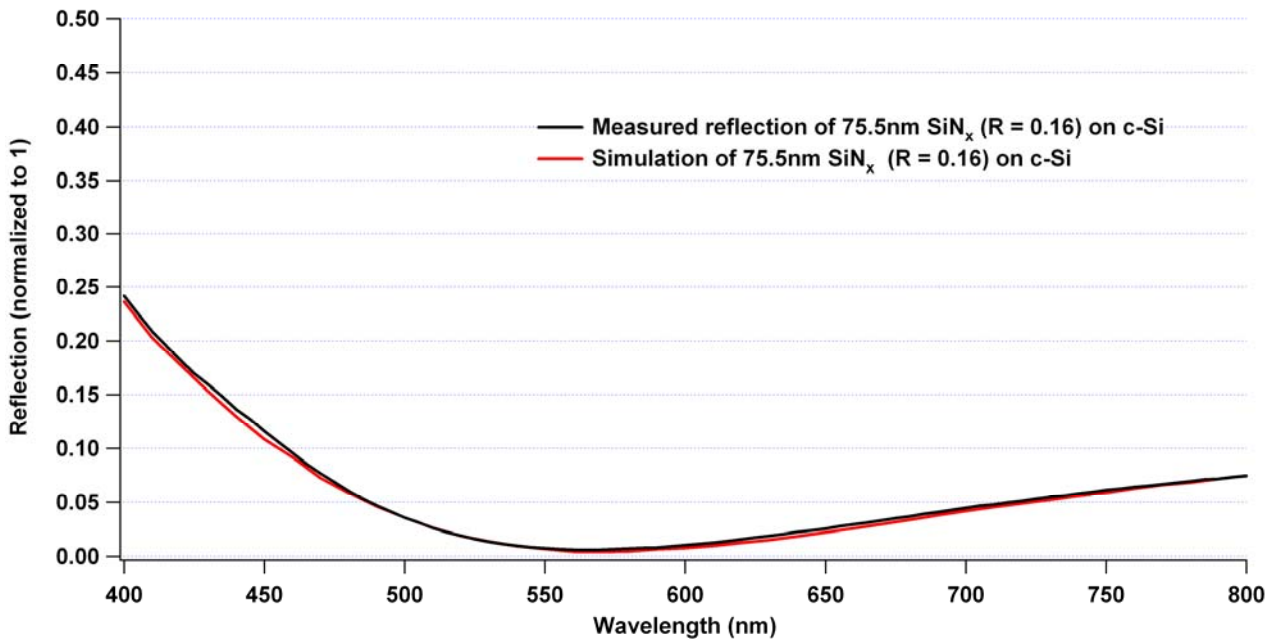
Fig. 22: Simulation (red line) and measurement (black line) of the reflection of a crystalline silicon substrate covered with SiNx. The silicon nitride is in this case 75.5 nm thick and was deposited under standard condition (R=0.16, n_{630}=1.866)

In order to see the modification induced by the refractive index and the thicknesses some simulations were performed. On the Fig 23, the same kind of silicon nitride (R=0.16, standard deposition parameters) was used. The simulations with three different thicknesses were done. The only big modification is the minimum of the reflection curve which is moving. We can also notice that the minimum position is sensitive to the thickness, if the layer is 20 nm thicker than the minimum of the reflection will shift by 150 nm. This can make
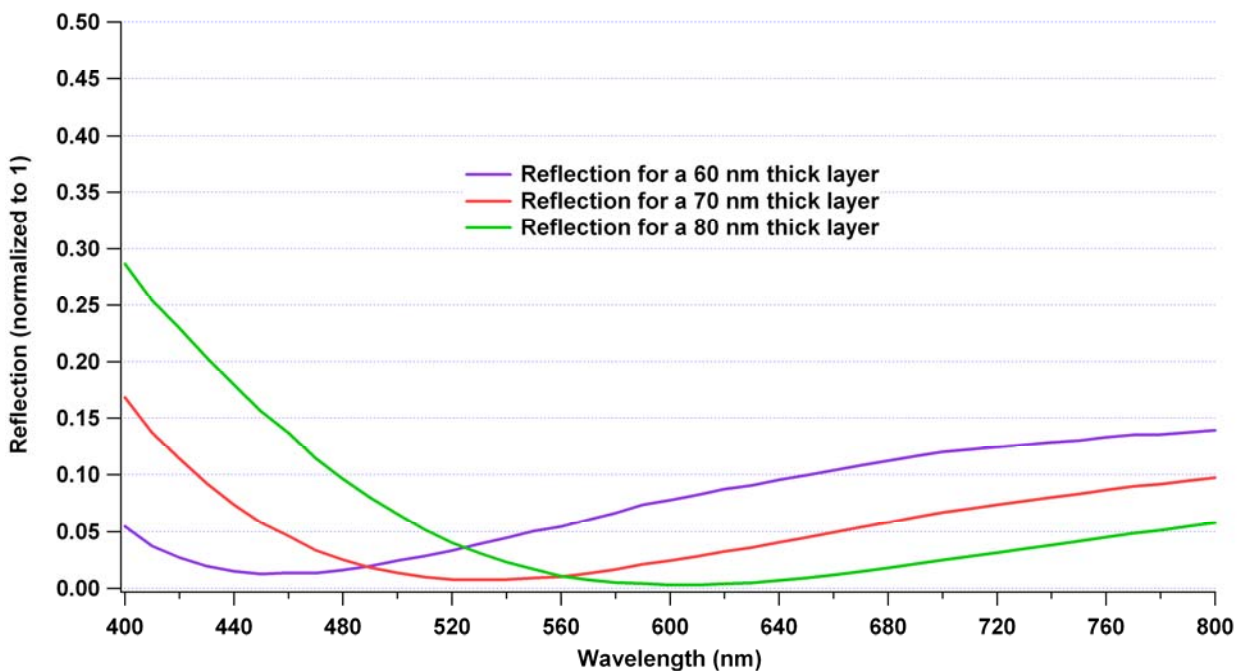
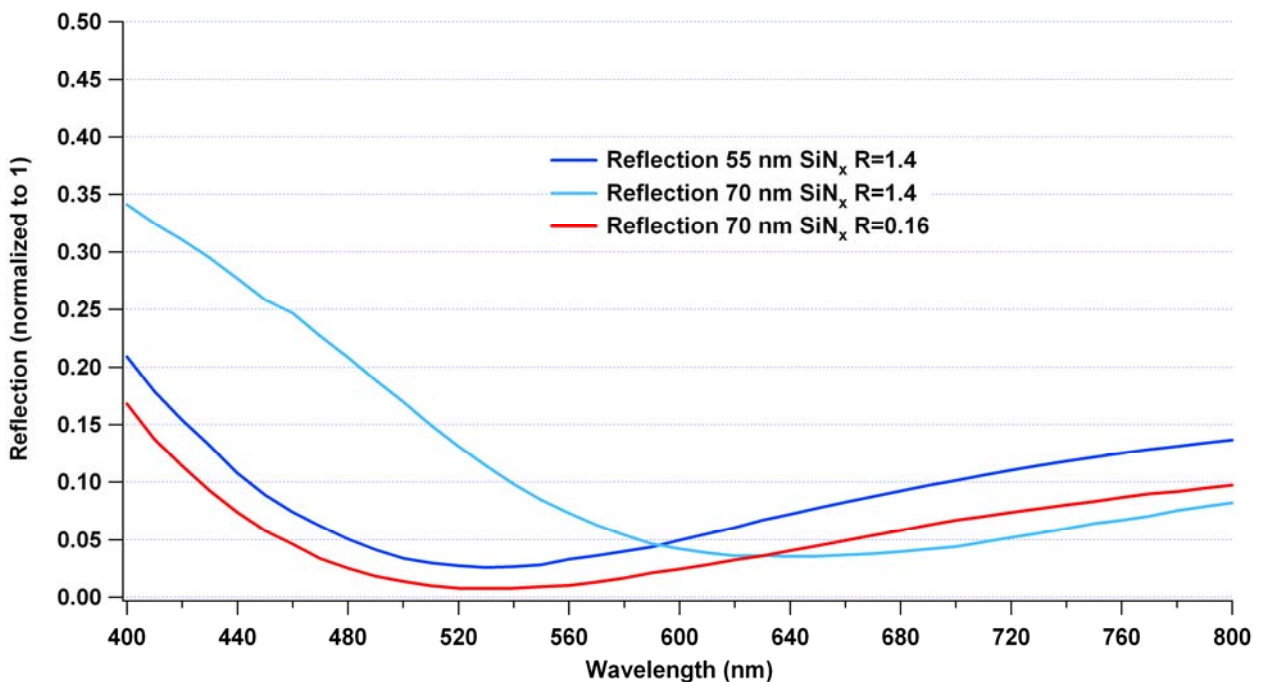**Fig. 23: Simulation of the reflection of a silicon substrate covered with SiN_x deposited under standard conditions (R=0.16, n_{630}=1.866) for three different thicknesses 60, 70 and 80 nm.**

a big difference concerning the final efficiency of a cell using SiN_x as front coating. Another point investigated was the effect of the refractive index. On the Fig.24, for the simulations, the same thickness was first taken for two different kind of silicon nitride deposited under the standard conditions but one with R=0.16 and the second one R=1.4. n=1.866 at 630 nm for R=0.16 and n=2.30 at 630 nm for R=1.4. Because of the big difference in the refractive indices the minimum of reflection will be highly shifted (nearly 120 nm). If the thickness is adjusted to have the same minimum of the reflection, then the influence of the refractive index is clearer. An increase of the refractive index leads to an increase of the reflection.

Fig. 24: Simulation of the reflection of a silicon substrate covered with SiN_x deposited under standard conditions (R=0.16, n_{630}=1.866 and R=1.4, n_{630}=2,30). The differences induced by the refractive index are shown (red and light blue lines) and the differences due to the modification of the thickness (red and deep blue line).

The anti-reflection property of the silicon nitride deposited on silicon is very sensitive to the properties of the SiN_x layer such as its refractive index and its thickness. The absorption will also play a role, but more for the light transmitted into the silicon than for the reflected light. This shows that the simulations are really important before starting deposition, especially for such sensitive systems, in order to save resources.

3.2. Electrical characterization

3.2.1 *Time Resolved microwave conductivity (TRMC)*

In the section about charge-carrier kinetics, this method was named TRPC referring to time resolved photoconductance measurements in general. Here the illumination is performed with microwaves, and we will call it TRMC (microwaves conductivity)

To study the behaviour of the charge-carriers inside a silicon wafer, we use a non destructive method called the Time Resolved Microwave Conductivity (TRMC) method. This kind of measurement is a contactless one. It means that no ohmic contact metalization has to be prepared. The measurement is based on the reflection of microwaves as a function of the conductivity of the studied material [III.5, 6].

The conductivity is connected to the mobility and the concentration of the charge-carriers by:

$$\sigma = n\mu_n e + p\mu_p e$$

(48)

These kinds of measurements are very useful to observe the behaviour of mobile charge-carriers induced by light in a sample [III.7]. The signal measured is the relative change of the microwave power reflected from the sample by a change of its conductivity. This is done by the generation of charge-carriers with a laser pulse (*see 2.1.2 interaction light matter second part*). The laser is a monochromatic light source. Two wavelengths are used, 1064 nm and 532 nm with pulse length 10ns (FWHM). The intensity of the laser is (for a radiation of 1064 nm and OD 0.0) 0.38 mJ.cm^{-2}. The Excitation density is $2.0*10^{15}$ cm². The first wavelength (1064 nm) due to the weak absorption coefficient of the silicon in this range generates electron-hole pair in the bulk (flat excess charge-carriers profile). The second one (532 nm) due to a high absorption in this range generates a sharp electron-hole pair profile at the surface (surface excitation). A gunn diode generates microwaves which are guided to the sample via a waveguide. A circulator separates the reflected wave from the incoming one and sends it to the detector.

The reflected microwave power is deduced from the Eq.12

$$\frac{\Delta R_{mw}(t)}{R_{mw}} = A.\Delta P(t) \tag{49}$$

Then:

$$\frac{\Delta R_{mw}(t)}{R_{mw}} = A.\int_0^d (\Delta n(x,t).\mu_n.e + \Delta p(x,t).\mu_p.e)dx$$

R_{mw} is the reflection of the microwaves and A is a constant. The physics behind this method is explained in the section *2.3 charge-carriers kinetics*
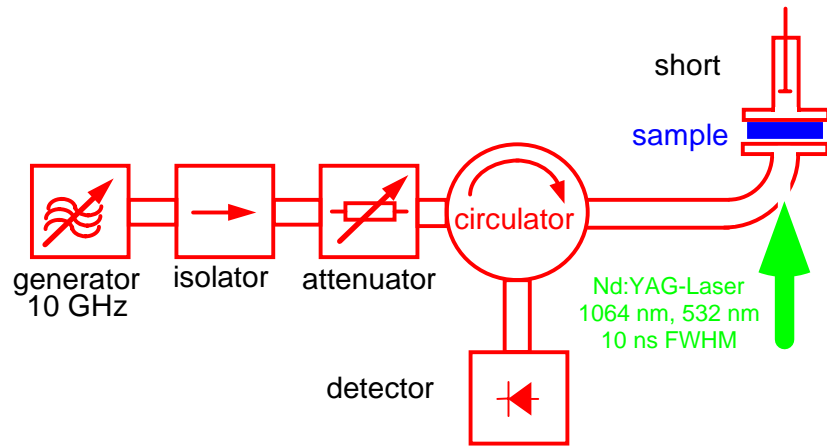

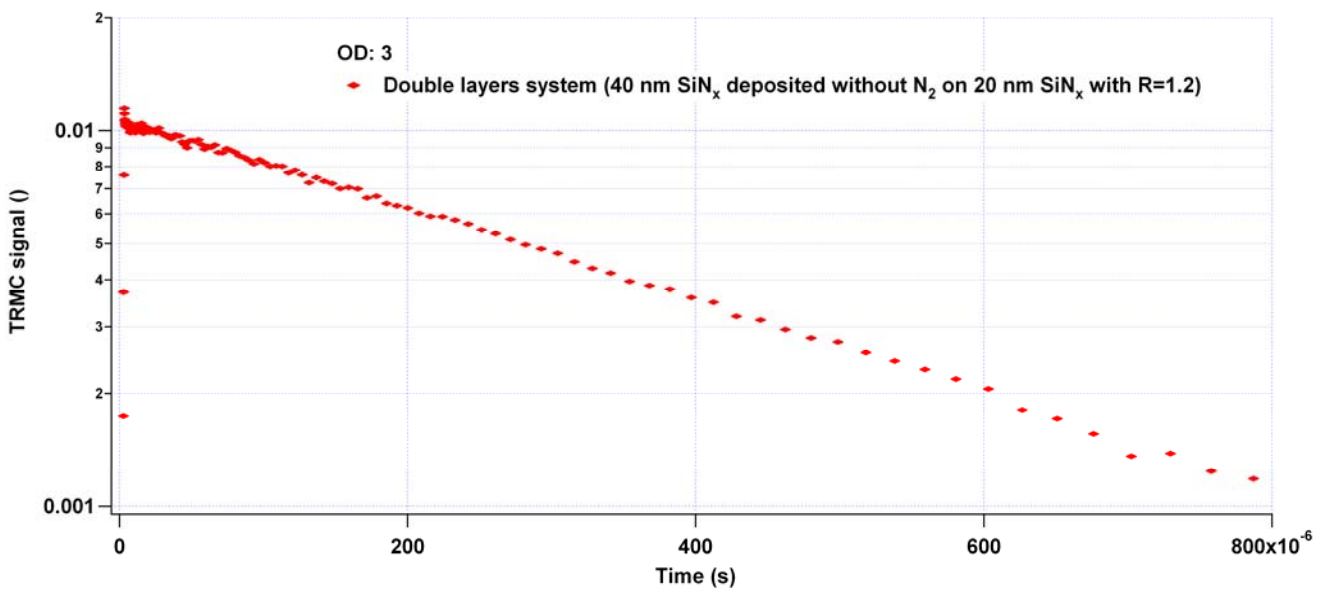.   **Fig. 25 : Scheme of the TRMC measurement principle.**

Fig. 26 : Typical measurements obtained by TRMC on a semi logarithmic scale. The decrease of the signal is due to the recombination of the excess charge carriers generated by the laser pulse. (1064 nm excitation, 10ns FWHM, the sample is a 1Ω.cm n-type silicon substrate 0.243 mm thick covered on both side with SiN_x)

47

The TRMC method is very useful to determine the lifetime and the surface recombination velocity of a sample [III.8]. The Fig.26, shows the evolution of the TRMC signal induced by a 1064 nm laser pulse on a silicon substrate covered with SiN_x. The graph is shown in a semi logarithmic scale suitable for an exponential decay. Fig.27 shows a TRMC signal in a log-log scale. This is more suitable for a non-exponential, extended decay. As it will be shown, this is particularly useful for p-type silicon substrate.
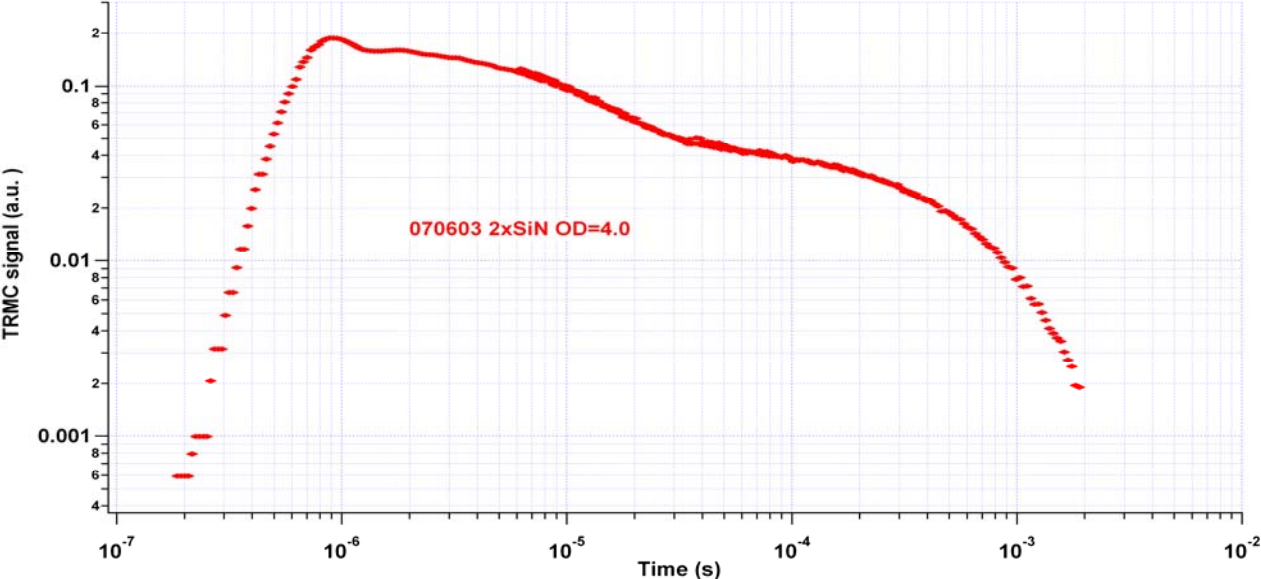
Fig. 27: Typical measurement obtained by TRMC. The log-log scale allows us to visualize the different decay processes occurring. Especially in the above case for p-type silicon covered with SiN_x. (1064 nm excitation, 10ns FWHM), The sample is a 100 Ω.cm p-type silicon substrate 0.530 mm thick covered on both sides with SiN_x

3.3. Structural characterization

The characterization of the structure of a layer is important in order to understand its behaviour. In this work, the three ways used to characterize the composition of the different layers are:

- The Elastic Recoil Detection Analysis (ERDA) measurement to give a quantitative overview of the different compounds present in the layer and their depth distribution.

- The XPS (X-ray Photoemission Spectrometry) to give an idea of the surfacial amount of different atoms (except hydrogen) but also their neighbours (using the shift of the peak).

- The Infrared spectroscopy to see the different bondings between the different atoms in the film.

This section will give an explanation of these different methods.

3.3.1 ERDA

To know the composition of a Silicon Nitride layer we can analyse directly the contribution of every atomic species by using the Elastic Recoil Detection Analysis (ERDA) method [III.9]. The measurements were carried out at the ISL (Ionen strahlen Labor) at the Hahn-Meitner-Institut [III.10] and at the Forschungszentrum Dresden-Rossendorf [III.11]. This characterization method is powerful because it allows us to determine the composition of a layer but it is a sophisticated method not available everywhere. The first measurements were performed at the HMI but after it has been closed the samples were sent to the Forschungszentrum Dresden-Rossendorfin Dresden.

The method consists of irradiating the sample with high energetic ions at a low angle (230 MeV Xenon ions at the H.M.I and 40 MeV Chlorine ions at the Forschungszentrum Dresden-Rossendorf). Due to the collision with the ions, atoms of the sample are ejected. With the measurement of energy, the time-of-flight related to the fixed flight path for the outscattered atoms (ions now) of the sample and according the formula: $E \equiv \dfrac{M}{2}V^2$, it is possible to identify and separate the different components using a plot of time vs. Energy.

The analysis of the ERDA measurements can give us the percentage of every atom present in the silicon nitride and also their depth distribution.

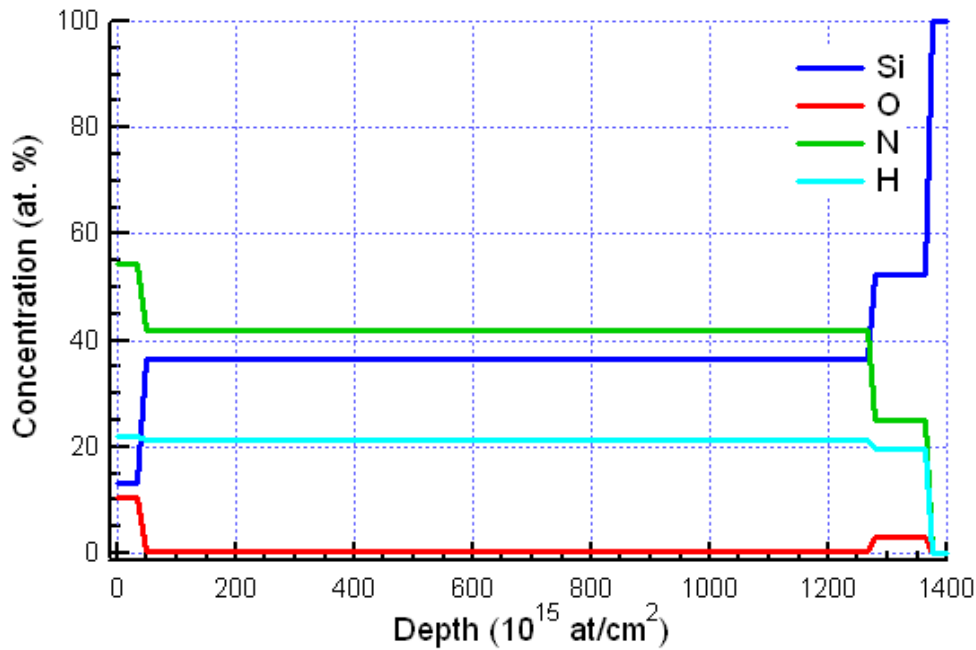The thickness of the layer can also be deduced from the formula:

$$d = \frac{N_m . <M_z>}{\rho . N_A}$$

(50)

d is given in at/cm². N_m is the area density in at/cm², $<M_z> = \sum f_z . M_z$ is the average atomic mass in g/mol (f_z the atomic fraction and M_z the atomic weight of the element Z), ρ is the density in g/cm³ and N_A the Avogadro's constant in mol^{-1} we can obtain d the thickness in nm.
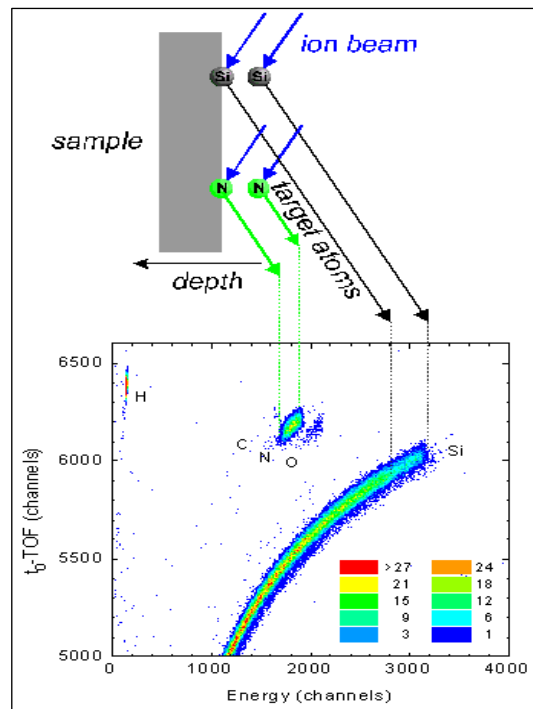
Fig. 28 : Principle of the ERDA measurements.

Fig. 29 : Evolution in the depth of the different compounds present in the silicon nitride layer deposited on a crystalline silicon substrate (100% on the right side). 100.10^{15} at/cm² represent 11 nm in this case.

With ERDA measurements we can see if the layer is homogenous in thickness. The oxygen observed at the interface between the silicon substrate and the silicon nitride is due to the oxidation of the substrate between the etching of the oxide layer by HF and the deposition. Indeed, the silicon is extremely reactive with oxygen. The measurement is not really sensitive for the first nm of the layer. However, there is more oxygen at the surface than inside the layer (because of oxidation). At the interface between silicon and silicon nitride we can see a structure (mixture of silicon, nitrogen, hydrogen and oxygen) which shows the damage on the silicon substrate caused by the ion impact during the deposition process. This interface is, nevertheless, very thin (less than 10 nm).

The relative error of the ERDA measurements is about 1-2%

XPS (or X-ray Photoemission Spectrometry) is used to determined the elemental composition of a sample at the surface. The principle of the XPS consists of the irradiation of the sample surface with an X-ray beam and subsequently to analyse the kinetic energy and the number of ejected photoelectrons. The X-rays are generated by a K_α line obtained with an Al or Mg anode (resp. 1.48 and 1.25 keV). An analyzer will select the electron in function of their energy and an electrons detector will count the number of electrons for each energy. More details about XPS can be found in [III.12,13]

However this kind of analysis has 2 weaknesses. It can not observe atoms with an atomic number below 3 (i.e. Hydrogen and Helium) and it is limited to the first 10 nm (depending on the material under investigation) because XPS is only measuring the electrons escaping from the surface All electrons generated deep inside the material will be recaptured before they escape to the vacuum. In our case the missing information about the quantity of hydrogen can be a problem because the SiN_x contains around 20% of hydrogen (number know thanks to the ERDA measurements).

A XPS measurement gives the number of electrons for each kinetic energy. Each element gives different peak(s) corresponding to their binding energies. Those characteristic peaks come from the electronic configuration of each core-level electron inside the atom (1s, 2s, 2p …). The peaks can be related to the corresponding atom and also to the amount of this atom in the material under investigation (in the 10 first nm approximately).
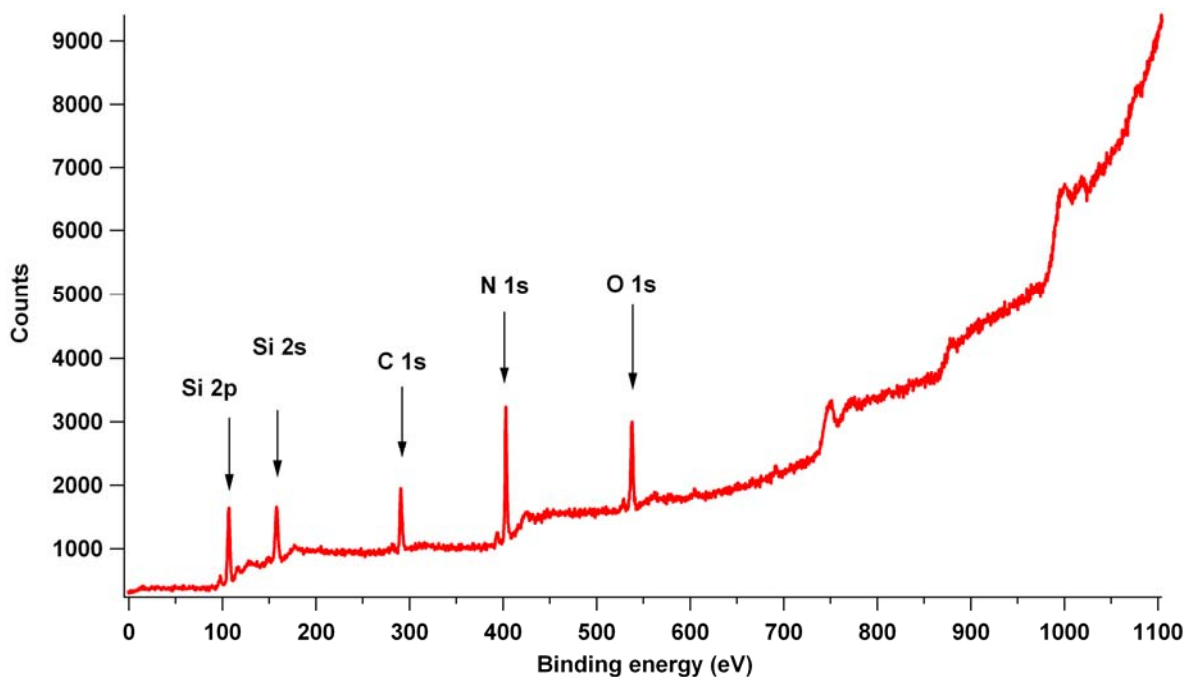

Fig. 30: XPS spectrum of a SiN$_x$ layer. The peaks represent the elements present at the surface of the layer. The percentage of each element in the layer is obtained by determining the area under each peak.

The samples were first etched with a solution of HF (2%) to remove the thin oxide layer (but also the other impurities therein) present at the SiN_x surface. The time of etching was not always the same (because the etching rate is different for different SiN_x deposited under different conditions). The sample was etched until the interference colour of the sample changed, indicating that the thickness was reduced. This step is important for XPS measurements because of the low analysis depth. Indeed, oxide at the surface will distort the results and will not show the real ratio of silicon and nitrogen inside the SiN_x layer. The relative error is about 3%.

The Fourier Transformed InfraRed Spectroscopy (FTIR Spectroscopy) [III.14] is a measurement technique based on the absorption of infrared radiation by the material. By studying the characteristic vibrations of the chemical bonds, an analysis of the chemical bonds present in the material studied is possible.

The molecule's vibrations are mostly included between 2.5 and 25 μm (400 cm^{-1} and 4000 cm^{-1}) corresponding to the infrared region. Not every vibration will lead to absorption, it will depend on the geometry of the molecule, the electronegativity of the atoms and their mass. In this work we will use values used in literature.

In a FTIR spectroscope, the light is guided through an interferometer (Michelson), the measured signal is the generated interferogram passing through the sample. Then, to obtain a conventional infrared spectroscopy like spectrum, a Fourier Transformation is performed. In the following table, the frequencies of vibrations for the compounds of interest in this work are given [III.15, 16]:

Si-Si	610 cm^{-1}
Si-H	630 cm^{-1}
Si-H2	630 cm^{-1}
Si-H3	630 cm^{-1}
Si-H rocking	665 cm^{-1}
Si-N stretching	840 cm^{-1}
Si-H2	845 cm^{-1}
Si-H3	862 cm^{-1}
Si-H2	875 cm^{-1}
Si-H3	907 cm^{-1}
Si-N stretching	957 cm^{-1}
Si-O-Si	1000 cm^{-1}
N-H3	1100 cm^{-1}
Si2N-H rocking	1170 cm^{-1}
N-H	1220 cm^{-1}
SiN-H2 bending	1550 cm^{-1}
Si-H	2000 cm^{-1}
Si-H2	2090 cm^{-1}
Si-H3	2140 cm^{-1}
N2Si-H stretching	2150 cm^{-1}
Si2N-H stretching	3350 cm^{-1}
SiN-H2 stretching	3450 cm^{-1}

Tab. 1: table giving the important frequencies vibrations used in this work.

An overview of the different oscillation mode (stretching, rocking …) is given here [III.17]

4. Coatings on silicon substrates

55

The aim of this work is the study of different coatings such as silicon nitride, amorphous silicon and silicon oxide on crystalline silicon, mostly n type but also p type are studied. These kinds of layers are used in silicon solar cells as passivation layers or anti-reflection layers.

An analysis of the different coatings with the measurements described before was performed. After a description of the deposition of the layers, results will be shown and analysed for different deposition parameters.

4.1. Deposition methods

This chapter will deal with hydrogenated amorphous silicon nitride a-H:Si_3N_4, named SiN_x in this work. The x means that the composition, i.e. the ration of silicon and nitrogen atoms, is not stoichiometric. The deposition was performed by Plasma Enhanced Chemical Vapour Deposition (PECVD) in a PlasmaLab 80 deposition chamber. The amorphous silicon was also deposited by PECVD but in another chamber (to avoid contamination), the principle remains the same.

The first step is the preparation of the substrate. Two kinds of substrates were used for this work. A quartz substrate was mostly used to determine the optical transmission of a SiN_x film. A wafer or wafer pieces of crystalline silicon (p and n doped) were used for all the other measurements. The standard size of a substrate (except for a whole wafer) is 27 * 14 mm. The silicon substrates were covered by a plastic foil and sawed at the desired size at the Fraunhofer-Institut für Zuverlässigkeit und Mikrointegration (IZM) Berlin.

The quartz substrates were cleaned with ethanol and water then dried under argon flow.

Two preparations of the silicon substrate were performed, a standard one and an oxide protected substrate one (using a Nitric Acid Oxidation of Silicon (NAOS) method [IV.1,2]). For both preparations the first steps are the same. Impurities such as particles or the thin native oxide layer have to be removed. Thereby, silicon substrates were cleaned by the process described in the following picture (Fig.31). Ethanol and Acetone remove the organic compounds. The piranha solution will create a chemical oxide layer which will be etched by the HF. The creation and etching of this layer will remove the oxide at the surface and the other impurities that stayed after the ethanol and acetone treatment. The etching will also generate H-Si bonds at the surface of the silicon. In this case, and to avoid a re-formation of the native oxide layer, the sample has to be placed as fast as possible into the deposition chamber. For the oxide protected substrate preparation after the handling described before, the sample is rinsed with water and staged for about 30 minutes in a 65% HNO_3 solution to create, chemically, a thin protective oxide layer (NAOS method).

The use of the NAOS substrate will be explained later in chapter *4.2 Silicon nitride*.

After the preparation and once the sample is placed into the deposition chamber, it can be coated by the silicon nitride. The deposition chamber uses a direct plasma and high frequency technology.

```
┌─────────────────────────────────────────────────┐
│   Clean with Ethanol under ultrasound (≈1 min)  │
└─────────────────────────────────────────────────┘
                      ↓
┌─────────────────────────────────────────────────┐
│   Rinse with water under ultrasound (≈1 min)    │
└─────────────────────────────────────────────────┘
                      ↓
┌─────────────────────────────────────────────────┐
│   Clean with Acetone under ultrasound (≈1 min)  │
└─────────────────────────────────────────────────┘
                      ↓
┌─────────────────────────────────────────────────┐
│   Rinse with water under ultrasound (≈1 min)    │
└─────────────────────────────────────────────────┘
                      ↓
┌─────────────────────────────────────────────────┐
│         10 minutes at 80°C in a piranha solution │
│   (50% H₂O₂ (50%), 50% H₂SO₄ (97%) in volume)   │
└─────────────────────────────────────────────────┘
                      ↓
┌─────────────────────────────────────────────────┐
│   Rinse with water under ultrasound (≈1 min)    │
└─────────────────────────────────────────────────┘
                      ↓
┌─────────────────────────────────────────────────┐
│       Etched 1 minute in a 2% HF solution       │
└─────────────────────────────────────────────────┘
```

10 minutes at $80°C$ in a piranha solution
(50% H_2O_2 (50%), 50% H_2SO_4 (97%) in volume)

Etched 1 minute in a 2% HF solution

Deposition with NAOS method

Deposition of the layer

Rinse with water under ultrasound (≈1 min)

NAOS method, 30 min in 65% HNO_3

Rinse with water under ultrasound (≈1 min)

Deposition of the layer

Fig. 31 : Scheme showing the preparation of the silicon substrate with the standard method or with the NAOS method

For the deposition of SiN_x we use a gas mixture of Silane (SiH_4), Ammoniac (NH_3) and nitrogen (N_2) in order to have all the compounds in the plasma phase. The nitrogen is used to dilute the gas mixture and provide also nitrogen atoms which will make the layer

57

more nitrogen rich [IV.10]. When the heating plate is at the desired temperature, the gases flow uniformly into the chamber by the showerhead upper electrode and are pumped radially toward the exit (pump on the scheme). There, a radio frequency about 13.6 MHz will ionize the molecules of the gases present between the 2 electrodes. The reactions in the plasma leading to the formation of the layers are complex and will not be detailed there, but four main reactions can be noted:

- Just after the ignition, the reactions between electrons and gas reactants lead, in the plasma, to a mixture of ions, gas radicals and electrons.

- The reactive species are migrating to the substrate (by convection, electric field …).

- The reactive species are absorbed on the substrate surface.

- There, the species will react and arrange them to form the growing layer. Some of the reaction products (the volatile one) will return into the plasma.

More information about plasma can be found there. [IV.3, 4]
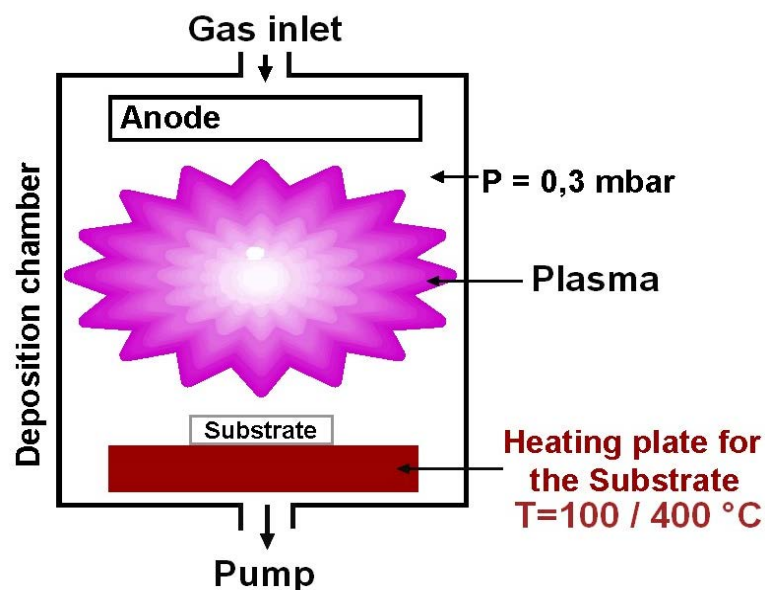
fig. 32 : Overview of the plasma deposition chamber. The substrate can be heat until 400 °C. The plasma is burning, over the sample.

The deposition process is made under a pressure of about 325 mTorr (0.4 mBar). Another parameter to take into account is the temperature of the sample. In this deposition chamber, we can heat the sample up to 400°C (by heating the heating plate). The temperature is automatically regulated by a digital controller (Honeywell UDC 3300). Those low

temperatures of deposition reduce the possibilities of contamination or degradations of the substrate and also the energy cost.

By varying the parameters such as temperature, gas mixture or pressure it is possible to modify the conditions of the depositions and thus adapt the layer to our needs. Different chemical compositions or deposition rates are available.

Both doping types of silicon will be used as substrate as well as glass or quartz. But in fact, in this chamber, all material which does not be degrade at those temperatures or will not contaminate the chamber can be used.

As previously mentioned, to make the amorphous hydrogenated silicon layers (a-Si:H) another deposition chamber is used but the principle is exactly the same. In this case no nitrogen is present in the layer, it means that only Silane is used in the plasma.

In the following, the standard conditions of deposition for the production of SiN_x layers are:

- Temperature: 350°C

- Pressure : 325 mTorr

- N_2 flux: 54 sccm (standard cubic centimetre)

The ratio R of the two main precursor gases (Silane and ammoniac) is defined by $R=[SiH_4]/[NH_3]$ and will, for the standard composition, be equal to 0.16.

It means: - Flux SiH_4: 32 sccm

- Flux NH_3: 200 sccm

If occasionally other deposition parameters (especially R) are used, this will be indicated.

4.2. Silicon Nitride

Silicon nitride in its crystalline form is found with the chemical composition Si_3N_4. It is a hard and solid substance which has a good shock and heat resistance and it is also a good isolator used in microelectronics [IV.5, 6]. For years silicon nitride has been used in the microelectronic industry as an insulator or as passivation layer for microchips and more recently in the photovoltaic industry. In our case, because of the deposition by PECVD, the silicon nitride is in an amorphous state. This means that we do not have a crystalline lattice. The other modification due to the PECVD deposition is an amount of nearly 20% (in atom quantity) of Hydrogen in the silicon nitride layer.

Silicon nitride is used in solar cells as a passivation and anti-reflection layer [IV. 7, 8, 9, 10, 11, 12]. The SiN_x layer on doped silicon will create an accumulation or depletion layer (on n-type respectively p-type) induced by its fixed positive charges [IV.13, 14]. The electrons (majority charge-carriers in n-type silicon) will accumulate at the surface. With its band gap of about 4.3 eV which avoids the absorption of the light for the wavelength higher than 300 nm and its refractive index $n_{SiNx} \approx 1.9$ which is between the refractive index of air $n_{air}=1$ and the one of silicon, $n_{Si}=4.5$, it's also a good coating for the anti-reflection.

To have a good understanding of the deposition process and the evolution of the properties of the SiN_x layer we study the effect of the precursor gasses (SiH_4 and NH_3) on the different properties by varying the ratio R of those gasses (R = [SiH_4] / [NH_3]). In addition, the variation of the deposition temperature was also studied.

To see the evolution of the composition, 5 different ratios R were used (R= 1.2, 1, 0.5, 0.16, 0.125). The flux of N_2 in the plasma was maintained. The deposition was performed at the temperature of 350°C on crystalline silicon FZ, n doped and with a resistivity of about 1 Ω.cm. A pressure of 325 mTorr is taken constant. Variation in the temperature, pressure or precursor gases (other than the Ratio R) will be indicated. Substrates used were mainly n type silicon, the use of p type is also indicated.

SiH_4/NH_3 ratio	Temperature of deposition (in °C)	Silicon (% of atomic content)	Nitrogen (% of atomic content)	Hydrogen (% of atomic content)
0.125	350 °C	32.6 %	44.7 %	21,7 %
	/	/	/	/
0.16	350 °C	33.6 %	44.4 %	22 %
	300 °C	31 %	45.6 %	22.5 %
0.5	350 °C	37 %	41.1 %	21.2 %
	300 °C	37.2 %	38.6 %	23.4 %
1	350 °C	39.4 %	38.7 %	20.9 %
	300 °C	42.4 %	33.1 %	23.8 %
1.2	350 °C	40 %	36.1 %	22.8 %
	/	/	/	/

Tab. 2: Evolution of the content of Silicon (Si), Nitrogen (N) and hydrogen (H) in the layer of SiN_x for different ratio of precursor gasses (R = [SiH_4] / [NH_3]) and different temperatures measured by ERDA.

A better overview of the evolution of the concentration of each compound can be done by a plot of the contribution of the different atoms to the composition of the film vs. the ratio R. (Fig.33 at 350°C and Fig.34 at 300°C)
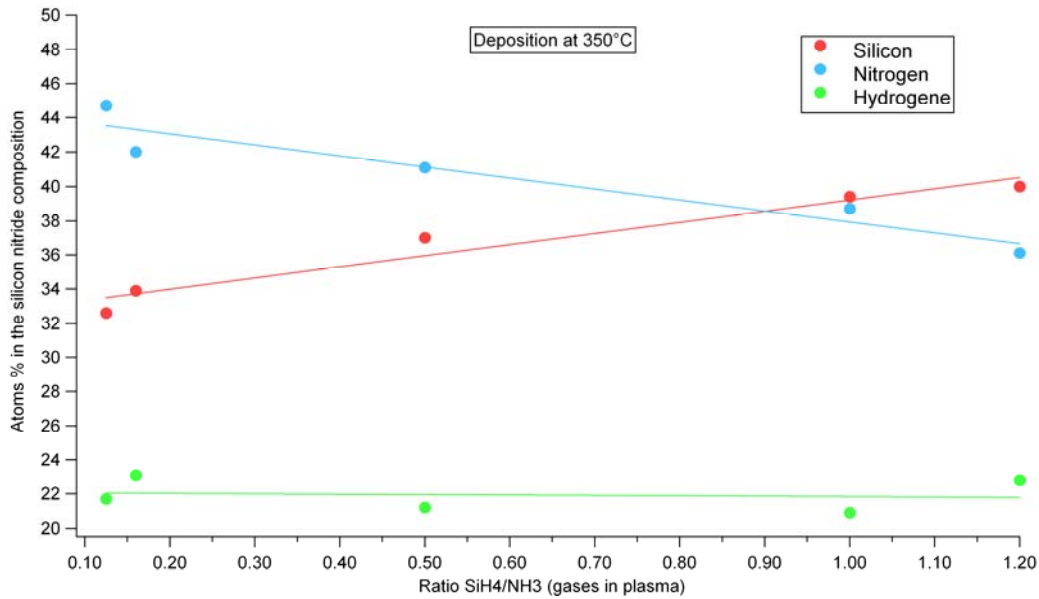
Fig. 33: Evolution of the relative contribution of the different elements to the composition of the silicon nitride layer for different ratios of the Silane and Ammonia in the plasma gases at 350°C. The lines were drawn as an aid for the eye.
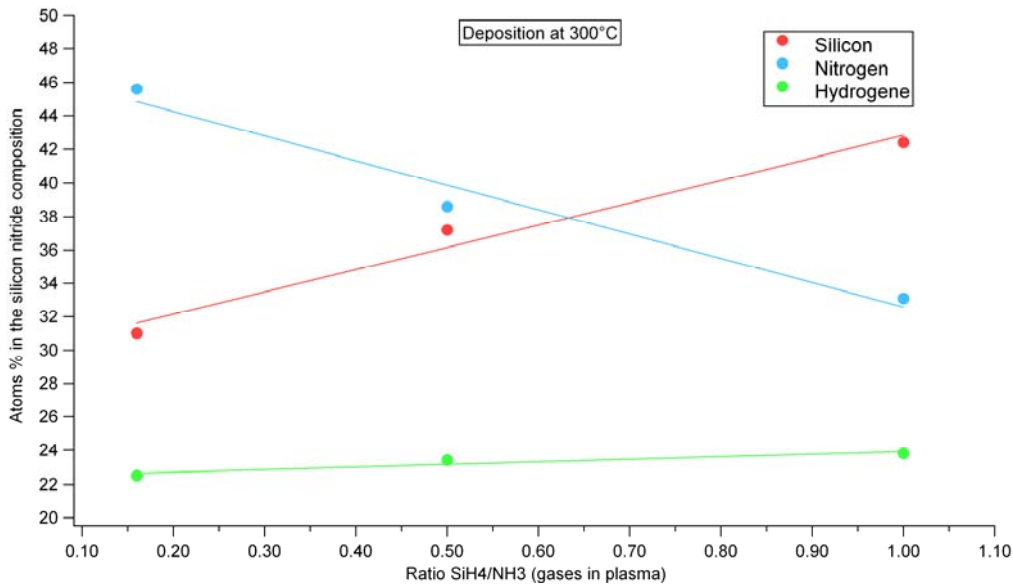
Fig. 34: Evolution of the relative contribution of the different elements (SI, N, H) to the composition of the silicon nitride layer for a deposition temperature of 300°C. The lines were drawn as an aid for the

We observe that the amount of hydrogen does not vary with the ratio R. The same thing was observed by J.-F. Lelievre in his thesis and G. Morello [IV.15, 16].

This is an important point for the future measurements with XPS which did not take the hydrogen into account.

62

After the closing of the ISL at the Hahn-Meitner-Institut it was more difficult to do ERDA measurements. We therefore tried to determine the composition of the layer by another method. XPS was the most comfortable one as it was fast and precise enough for our needs. An explanation of the XPS measurements was given in the section *3.3.2. XPS.*
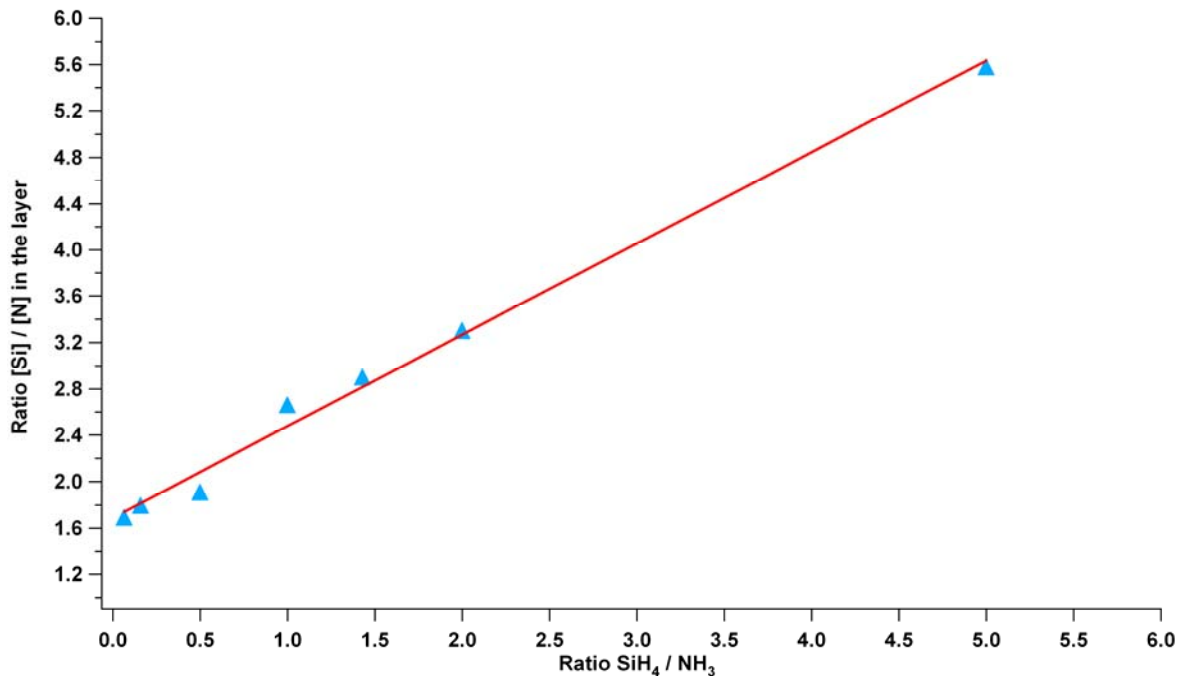
Fig. 35: XPS measurements showing the ration r = Si / N of the compounds in the layer as a function of the ratio R of the precursors gases in the plasma. Temperature of deposition = 350°C, pressure = 325 mTorr, N_2 flux 54 sccm.

Another set of samples was performed over a wide range of R (= 0.065, 0.16, 0.5, 1, 1.43, 2, 5 and 0.16 without N_2 notice 0.16_{-N2}). After the deposition, and before the XPS measurements, the samples were etched with HF (2%). This step is important to removed the first oxide layer and avoid the pollution due to the thin oxy-nitride layer on the surface. Indeed after the deposition we observed the formation of a thin oxide layer on the surface of the Silicon nitride. Even if the sample is cooled down in the chamber under vacuum the oxide is still present. The XPS spectra of a sample removed from the chamber directly after the deposition (i.e. when it is still warm) and the spectra of a sample removed after cooling down of the chamber under vacuum are the same. The time of etching was not the same for all samples. The different compositions made the SiN_x harder or softer. To remove enough matter, the samples were dipped in the HF solution and removed after the change of the interference colour. If the surface interference colour changes, it means that the thickness of the coating became thinner (more than a few nanometres). The oxide layer is then completely removed.

The ratio r = [Si] / [N] of the different compounds (Silicon and Nitrogen) in the layer was found to be proportional to the ratio R (ratio of the precursor gases in the plasma). In the following we will only use the ratio R, more practically because it is directly related to the parameters of the deposition chamber.

As shown, the precursor gases play an important role in the final composition of the silicon nitride layer. The more silicon in the plasma, the more silicon in the layer. And thus, all properties related to the amount of silicon will be changed.

A good overview of the effect of the ratio R on composition of the layer can be seen in the FTIR spectra Fig.36. The three samples measured were deposited under three different ratios R {0.16, 0.5 and 5}. All the samples have the same thickness. The more silicon ions in the plasma, the more Si-H bonds in the layer (and less N-H bonds). The number of Si-N bonds seems to be constant. This modification of the bonding inside the layer will have an impact on the optical properties like the refractive index or absorption and on the electrical passivation.
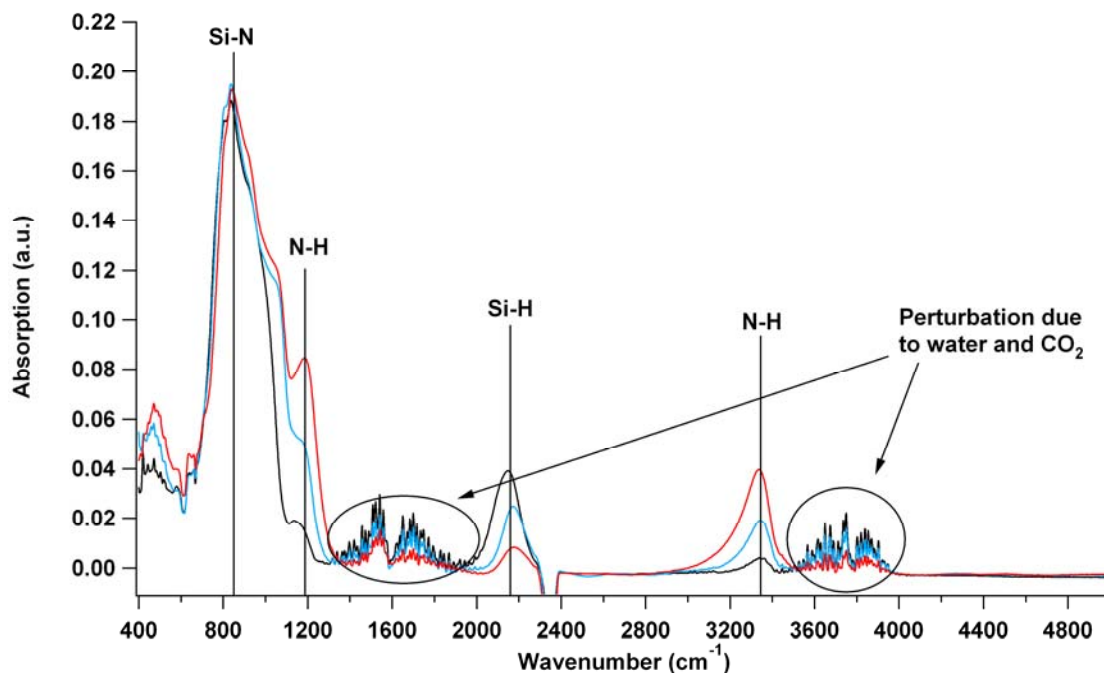
Fig. 36: IRFT spectra of different SiNx deposited with different ratio R. The red curve is the SiN$_x$ with the smallest quantity of silicon (R=0.16) and the black curve is the layer with the biggest quantity of silicon (R=5)

The precursor gases influence also the deposition rate. Before the study of the thickness of the SiN$_x$ layer we have to be sure that the deposition is homogenous in the lateral plan, otherwise the use of the thickness will make no sense. Fig. 37 shows a picture of two

samples. The colour of each sample is uniform. Silicon nitride is a transparent compound, so the colour is due to interferences. As seen in the chapter 1, the interferences are a function of the refractive index and the thickness of the layer, therefore, the uniformity of the colour means that the effective refractive index and thickness are identical over the whole area (i.e. in the lateral plane) for each sample. The effective index will be the average of the possible variation of the refractive index in the normal direction.
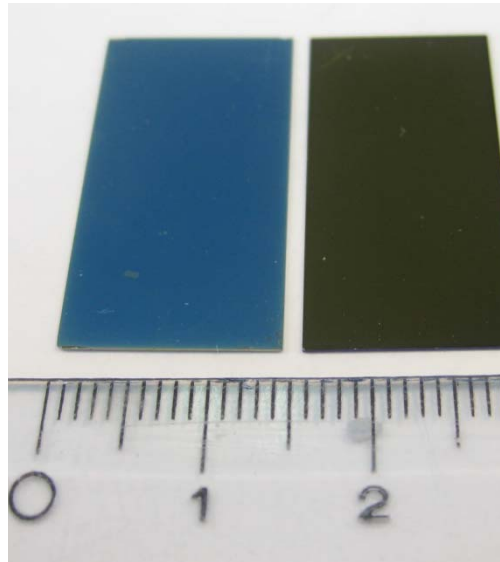
Fig. 37: Picture of two samples (silicon nitrite layer on n type mono-crystalline silicon substrate). The colour due to the interferences is uniform for the whole area of each sample. Interferences are a function of the refractive index and the thickness of the layer, therefore, the uniformity of the colour means that the effective refractive index and thickness are identical over the whole area (i.e. in the lateral plane) for each sample..

To quantify this, measurements have been performed with the monochromatic ellipsometer on 5 spots spread over the whole area for three samples. These experiments yield the thickness and the effective refractive index on every spot. The results of those measurements show a good uniformity of the deposition over the whole area of each sample.
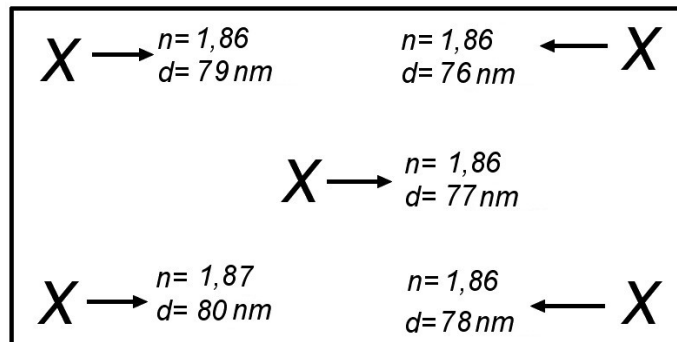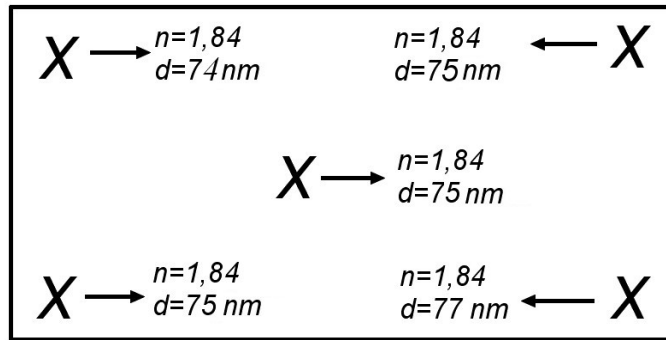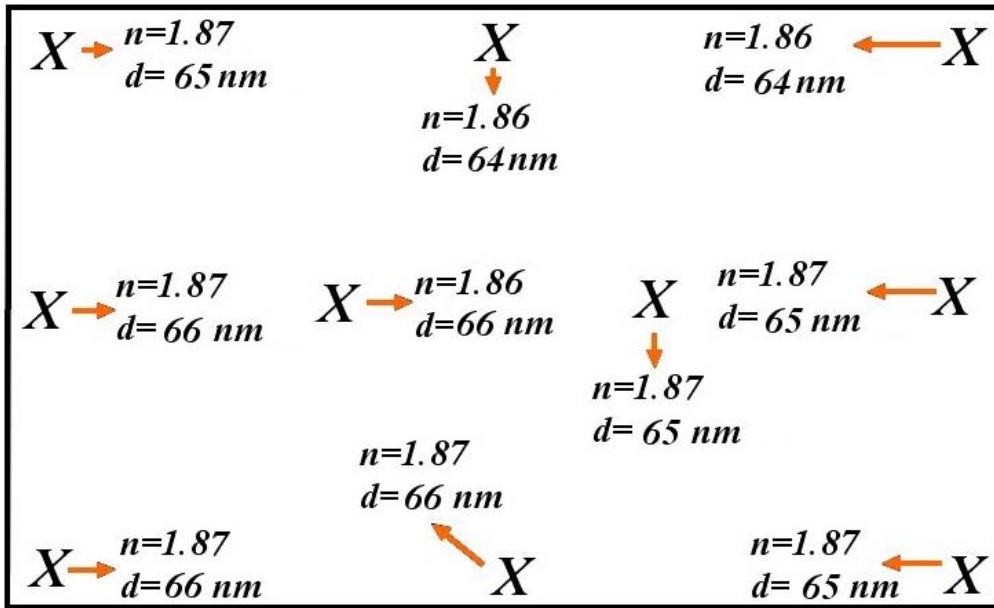
Fig. 38 : Measurements of the thickness and refractive index (at λ=630 nm) of three different samples made by a silicon nitride on a silicon substrate. The Xs give the points where the measurements were done. n is the refractive index at the point X and d the thickness.

These measurements show that the thickness varies only in the percent range over the area of each sample. The effective refractive index varies only slightly in the percent range. Both variations are within the error range of the measurements and so the samples can be considered homogeneous over their whole area (i.e. in the lateral plan). In the following, all samples used to characterize the thickness were measured with the monochromatic ellipsometer at two distinct points in the middle of the sample

Fig.39 shows the thickness of the layer as a function of the deposition time. The deposition was performed on substrates of the same batch (n-Si, CZ, <111>, 1 Ω.cm) at the same temperature (350°C) and under the same pressure (325 mTorr).
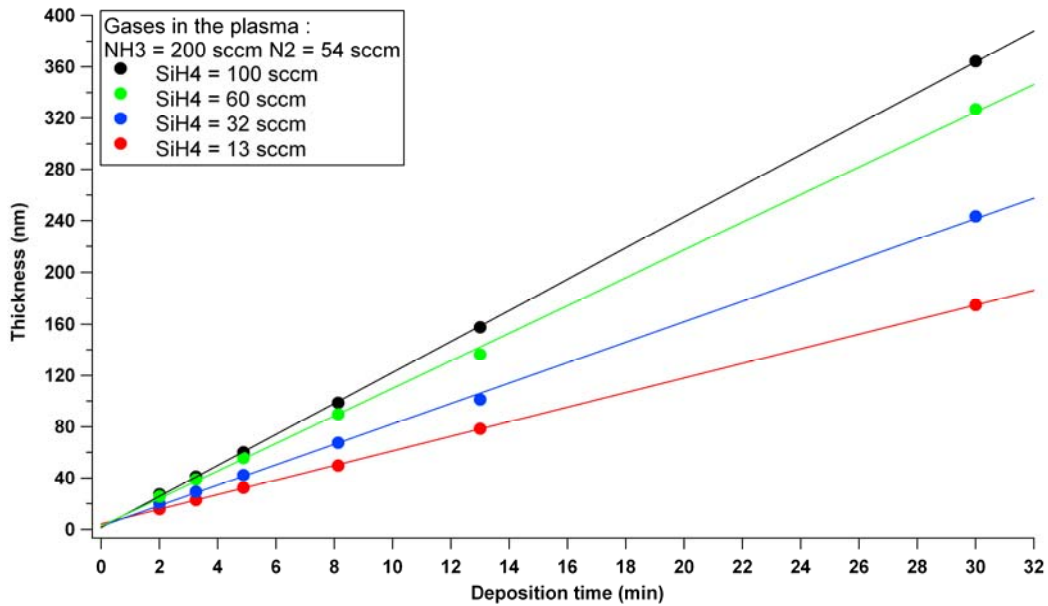
Fig. 39: Representation of the thickness (in nm) of the silicon nitride layer as a function of the deposition time (in min.) for 4 different concentrations of gases in the plasma during the deposition process. (The lines are drawn as a guide to the eye).

It is clear that the more silicon we have in the plasma, the faster the deposition will be. A good overview is shown by the plot of the deposition rate vs. the deposition time. The deposition rate is the thickness at a specific time divided by the deposition time.
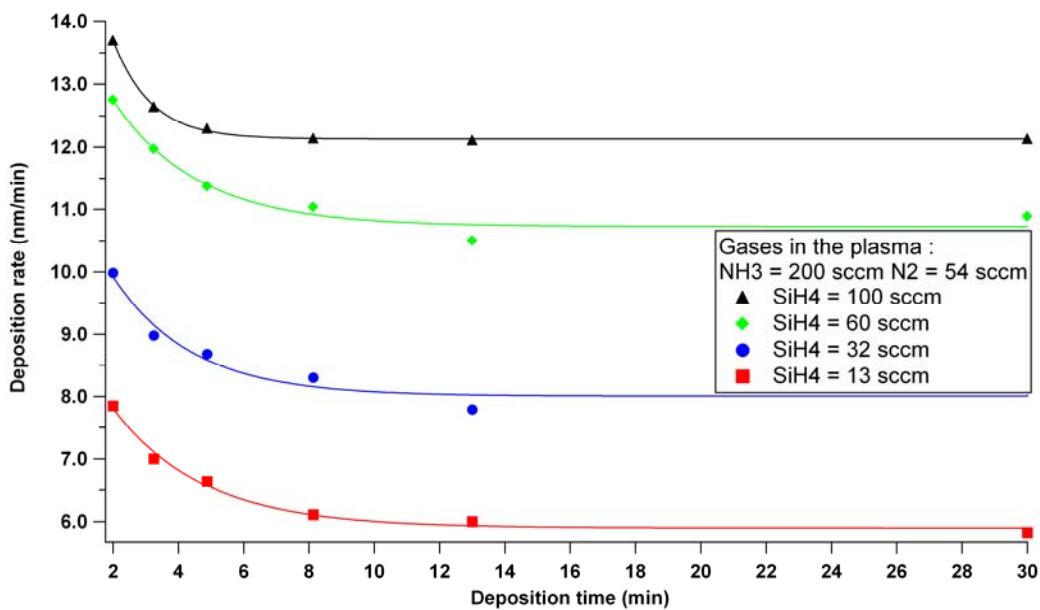
Fig. 40: Deposition rate (nm/min) of the silicon nitride as a function of the time (min) for 4 different ratios R.

evolution of the refractive index with the time of deposition. (Fig.41)

In this picture the refractive indices of a silicon nitride layer were measured by ellipsometry at λ=630 nm (monochromatic ellipsometer). The layers were deposited under the same conditions (Temperature = 350°C, Pressure = 325 mTorr, gases flux: SiH_4 = 100 sccm; NH_3 = 70 sccm; N_2 = 54 sccm) but for different times of deposition. This gas mixture was used because it was the only one giving a result of the refractive index for the thinner film (2 minutes). The same behaviour is observed for the other compositions without the thinner film (2 minutes).
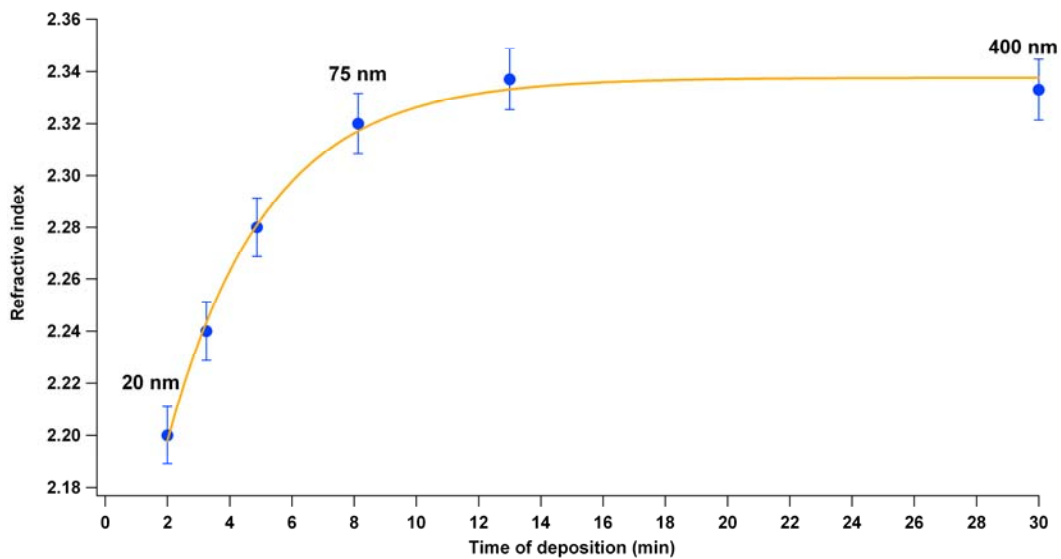
Fig. 41: Evolution of the refractive index as a function of the time of deposition. All samples were deposited under the same condition given at the beginning of the chapter (temperature, pressure, substrate) and with the same precursor gases (SiH_4 = 100 sccm; NH_3 = 70 sccm; N_2 = 54 sccm).

On these graphs we can see that, at the beginning, the layer grows quickly and after around 8 minutes the deposition rate becomes constant. The same evolution in the time is observed concerning the measured refractive index. Two explanations are possible:

- The refractive index is identical in the whole layer but increases during the deposition due to thermal effects or diffusion of compounds

- The first layer has a lower refractive index than the subsequently deposited one. Measurements will give the average of the refractive index. (i.e. the effective refractive index)

68

If we compare Fig.40 with Fig.41, the second case seems to be the more plausible one. Amodel for this case is that the substrate (Silicon) is very reactive at the beginning so the radicals are reacting quickly with it. After this first step, the radicals will have to grow on another "substrate" which consist of silicon nitride. The SiN_x is less reactive and the radicals will react slower with it. This gives, a somewhat different film structure, also. We can then assume that we have a gradient of refractive index in the normal direction for the first 75 nm.

For this ratio R, the maximal density is obtained for layers thicker than 75 nm (after 8 minutes of deposition). This can be problematic for the characterization of thin layers as if the refractive indices are lower the density will vary. This will lead to a change in the composition or arrangement of the atoms and thus the properties. The thicknesses used for our application are thicker than 70 nm so we can assume that the refractive index is the maximum one and all the properties will be fixed.
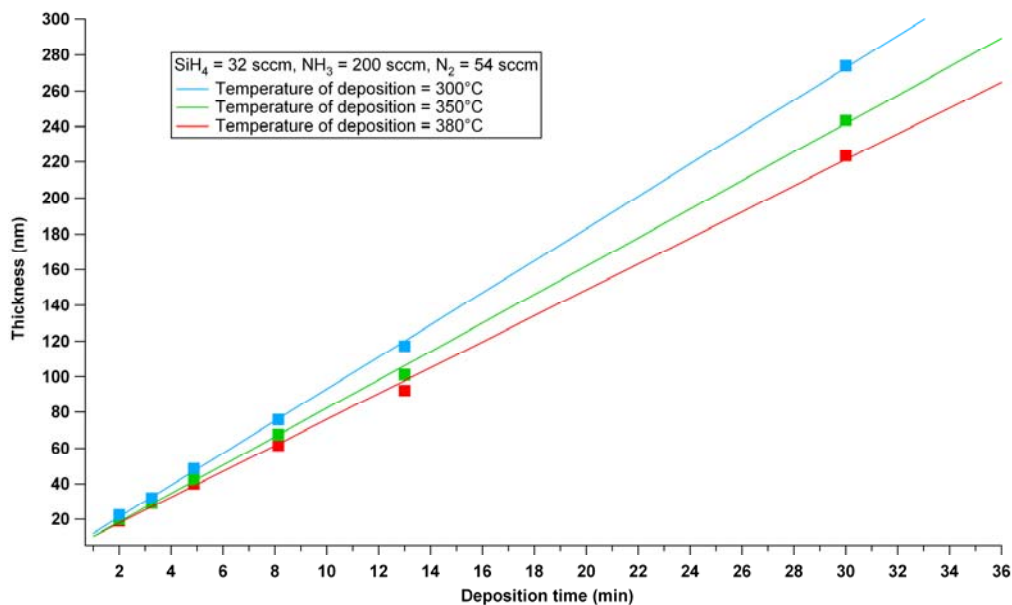
Fig. 42: Thickness as a function of the deposition time for 3 layers deposited at different temperatures but with the same composition of the precursor gases. (The lines are drawn as an aid to the eye)

The deposition rate (and so the thickness vs. the deposition time, Fig.42) depends on the substrate temperature. The Fig.43 shows the deposition rate as a function of the deposition time for 3 layers deposited with the same precursor gas mixture but at 3 different temperatures (300°C and 350°C). The deposition at low temperatures is faster than at high temperatures. The reason for this could be the heat of the surface of the substrate, the more the surface is excited the more the reactive ions in the plasma will have difficulties to stabilize themselves.
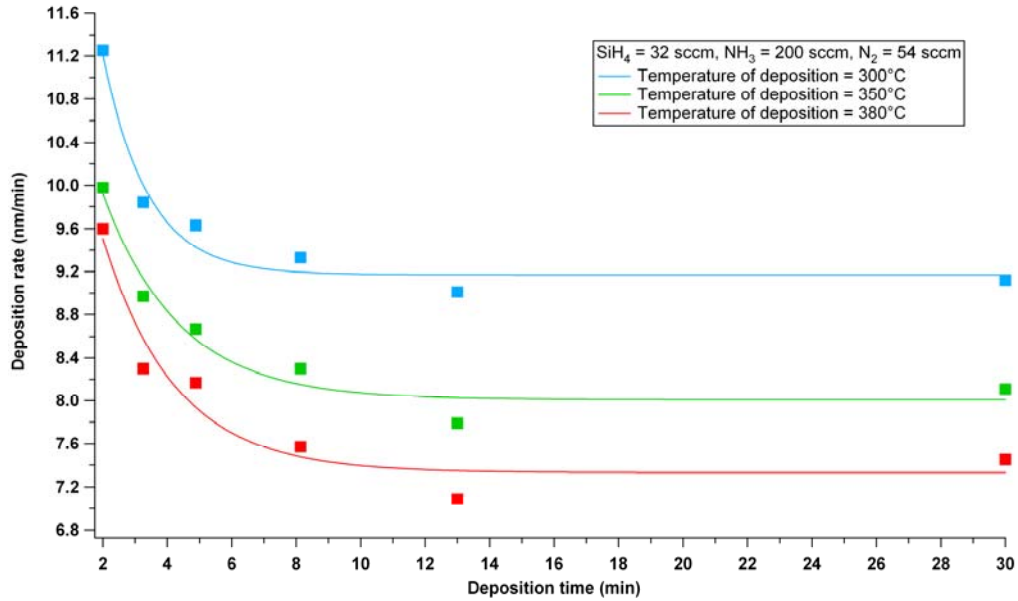
Fig. 43: deposition rate of SiNx layers for the same composition of the precursor gasses and three different temperatures (300°C, 350°C and 380°C)

One problem for the reproducibility and the conception of SiN_x layers with specific and precise properties is to understand the evolution of the layer during the deposition process, in function of the deposition parameters. Two parameters are important to understand: the thickness in function of the deposition time and the final composition of the SiN_x.

To have a good evaluation of the thickness it will be helpful to have an idea of the deposition rate as a function of the ratio R: The deposition rate is changing with the ratio R. If we plot the deposition rate (for high deposition time) in function of the ration R (Fig.44) we see that this evolution can be fitted with an exponential equation.

From this graph we can see that there is a saturation at a slope of about 12.8 nm/min. The second piece of information from this graph shows that we can have a good idea of the thickness of a sample knowing the ratio R and the time of deposition. The deposition rates vary with the temperature (Fig.43), it is necessary to do this plot for every desired deposition temperatures.
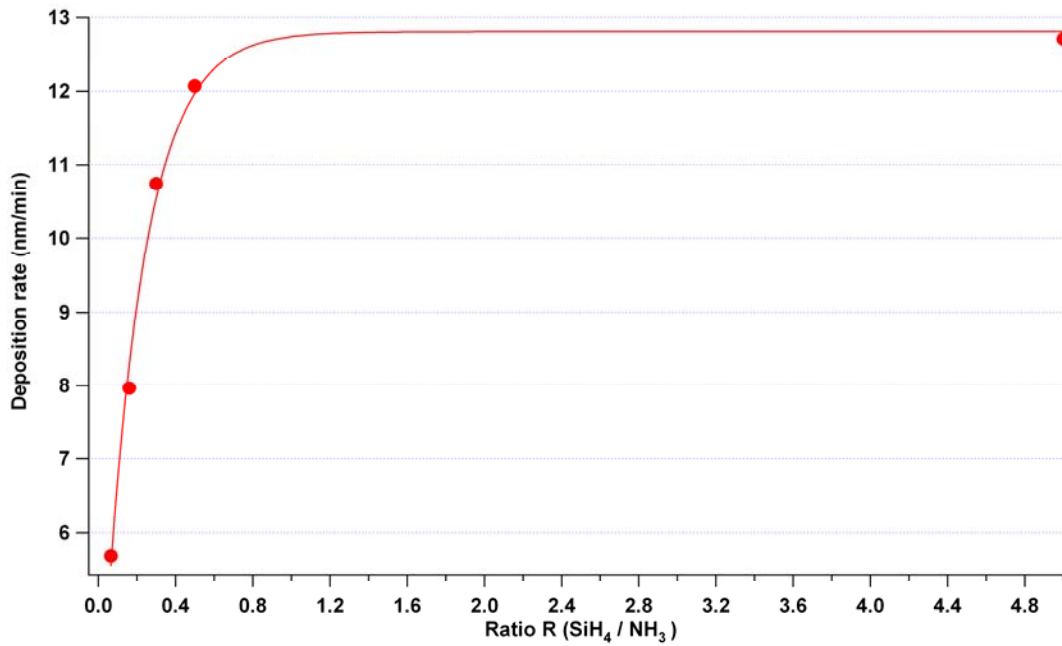
Fig. 44: Plot of the deposition rate (for 30 min of deposition and deposition at 350°C) vs. ratio R of the precursor gases in the plasma. If the temperature varies, the deposition rates will vary too.

4.2.2. Refractive index

As seen before, the modification of the ratio R leads to a modification of the deposition rate and, as shown with the ERDA and XPS measurements, of the ratio of the silicon and nitrogen inside the layer. The modification of the composition will influence the behaviour of the layer. An investigation of the optical properties was performed. Firstly, in order to see the modifications induced by the gases (i.e. the composition) different layers were deposited under the same condition (Temperature = 350°C, pressure = 325 mTorr) but the ratio R, of the precursor gases SiH_4 and NH_3 was modified. The values of R used are the following: R $([SiH_4]/[NH_3]))$: { 0.065 ; 0.16 ; 0.3 ; 0.5 ; 1 ; 1.43 ; 2 ; 5 }

The amount of N_2 was taken constant (54 sccm). The N_2 plays a role in the deposition process [IV.18], which is why it is taken as a constant. The different samples were analysed by ellipsometry in order to find out their refractive index n and their extinction coefficient k. The layers were made thick enough (<80 nm) to avoid the problem with the refractive index gradient shown before. As shown on the Fig.45, the increase of the ratio R induces an increase of the refractive indices. The refractive index is related to the density of the material, in our case the increase of the density is directly related to the increasing amount of silicon inside

71

the layer. It must be remarked that for high R (R=5) the insertion of nearly 40% of silicon clusters in amorphous silicon nitride in the model was necessary to obtain a good fit between the calculation and the ellipsometrical measurements. This can also explain the high absorption of the layer shown in the section *4.2.3 absorption*.
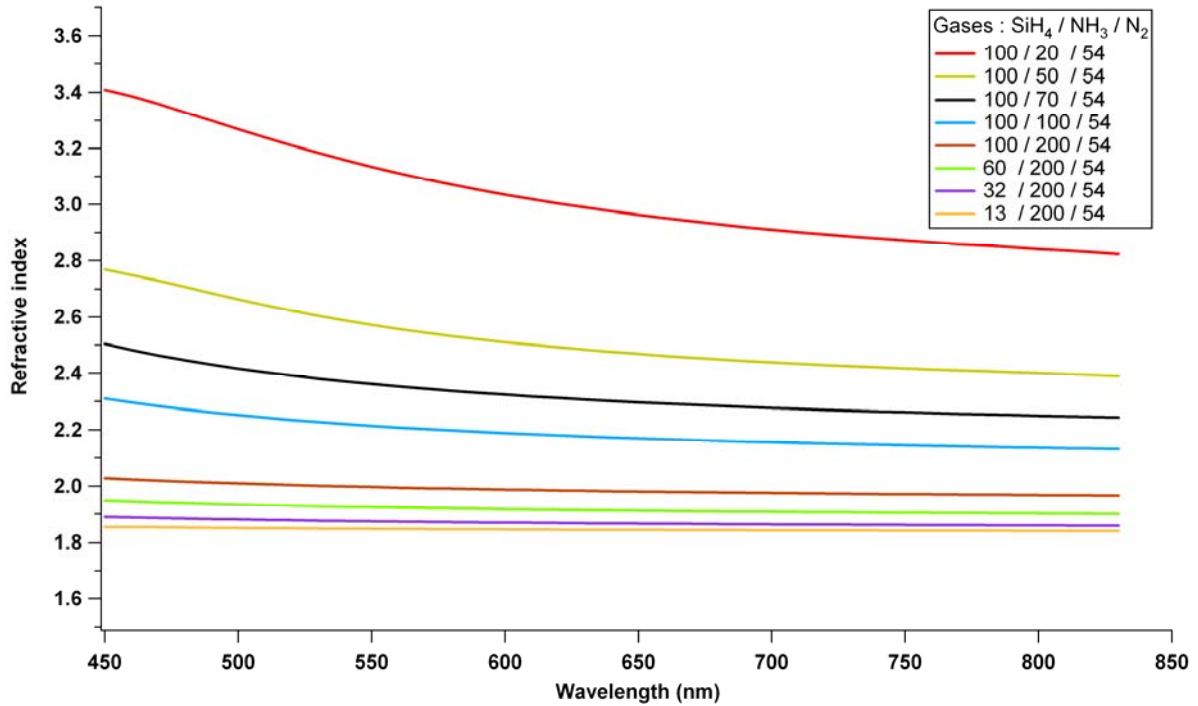
Fig. 45: Evolution of the refractive indices for different ratio of the precursor gases (R). The layers were deposited under the same conditions of temperatures (350°C) and pressure (325 mTorr). The flux in Standard Cubic CentiMetres (sccm) of each gases are given on the graph.

We can also observe the same as Dauwe [IV.19], the evolution of the refractive index of a layer follows a linear equation in function of the ration R (different for each wavelength) in Fig.46. In our case, for a wavelength at 630nm:

$$n = 1.817 + 0.31 * (SiH_4/NH_3) \tag{51}$$
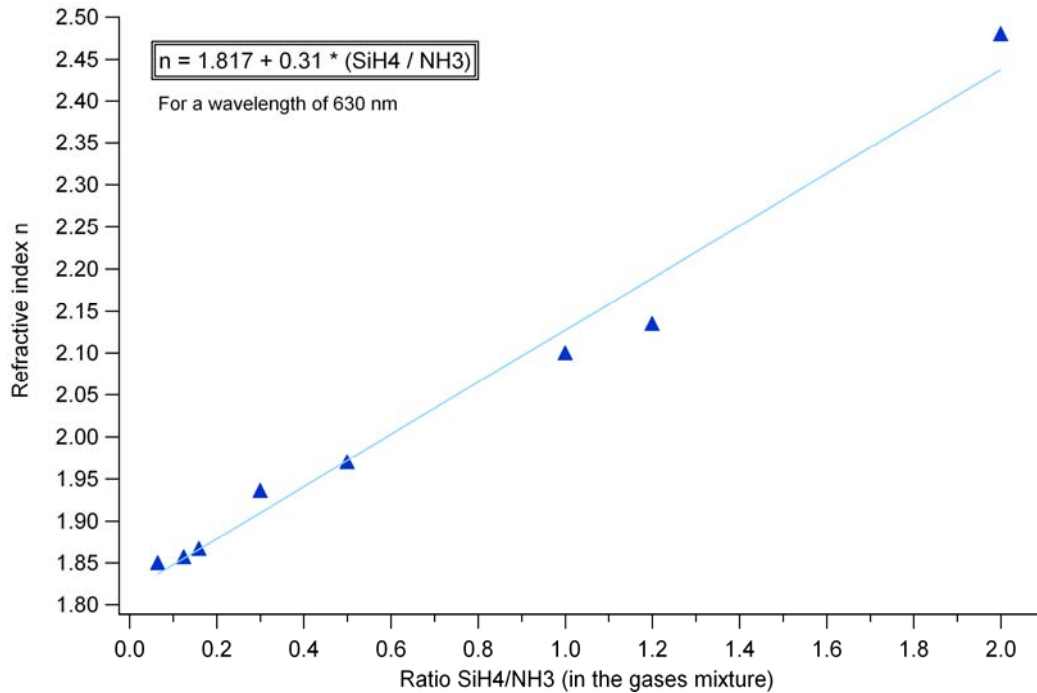
Fig. 46: Evolution of the refractive index for a wavelength of 630 nm as a function of the ratio R of the precursor gases.

The variation of the refractive index was also observed for other parameters. In a second series of experiments, the temperature was modified but the precursor gases and the pressure stayed the same. The Fig.47 shows the refractive indices for four different temperatures of deposition (t= 250°C, 300°C, 350°C, 380°C)
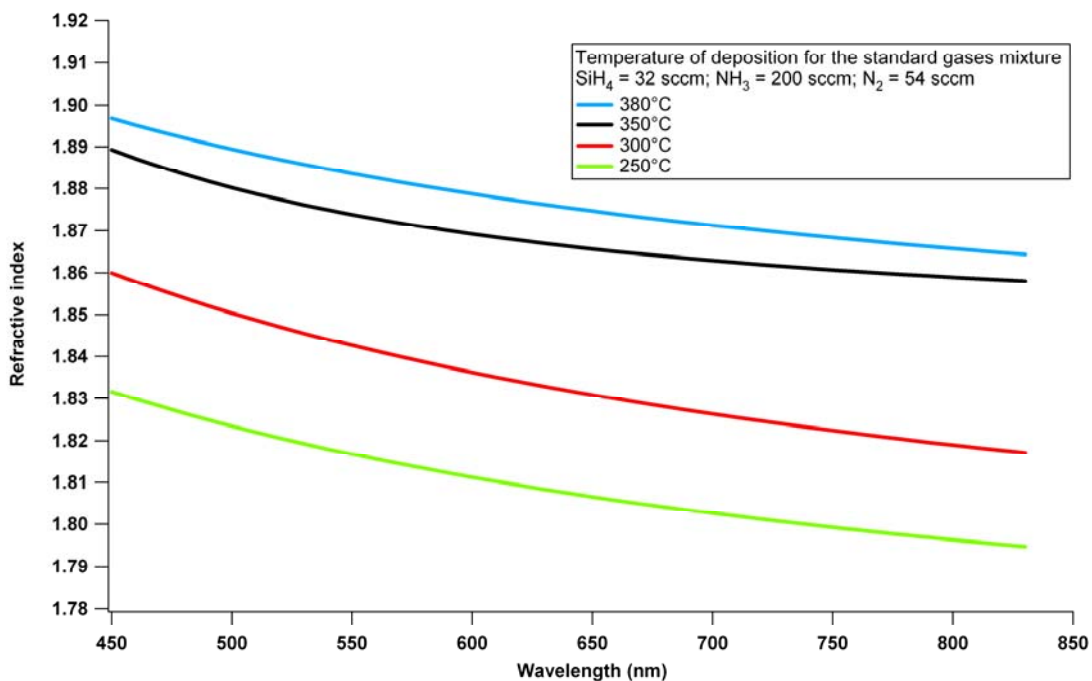
Fig. 47: Refractive indices for four different temperatures of deposition (250°C, 300°C, 350°C, 380°C). The composition of the precursor gases and the pressure remain constant.

This variation shows that the layers made under low temperature are less dense. As for the variation of the ratio R, the evolution of the refractive indices can be related to the temperature of deposition (for one wavelength) by a linear equation (Fig.48).
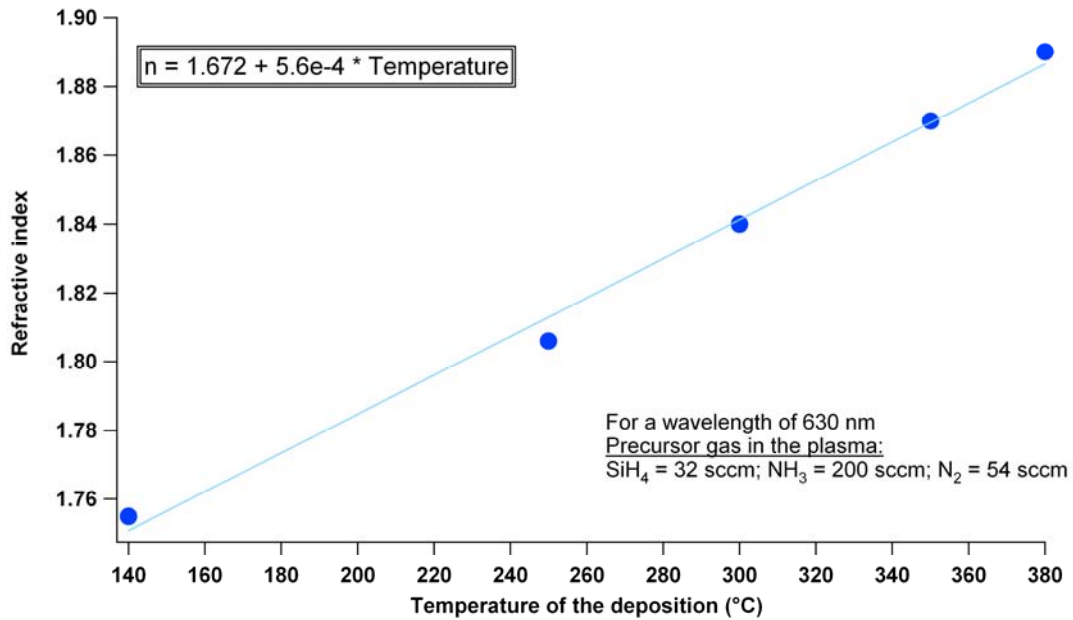
Fig. 48: Evolution of the refractive indices as a function of the temperature of deposition at a wavelength about 630 nm.

4.2.3. *Absorption*

Another property modified by the silicon content is the absorption of the light in the layer. The absorption is a very important point to know and to control. The silicon nitride will be deposited on the silicon (to reduce the reflection) which is why it must have the lowest absorption possible in order to let the maximum of light interact with the active part of the device. Silicon nitride deposited under the same conditions of temperature and pressure, but with different precursor gases, were analysed with ellipsometry. The results on the Fig.49, clearly show an increase of the extinction coefficient with the silicon content in the coating. The high absorption for the SiNx deposited with a big ratio R (red line, R=5) can be explained by the presence of silicon clusters inside the coating. The presence of the clusters was only proved by the ellipsometrical measurements here but it was already observed here [IV.16]. The absorption α is directly related with the extinction coefficient k by the formula:

74

$$\alpha = \frac{4\pi k}{\lambda} \quad cm^{-1} \tag{52}$$
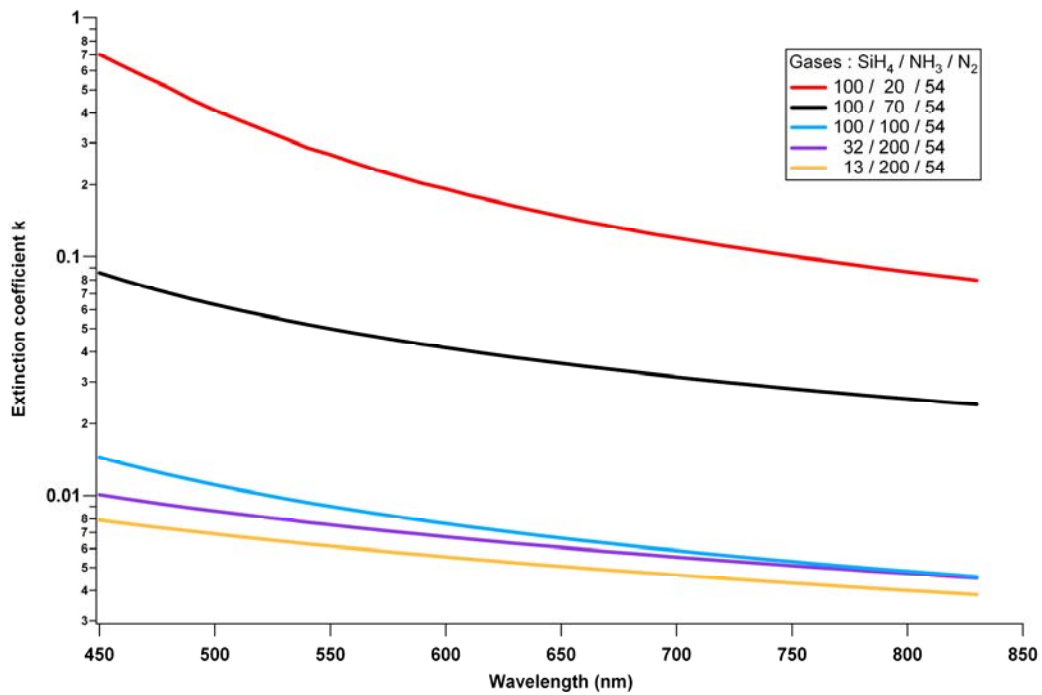
Fig. 49: Extinction coefficient k of different SiN$_x$. The ratio R of the precursor gases is the only variable parameter. The measures were done for R = {0.065, 0.16, 1, 1.43, 5}.

In order to investigate the light passing through the layer, transmission measurements were performed. The studied layers were all 100nm thick. For low values of R, the absorption is very low and well suited for our needs.
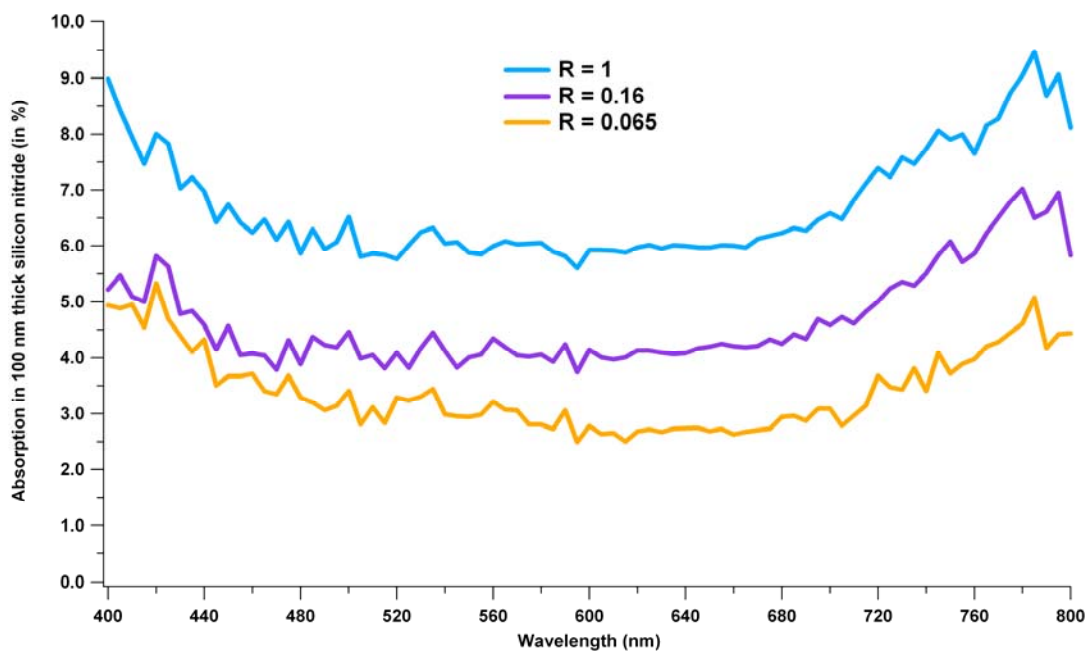
Fig. 50: Absorption of different layer of SiNx with different ratio R of precursor gases. All layers were 100 nm thick.

Using the optical parameters obtained before, the deposition of an anti-reflective layer was performed. A layer was deposited under the standards condition with a ratio R=0.5. in order to obtain a refractive index near 2 (n_{560}=1.99). The optimal thickness to have no reflection for the wavelength of 560 nm is 70 nm. The Fig.51 shows the measured reflection. The reflection at 560 nm was found to be 0.03%
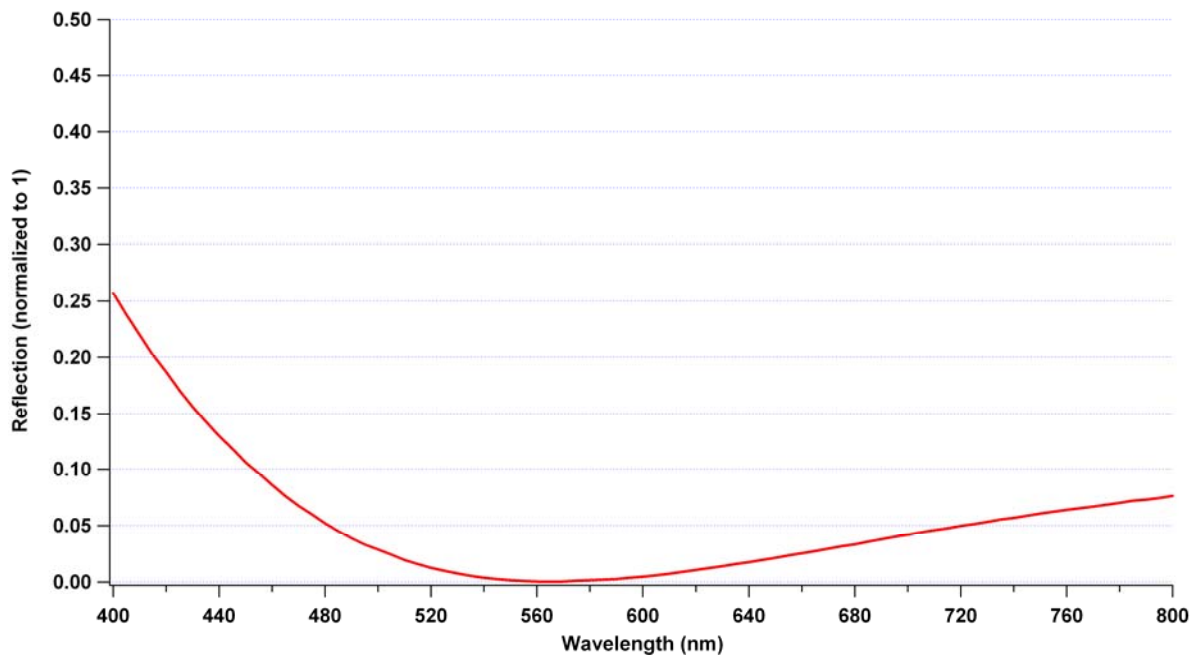
Fig. 51: Reflection of a crystalline silicon substrate covered with SiN$_x$. The silicon nitride is in this case 70 nm thick and was deposited at 350°C (R=0.5).

The anti-reflection for one wavelength is good, but the overall reflection has to be enhanced. In order to find the best SiN$_x$ composition, the electrical passivation effect must also be taken into account.

In the following, the intensity of the laser used is (for a radiation of 1064 nm and OD 0.0) 0.38 mJ.cm^{-2}. The Excitation density is $2.0*10^{15}$ cm².

The SiN$_x$ coating on silicon substrate has a double function when it is integrated into the inverted silicon solar cell. The anti-reflection, as seen before, and the passivation. The passivation can have two aspects: the bulk and the surface passivation. By using multi-crystalline silicon, a part of hydrogen contents of the SiN$_x$ will diffuse in the bulk and thus lead to a reduction of the bulk defects (dangling bonds) [IV.20, 21]. In this work we are only working with mono-crystalline silicon, the hydrogen diffusion will be irrelevant. The silicon substrates used are pure enough (i.e. without many defects) and the hydrogen diffusion will not enhance its quality, the diffusion of hydrogen could also decrease the quality of the substrate (generation of stress in the lattice, …). In this work the SiN$_x$ coating will be used as an electrical passivation of the surface. The Fig.52, shows the TRMC signal induced by a 532nm laser pulse on one sample covered on one side (brown curves) and a sample covered on both sides (blue curve). The pulse only induces charge-carriers at the surface (because of the strong absorption). When the side without SiN$_x$ is illuminated, the surface recombination is so high that the charge-carriers will recombine very quickly. If the illumination is done on the covered side, the recombination disappears at the beginning because of a low surface recombination due to passivation by the SiN$_x$ coating. However as soon as the charge-carriers attain the opposite non-covered side (where they will recombine), the recombination process will rapidly increase. On the blue curve, as for the brown curve (illumination of the covered side) there is no recombination at the beginning. The difference appears when the charge-carriers attain the opposite side. In this case, due to the passivation of the opposite side induced by the SiN$_x$ coating on this side there is no relevant decay of the signal. This shows the electrical passivation effect of the silicon nitride.
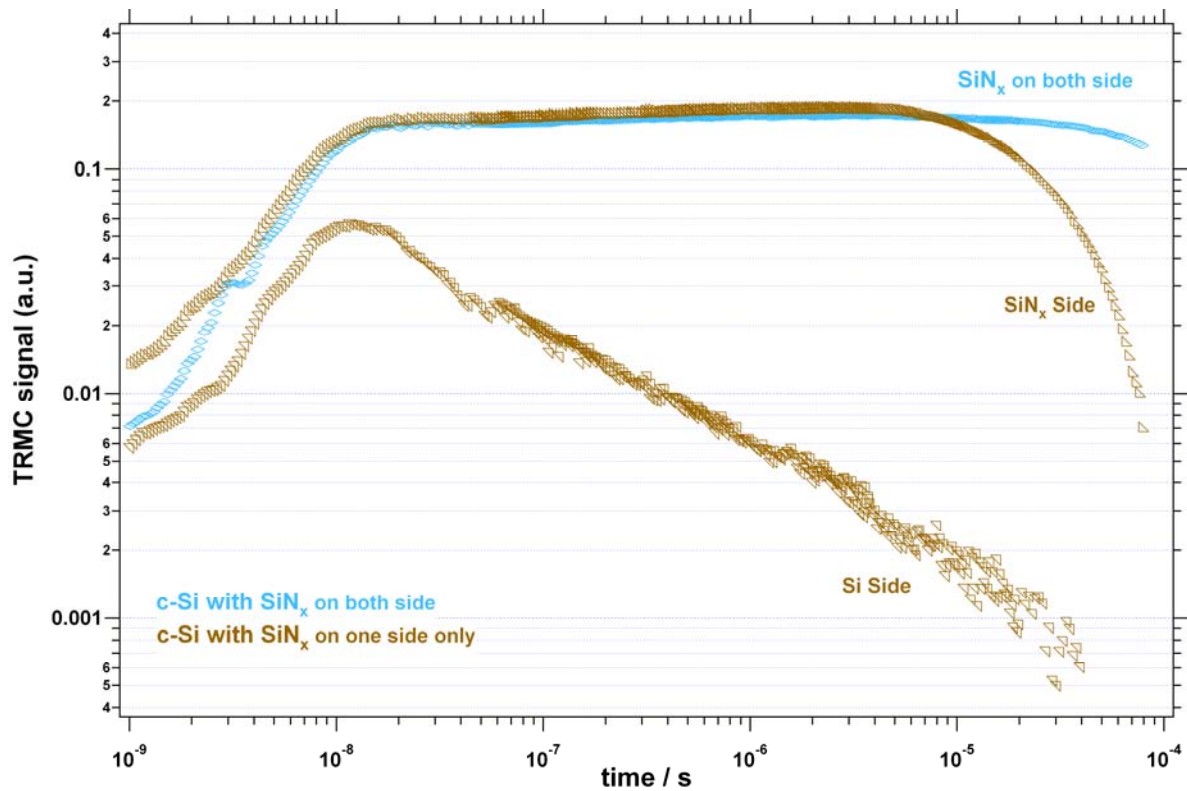
Fig. 52: TRMC signal showing the decay of the excess charge carriers in two silicon substrate. One of the samples was covered with SiNx on one side, the other on both sides. The silicon used as substrate is the same in both case, n-type (1Ω.cm). The excess charge carriers were generated by a 10 ns laser pulse with a wavelength of 532 nm in order to generate charge carriers only at the surface (1 μm).
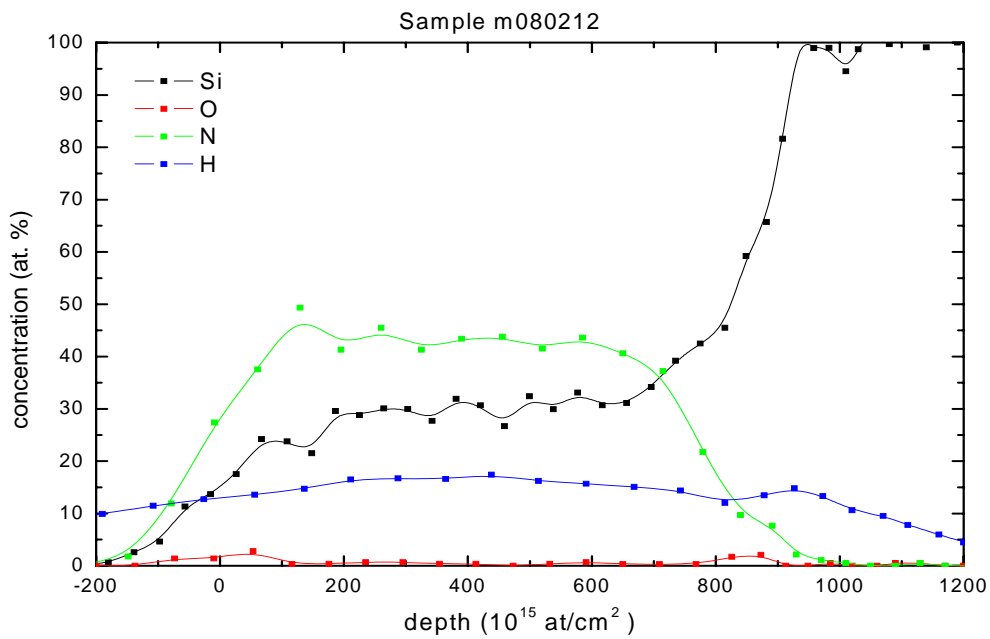

Fig. 53: ERDA measurement of a SiN$_x$ layer. The evolution of the concentrations of the principal elements present inside the layer (Si, N, H, and O) is show. The substrate is on the right side (100% of Silicon. 100 at/cm² ≈ 10 nm

78

The big disadvantage of this coating is the damages induced at the surface during the deposition. As shown on the ERDA measurement Fig.53 showing a spectrum of a silicon nitride layer on a silicon substrate, the interface between the SiN_x coating and the silicon surface is not abrupt. Indeed, during the deposition by PECVD the surface of the substrate is damaged by the impacts of the ions. This will lead to an increase of the defects at the surface.

The passivation effect of the silicon nitride is due also to its fixed positive charge. Calculations made by Hui YAN et al. [IV.22] Show that nitrogen dangling bonds produce a density of states near the top of the valence band and the Silicon dangling bond produce a density of states near the midgap.

The K center has been identified as an unpaired spin mainly located on silicon atoms bonded with three nitrogen atoms [IV.23]. K centers can be found in three charge states, K0 (paramagnetic), K+ and K- (diamagnetic). Two other paramagnetic centres located on nitrogen atoms were found [IV.24]. One is located on a Nitrogen atom bonded with two silicon atoms, the second is attributed to an unpaired electron localized on two inequivalent nitrogen atoms bonded to each other. To compare with the silicon oxide, where the fixed charges are due to O_3-Si configuration, but the number of fixed charges is higher inside the SiN_x [IV.25, 26]. The experiments have shown the fixed charges are present only in the first 20 nm. [IV.27]

In this work the substrate used to determine the electrical passivation of the silicon nitride was always the same. The substrate was n-type crystalline silicon Mitsubishi 1.6-2.4 Ω.cm. 0.240-0.260 mm thick. Before all measurements, the minority carrier diffusion constant and the resistivity of the wafer were measured. TRMC signals induced by 532 nm have shown that both surfaces can be considered as infinite sinks. Thus the excess charge-carriers density at the surface is effectively zero. With these results, the diffusion constant can be determined. Preliminary investigations were performed with silicon nitride on both side of the substrate in order to know the lifetime in the bulk. The lifetime was found higher than 500 µs, thus $\frac{1}{\tau_v} \to 0$. The Fig.54 shows the TRMC measurements induced by 1064 nm of the bare n-type silicon substrate we used. The lifetimes for the different intensities are:

$$\tau_{eff}^{OD=1.6} = 5.77 \mu s$$

$$\tau_{eff}^{OD=2.0} = 5.58 \mu s$$

$$\tau_{eff}^{OD=2.3} = 5.57\,\mu s$$

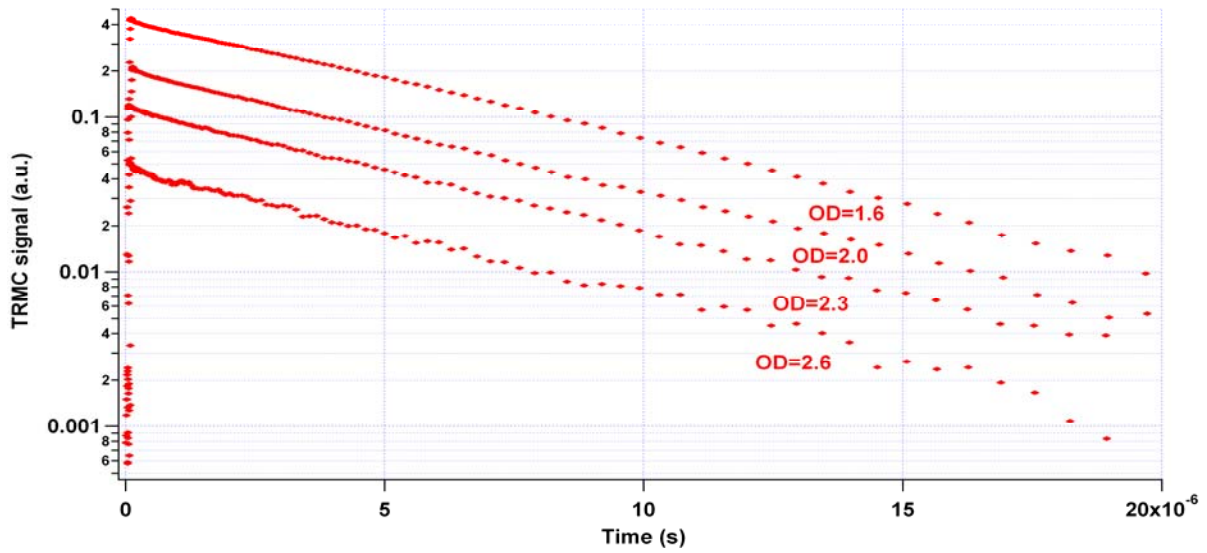$$\tau_{eff}^{OD=2.6} = 5.42\,\mu s$$

Fig. 54: TRMC signals induced by a 1064 nm laser pulse on bare n-type 1.6-2.4 Ω.cm. 0.240-0.260 mm thick, for four intensities.

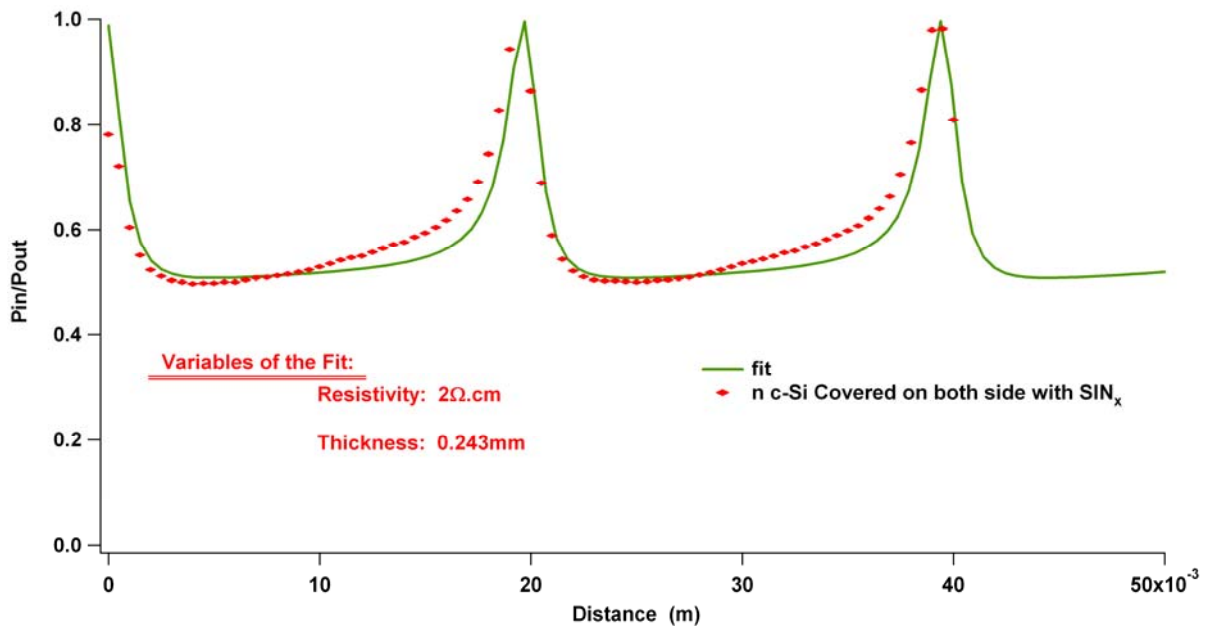**Fig. 55: Fit (green line) of the resistivity measurement (red curve). The resistivity is founded to be 2Ω.cm**

So Eq.34 can be used. The average of the lifetime is 5.58 µs. The diffusion is:

$$\frac{1}{\tau_{eff}} = \frac{D\pi^2}{d^2} \quad \Rightarrow \quad D = \frac{d^2}{\pi^2 \tau_{eff}}$$

With the thickness of the substrate was measured 0.243 mm then:

D=10.7 cm².s

Next the resistivity was measured. The resistivity is also measured in the same equipment as the TRMC measurements. Detailed information about this measurement method can be found in the reference [IV.28]. The result obtained by the fit of the resistivity measurements is a resistivity of 2 Ω.cm. (Fig.55) and is in good accordance with the data given by the manufacturer.

The surface passivation by field effect (see *2.4. Passivation*) is directly related with the bonds inside the SiN$_x$ layer [IV.23]. The modification of the amount of each compound will modify the number of bonds and then lead to a variation of the passivation. The lifetimes of 3 samples made under the same conditions of temperature and pressure but with different ratio R were measured by TRMC (Fig.56). The SiN$_x$ layers on the three samples have the same thickness (≈74nm). The first measurements were made with a 1064nm laser pulse, in order to generate homogeneously charge-carriers in the bulk. A difference in the decay time can be observed between the three samples. Using Eq.16 a maximum value for the surface recombination velocity can be obtained.

$$\frac{1}{\tau_{eff}} = \frac{1}{\tau_v} + \frac{1}{\tau_s} \quad \text{(Eq.16)}$$

S^{max} is obtained when the lifetime is determined only by the surface lifetime ($\tau_v \gg \tau_s$)

$$\text{then } \frac{1}{\tau_{eff}} = 0 + \frac{1}{\tau_s} = \frac{2S^{max}}{d} \tag{53}$$

The electrical passivation properties if SiN$_x$ films on the same substrate can be compared by comparison of the values of S^{max}

$$\tau_{eff}^{R=0.16} = 495\mu s \quad \Rightarrow \quad S_{R=0.16}^{max} = 24 \, \text{cm.s}^{-1}$$

$$\tau_{eff}^{R=0.5} = 418\mu s \quad \Rightarrow \quad S_{R=0.5}^{max} = 29 \, \text{cm.s}^{-1}$$

$$\tau_{eff}^{R=5} = 314\mu s \quad \Rightarrow \quad S_{R=5}^{max} = 38 \, \text{cm.s}^{-1}$$

The amount of silicon inside the layer has a influence on the electrical passivation, but these differences are not so important.
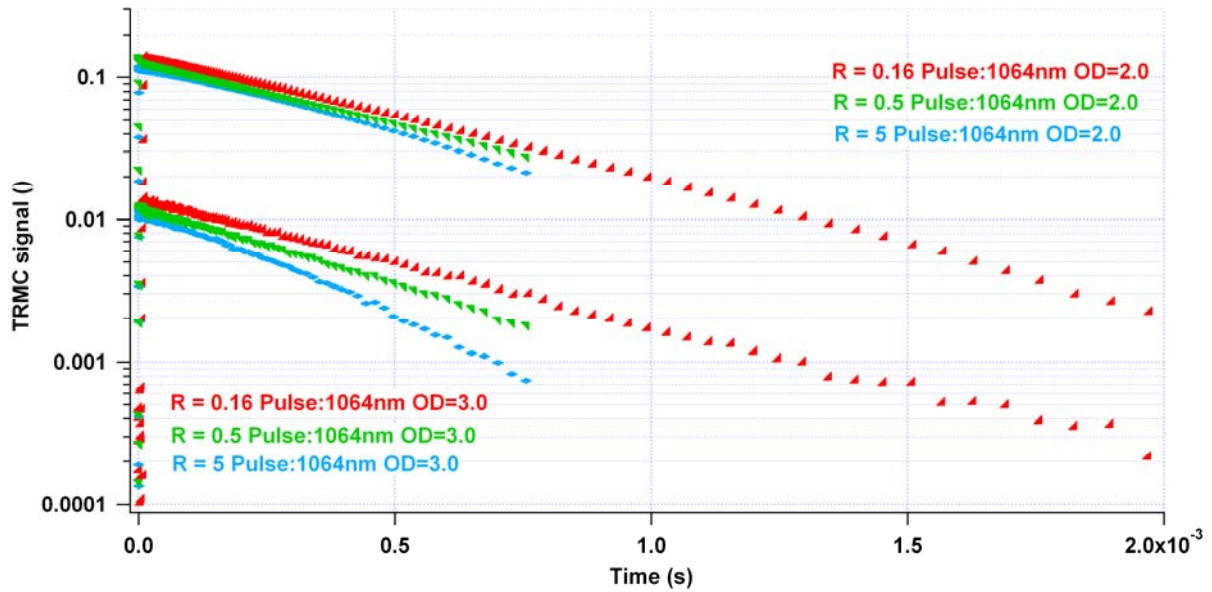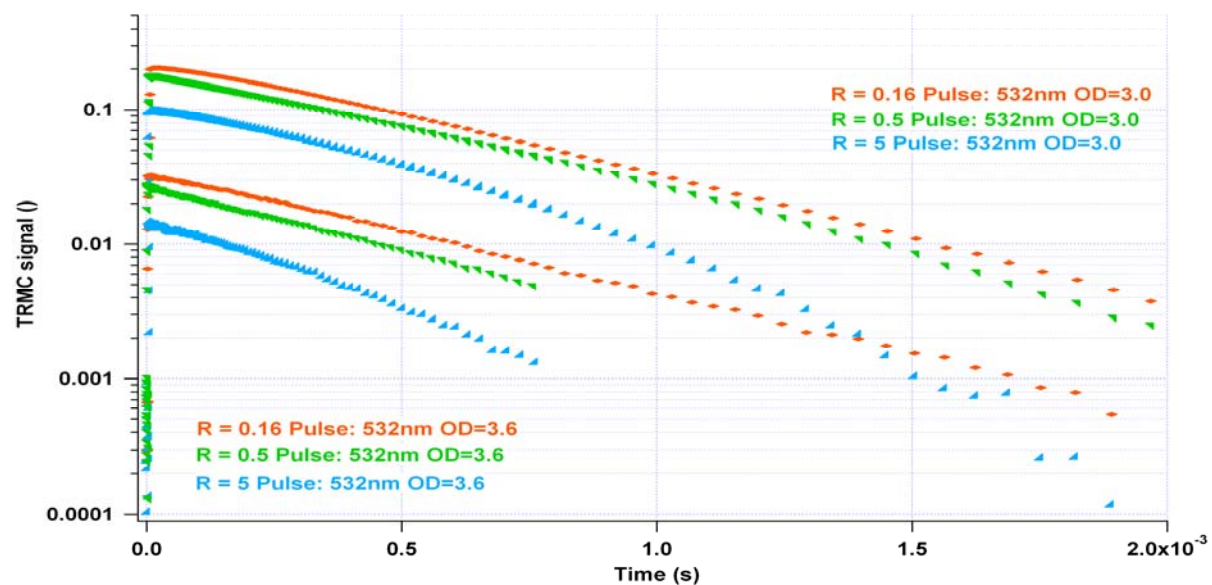

Fig. 56: TRMC measurements of three samples with three different ratios R {0.16, 0.5, 5}. The generation of the charge carriers was made by a 10ns laser pulse with a wavelength of 1064 nm.

The same measurements but with a surface excitation realized by a laser pulse with a wavelength of 532 nm were performed (Fig.57). The same difference appeared in the lifetime but in this case, the effect of the coating itself can also be observed. The samples with R=0.16 and R=0.5 have approximately the same amplitude, but the third sample with R=5 has a much lower amplitude.

Fig. 57: TRMC measurements of three samples with three different ratios R {0.16, 0.5, 5}. The generation of the charge carriers was made principally near the surface by a 10ns laser pulse with a wavelength of 532 nm.

This difference can easily be explained by two factors. The first one is that the layer has a high refractive index (3.15 at 530 nm), which reduces the anti-reflection effect. More light, especially for the laser excitation at 532nm, is reflected and will not generate charge-carriers. This can be seen on the Fig.58 showing the reflection of a bare silicon substrate and silicon cover with SiN_x deposit with R=5 and SiN_x deposit with R=0.5.
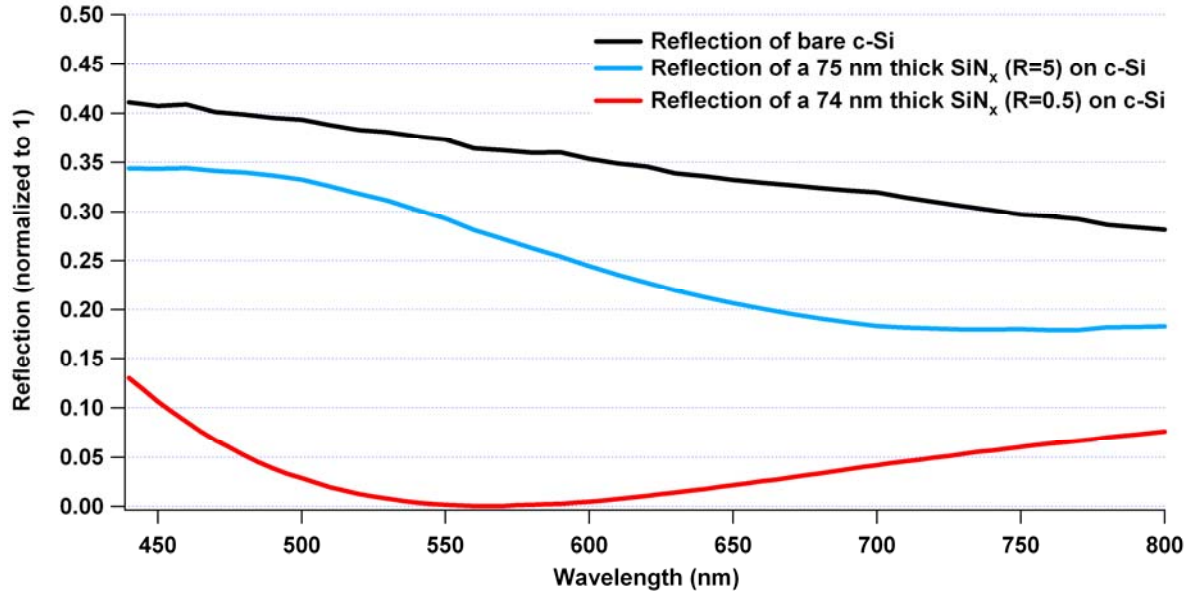
Fig. 58: Reflection of a bare silicon substrate (black curve) and silicon cover with SiN_x deposit with R=5 (blue curve) and SiN_x deposit with R=0.5 (red curve).

Another reason for this low amplitude is the absorption in the SiN_x film. For coating deposit with a low R, the absorption is not so high, but for R=5 the absorption coefficient at a wavelength of 530nm is about $6.7*10^4$. This is high enough to reduce the generation of charge-carriers in the silicon substrate.

The silicon content in the SiN_x coating does not seems to be the principle factor for the passivation, even if it plays a role. This implies that the Si content can be optimized in view of the anti-reflection and absorption properties of the films only. To gain an overview of the kind of coating we are able to deposit, the influence of the temperature was also measured. The Fig.59, show the TRMC measure of two samples covered with the same SiN_x (same ratio R) but deposited at two different temperature (300°C and 350°C). The lifetime is 190 μs for the sample deposited at 300°C and 710 μs for the one deposited at 350°C. The surface recombination velocities are thus:

$$S_{300}^{max} = 60 \, cm.s^{-1}$$

$$S_{350}^{max} = 16 \, cm.s^{-1}$$

So the temperature of deposition plays an important role in the electrical passivation effect of the layer.
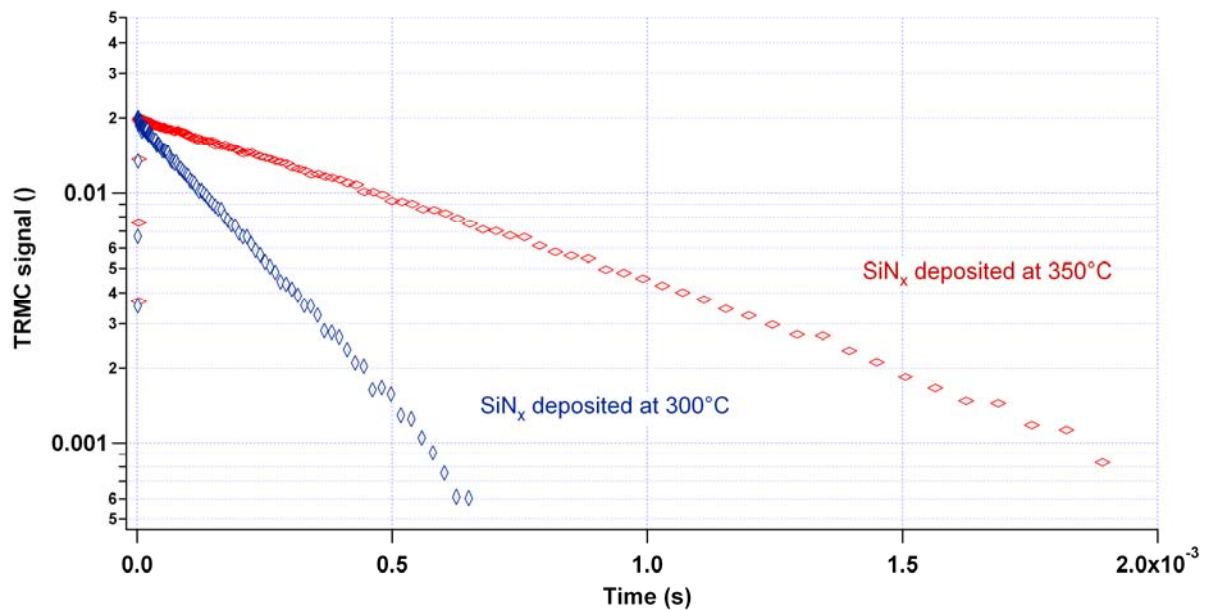

Fig. 59: TRMC signal of two samples deposited at two different temperatures (300°C and 350°C). The pressure and the precursor gases was the same during the two depositions.

Another parameter seems to have an influence on the passivation effect, the nitrogen (N_2) used as precursors gas. The TRMC measurement of a layer of SiN_x deposited without N_2 in the precursors gases is compared on Fig.60 with the other layer deposited with different ratio R and with N_2 in the precursor gases.
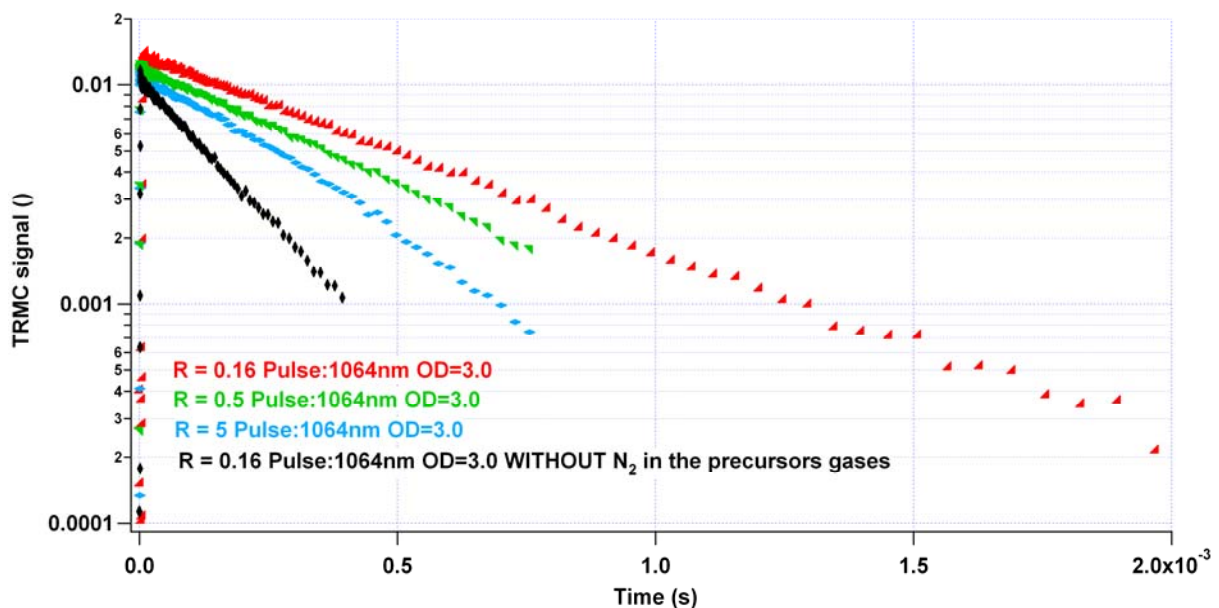
Fig. 60: Comparison of TRMC measurements of SiNx layers deposited without N_2 in the precursor gases (black line) and three samples deposited with three different ratios R {0.16, 0.5, 5} and N_2 in the precursor gases . The generation of the charge carriers was made principally near the surface by a 10ns laser pulse with a wavelength of 532 nm.

84

The surface recombination velocities show a significant difference between the deposition with N_2 and the one without N_2 in the precursor gases.

$$S_{SiN_x\_without\_N_2}^{max} = 62\,\text{cm.s}^{-1}$$

$$S_{SiN_x\_R=0.16}^{max} = 24\ \text{cm.s}^{-1}$$

However, even if the TRMC shows a difference, we have to be careful when dealing with the value of the surface recombination velocity of the sample deposited without N_2. In fact, as it will be explained in the following sub-chapter, a problem with the reproducibility occurred in this work. The only thing clear is that the passivation effect induced by the layer deposited without N_2 is worse than the one deposited with N_2. Quantitative results are not available yet. However, this effect can be explained. The N_2 provides more nitrogen in the plasma and its suppression will lead to an increase of the silicon content (which reduces the passivation effect, as seen with the other three curves).

4.2.6 *Problem of the reproducibility of the layer*

During examination of the passivation, a difference of the passivation for samples prepared under the same conditions was observed. Samples not prepared at the same time but with the same precursor gases, under the same pressure and at the same temperature show clearly a surface passivation sometimes 4 or 5 times different from each other. The first idea was a non-homogeneity in the bulk of the silicon wafers used as substrate. The difference appeared with samples coming from the same wafer but also with those cut from different wafers (of the same batch), the substrate cannot be the reason for these differences.

For a first attempt to check the reproducibility three samples were prepared under the same conditions:

Precursor gases: SiH_4 = 32 sccm; NH_3 = 200 sccm; N_2 = 54 sccm

Time of deposition = 11 min 23 sec.

Temperature = 350°C

Pressure = 325 mTorr

The samples were made separately (three different depositions). The results of the measurement of the passivation obtained by TRMC are the following:

Sample n080209, $\tau_{eff} = 507$ µs

Sample n080207, $\tau_{eff} = 290$ µs

Sample n080211, $\tau_{eff} = 181$ µs

ERDA, ellipsometry and infrared spectroscopy were performed on the samples in order to determine the reasons for this difference. The interference colours of the samples are the same and there is not, at first sight, a big difference in the thickness or refractive index.

The measurements made with ERDA (Fig.61) do not give a clear answer, the three spectra are more or less the same and can not explain the difference. Even the oxygen peak at the surface of the sample n080207 can not be an explanation because this peak does not appear on the sample n080211. Also the penetration of the different elements due to the deposition process can not explain the differences. On the other hand, ERDA measurements show a reproducibility in the composition of the layer, the problem is not due to the composition (i.e. the quantity of each element, Si, N, H) of the layer.
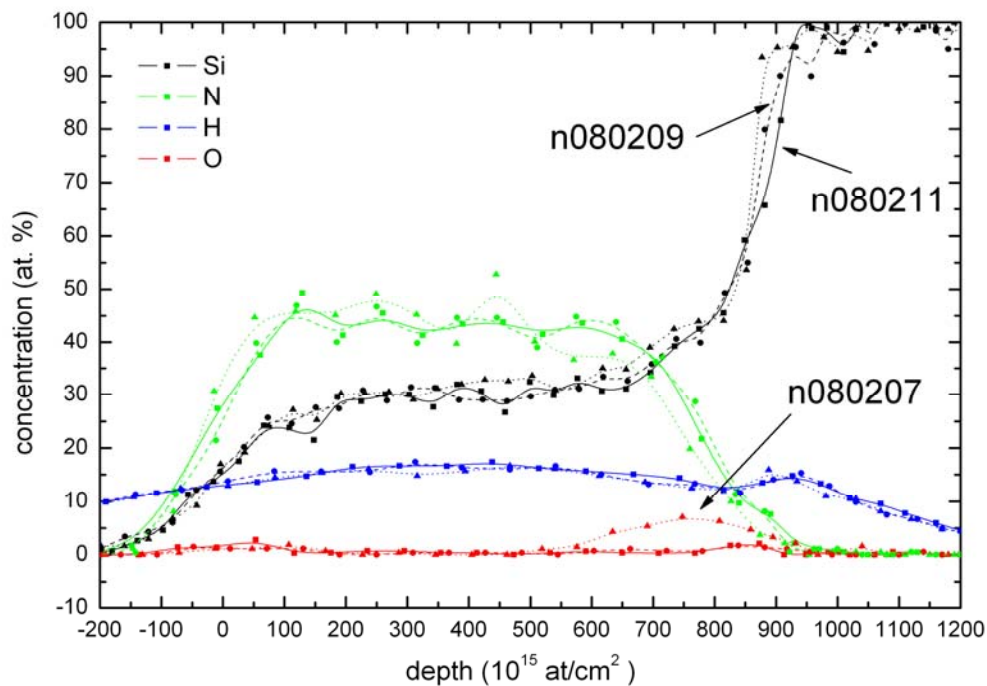
Fig. 61: ERDA spectrum of the three sample n080207 (dots) n080209 (dash) and n080211 (line). The composition of the layer is the same, i.e. the same amound of elements (Si, N, H).

Following on from this, a measurement by ellipsometry (Fig.62) was performed in order to determine the refractive index of the three different samples. The refractive index, related to the density for example, could provide useful information. But also in this case the measurement did not give any answers. The sample n080209 and n080211 with the biggest difference in the passivation have exactly the same refractive index. The difference is not due to the density of the layers or to their permittivity. The three thicknesses were also measured and the results are:

n080209: 88.5 nm

n080207: 88.3 nm

n080211: 88.6 nm

As expected by the colour, the three samples have exactly the same thickness. If we suppose that the fixed charges are only located in the first 20 nm [IV.27] this means that we have the same number of charges in all the three samples (if the composition is assumed to be the same).
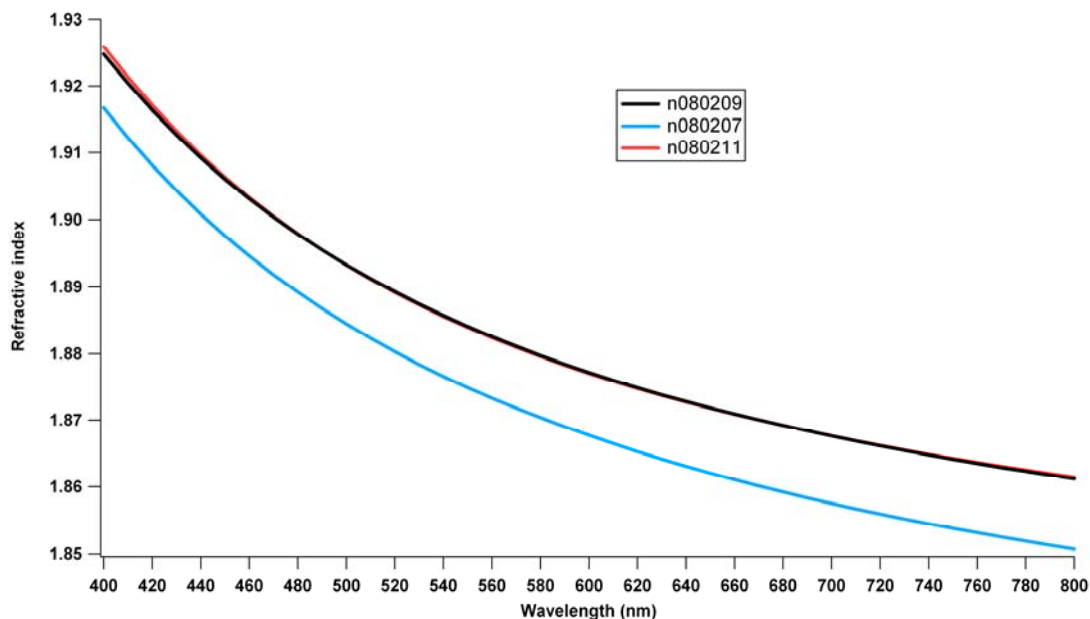
Fig. 62: Refractive index of the three samples for wavelength between 400 and 800 nm

The third measurement performed on the samples was the Fourier transform infrared spectroscopy (Fig.63). Here the results can give us an indication of the reason for this difference. The main peak, giving mostly the Si-N bond, is decreasing with the passivation. Secondary peaks related to the $Si-H_x$ and $N-H_x$ bonds are the same for the three samples. The decrease of the main peak is due to the decrease of the Si-N bond in the layer. Indeed, the Si-

H_2 vibration at 2090 cm^{-1} stays the same, the contribution of this vibration in the main peak does not change. The Si_2N-H and N-H vibrations at 1170 and 1220 cm^{-1} do not change either. This measurement tends to shows that the decrease of the main peak is mainly due to the decrease of the Si-N bond density inside the layer. However, it has been found [IV.29] that the passivation is related to the Si-H bond. The more Si-H bonds we have the better the passivation. The Si-H bonds are related with the Si-N bonds, the more Si-N bonds we have the less Si-H bonds we have. This suggests that a good passivation is obtained from a small amount of Si-N bonds, which is not the case here. In this situation it is impossible to link the passivation with the FTIR measurements. This will be confirmed later in this section.
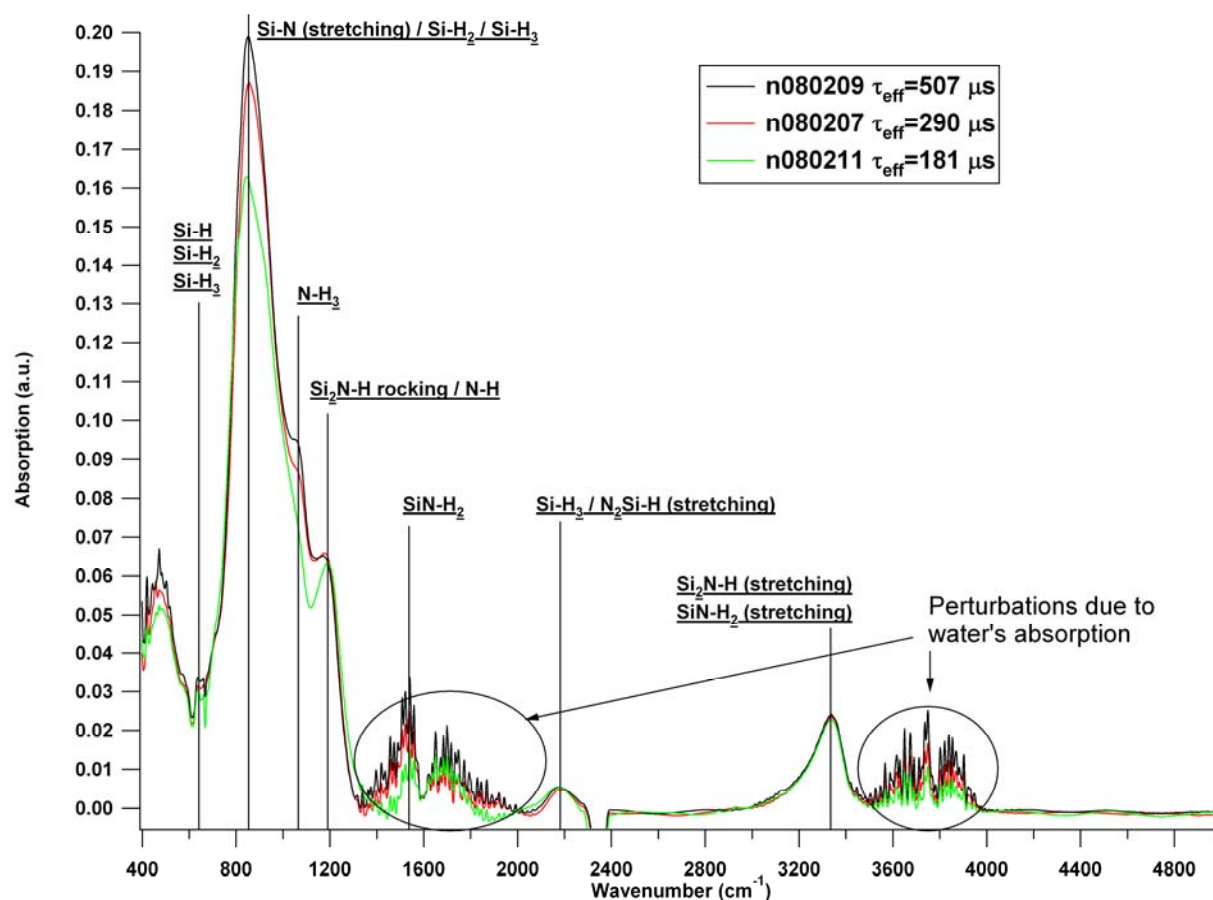
Fig. 63: Infra-red Fourier Transform spectra of 3 samples with different passivation induced by layers deposited under the same conditions.

The TRMC measurements are different. The origin of this difference in the passivation effect can be caused by a variation of the fixed charge in the SiN_x layer or by a variation in the density of surface states leading to recombination processes. The measurements performed here can not clearly identify the reason.

This difference between samples deposited under the same condition is problematic. If the reason for the difference is the variation of the bonds inside the coating, the problem will be difficult to solve, but if the surface states are the cause then a possible solution can be worked out.

This is why, in order to suppress or at least reduce the difference, a thin layer of silicon oxide was first grown on the substrate. The oxide layers were chemically grown by the NAOS method (Nitric Acid Oxidation of Silicon). The chemical oxides are not the best oxides (in terms of homogeneity or defects) we can use (compared with thermal oxides), but they have the advantages of being simple to handle and fast to produce. The thickness of the oxide is around 2-3 nm. Three series of samples were prepared.

Three samples with an oxide layer were separately covered with SiN_x. At the same time three sample (the same substrate) without this oxide layer were also covered.

The conditions of the depositions were exactly the same for each pair of samples.

- Precursor gases: $SiH_4 = 32$ sccm; $NH_3 = 200$ sccm; $N_2 = 54$ sccm

- Time of deposition = 9 min 43 sec.

- Temperature = 350°C

- Pressure = 325 mTorr
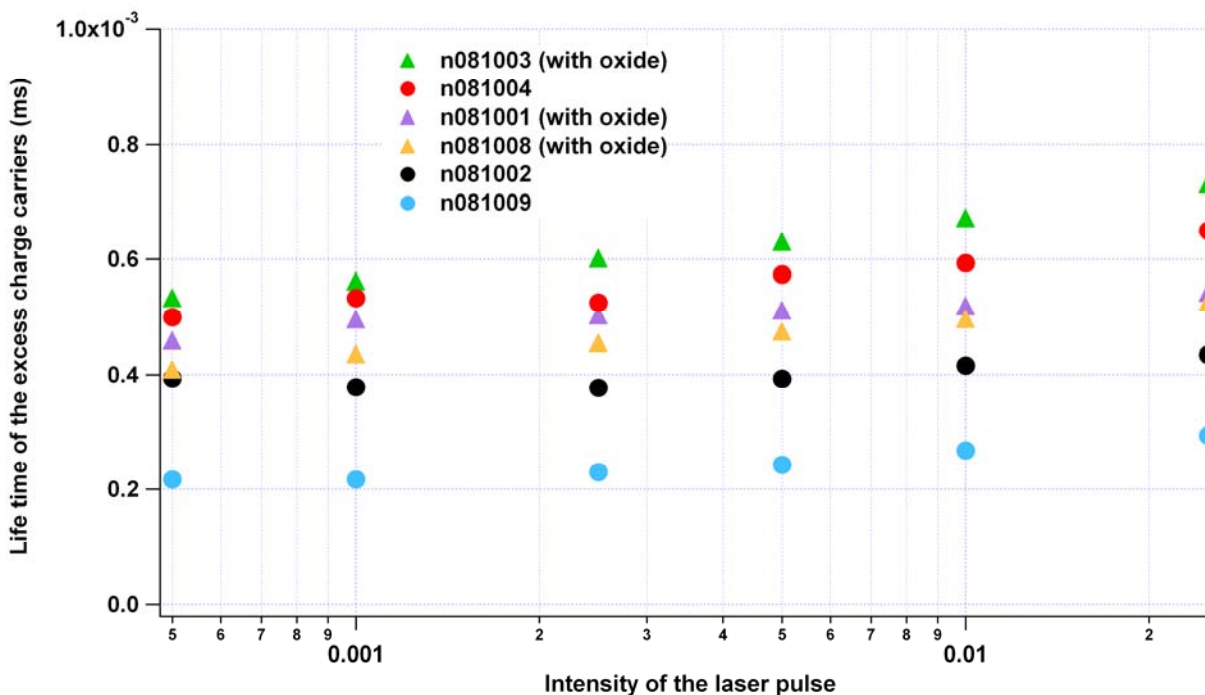
Fig. 64: Representation of the lifetime of the samples in function of the intensity of the laser pulse

Ellipsometry, TRMC and FTIR were performed on those samples too.

Samples named n081001, n081003, n081008 were oxidized before the SiN_x deposition and samples n081002, n081004, n081009 were covered with SiN_x just after the HF etching.

The results of the TRMC measurements always show a difference in the lifetime (Fig.64).

Sample name	With an oxide layer	Thickness of the SiN_x (nm)	Refractive index	Lifetime (μs)
N081001	✓	72	1.87	510
N081002		73	1.86	390
N081003	✓	72	1.87	630
N081004		72	1.86	570
N081008	✓	75	1.87	480
N081009		76	1.86	240

Tab. 3: Overview of the lifetime and the refractive index of the samples with and without the thin oxide layer between the silicon substrate and the SiN_x coating.
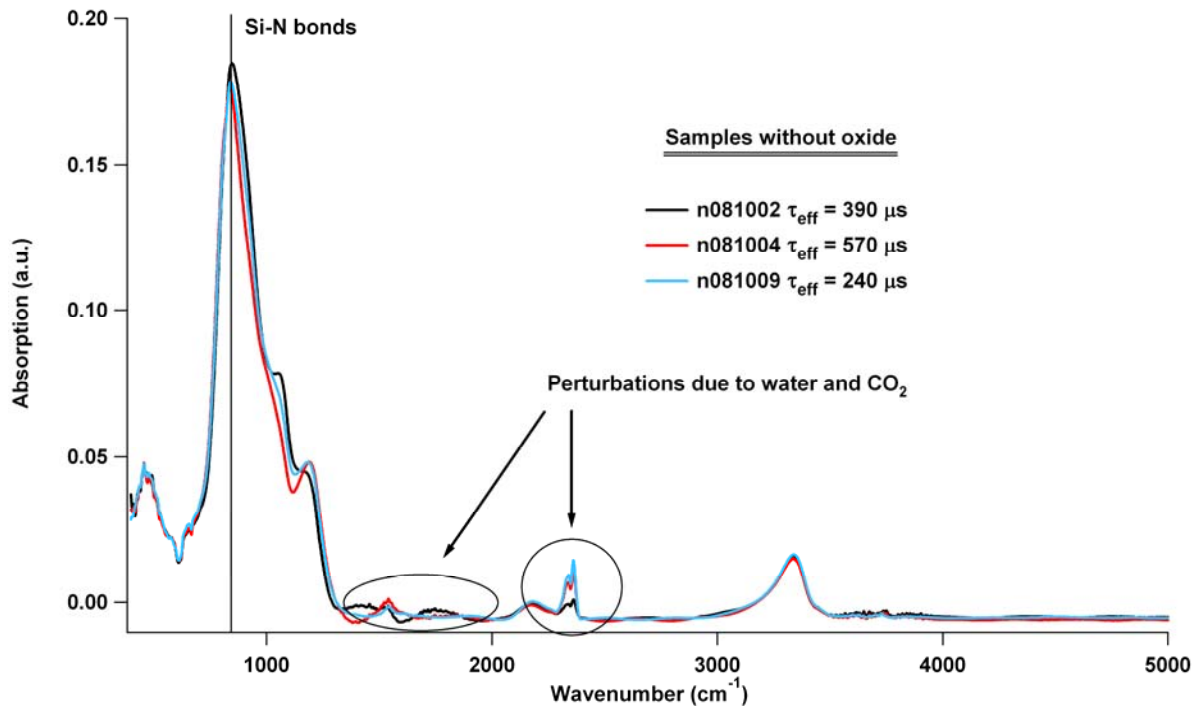
Fig. 65: FTIR spectra of the three samples without the oxide layer between substrate and SiN_x coating.

An initial look at the TRMC results shows that the difference does not disappear with the introduction of the thin oxide layer. However, the difference in the measured lifetime between each oxidized samples appears to be lower than the difference between the non-oxidized one.

The refractive indexes are the same for each sample like the thickness. A variation of the composition is subsequently not possible, and as shown on the Fig.65 and Fig.66 the variation in the bonds is not an explanation either.
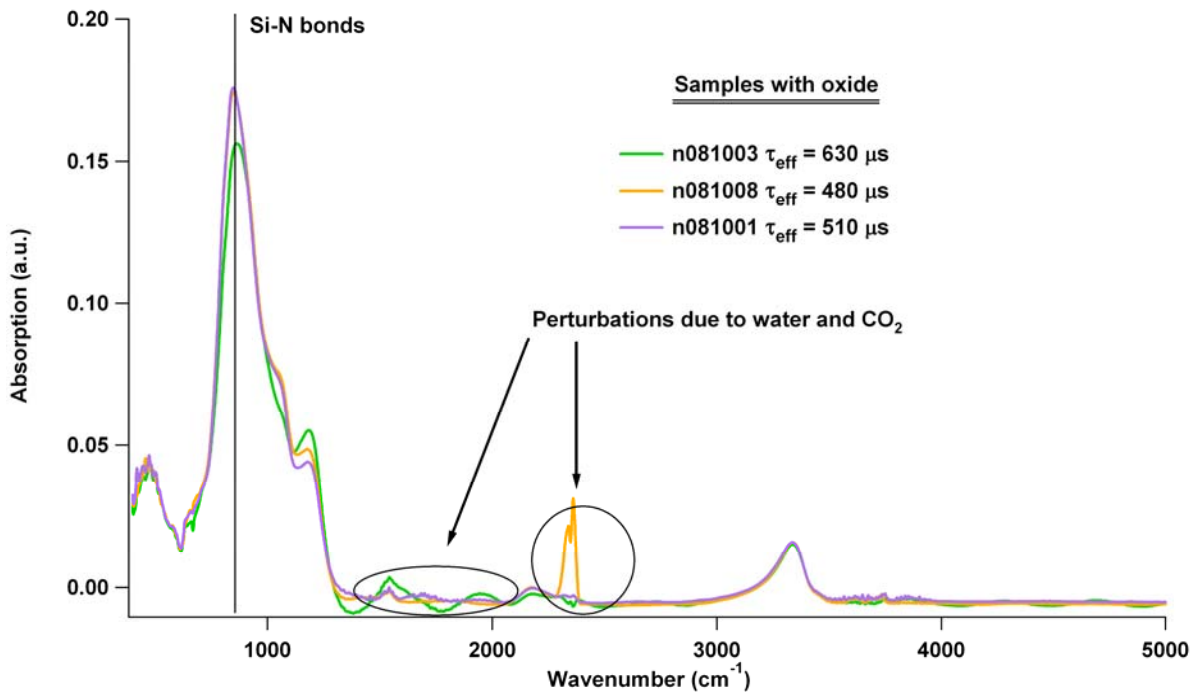
Fig. 66: IRFT spectra of the three samples with the thin oxide layer between substrate and SiN$_x$ coating.

As for the three first samples, the Infra red spectra show a difference in the bonds present in the coating between all layers. However, this difference cannot explain the difference of the passivation effect observed by the TRMC measurement.

An oxide layer at the interface between the silicon substrate and the SiN$_x$ seems to reduce the observed difference of passivation. If the origin of the effect is the surface states, an oxide with a better quality or a thicker oxide layer can suppress this problem.

4.2.7 Annealing

The effect of the annealing on the samples was studied. Two annealing temperatures were used, at 400°C and at 900°C. The samples were placed for 15 minutes in an oven at the desired temperature under a constant flux of N_2. The use of forming gas containing 20% of H_2 was observed not to be necessary. The molecules of Hydrogen will in every case not diffuse into the SiN_x layer. As shown by [IV.30] the hydrogen inside the Silicon nitride layer will form Hydrogen molecules and diffuse out of the layer under thermal excitation.

- *Low temperature annealing (400°C)*

In the first case, the effect of an annealing at 400°C on the passivation was studied. The sample was annealed for 15 minutes. TRMC measurement on Fig.67 shows the measurements made on the same sample before and after the annealing. No significant modifications of the TRMC signal are visible.
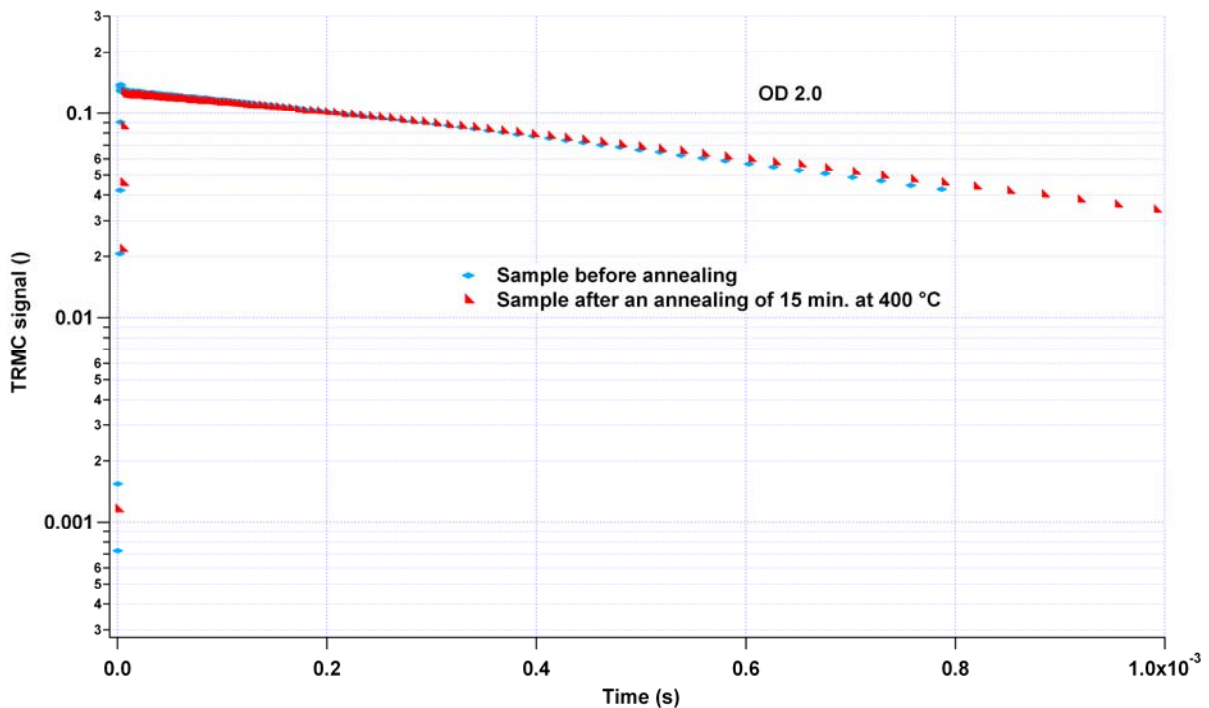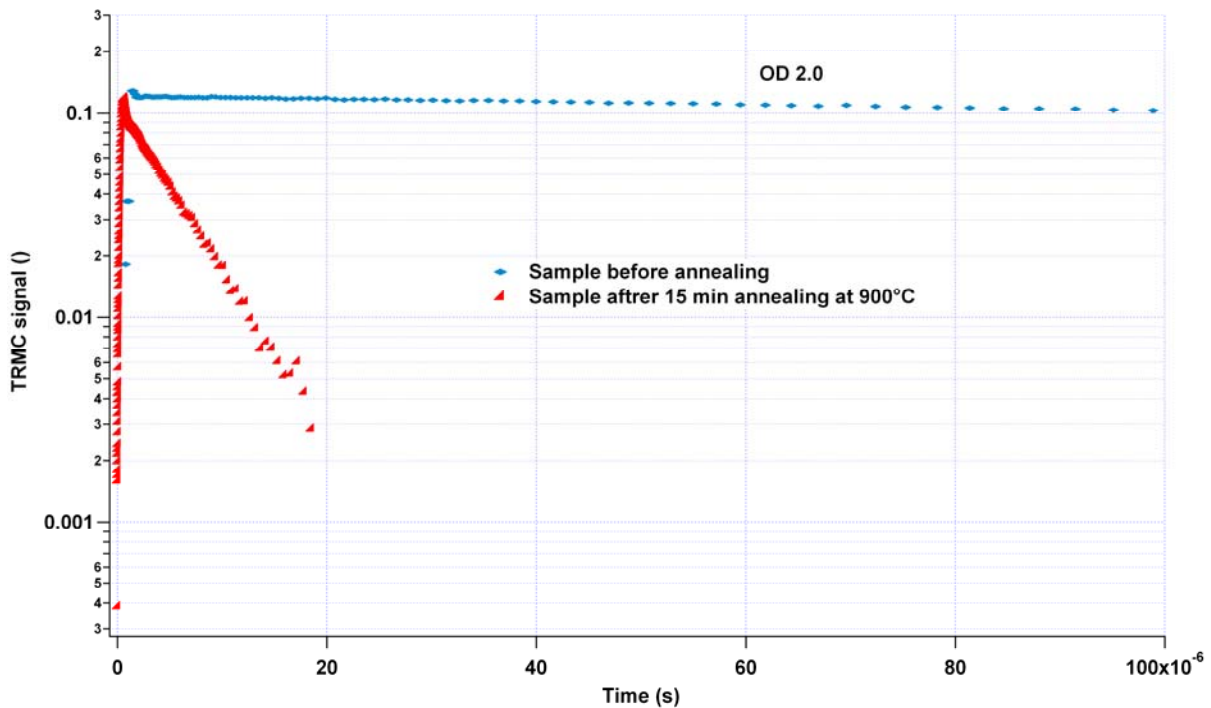

Fig. 67: TRMC measurements of a sample (silicon substrate covered by a 65 nm thick SiN$_x$ with R=0.16) before (blue curve) and after (red curve) a 15 minutes annealing at 400 °C.

The surface recombination velocities obtained by the measurements are:

$$S_{before}^{\max 400} = 15 \, \text{cm.s}^{-1}$$

$$S_{after}^{\max 400} = 14.6 \, \text{cm.s}^{-1}$$

The annealing at 400°C does not increase the electrical passivation for SiN$_x$ deposited on crystalline silicon. Even if the hydrogen bonds start to break at 350°C (Si-H first) [IV.31] we observed that for 15 minutes annealing at 400 °C the number of Si-H bonds did not drastically change. The Fig.68 shows an FTIR spectrum of the sample before and after the annealing. This measurement shows that there is no modification of the bonding inside the silicon nitride layer. The very small differences could come from the non-homogeneity of the bonds on the surface of the sample.
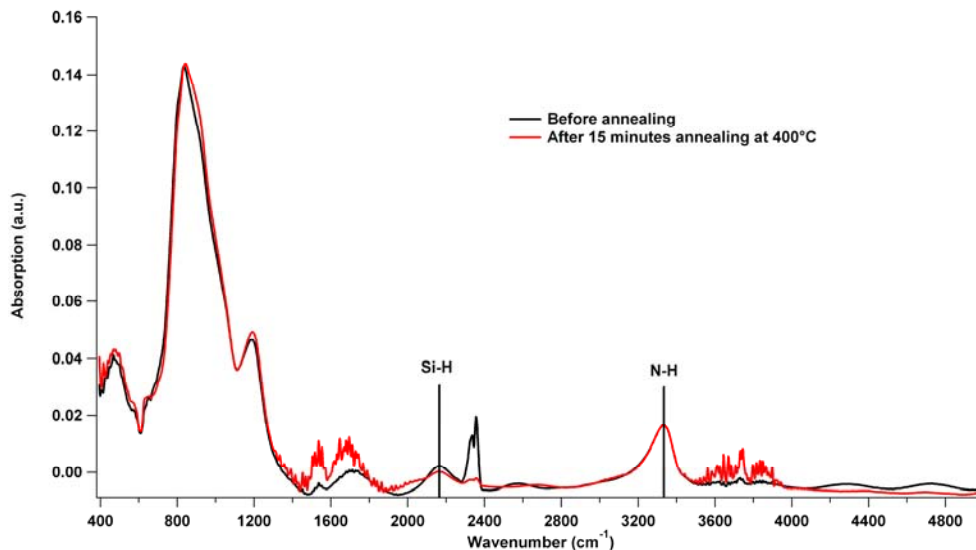
Fig. 68: IRFT spectra of a SiN$_x$ coating on crystalline silicon. The black curve is the spectrum of a sample deposit with R=0.16 before the annealing. The red curve is the same sample after 15 minutes annealing at 400°C.

For our purpose, silicon nitride on crystalline silicon, the annealing process at low temperature will not increase (or decrease) the electrical passivation effect of the SiN$_x$ layer.

In this case the sample was also annealed for 15 minutes. But at such a high temperature, the effect of the annealing is different. Firstly, the electrical passivation induced by the SiN_x layer disappears. As shown on the TRMC measurement on Fig. 69, the signal of the measurement for the annealed sample (red one) decreases much more rapidly than the one before annealing (blue one). Before annealing the surface recombination velocity is:

$$S_{before}^{\max\_900} = 27 \text{ cm.s}^{-1}$$

But after the annealing it is quasi infinite and the process is only controlled by diffusion. (*2.3. Charge-carriers kinetic*).

Fig. 69: TRMC measurements of a sample (silicon substrate covered by a 65 nm thick SiN_x with R=0.16) before (blue curve) and after (red curve) a 15 minutes annealing at 900 °C.

To gain a better understanding of the modification induced by the annealing, ellipsometry and FTIR measurements were performed on the sample (Fig.70).
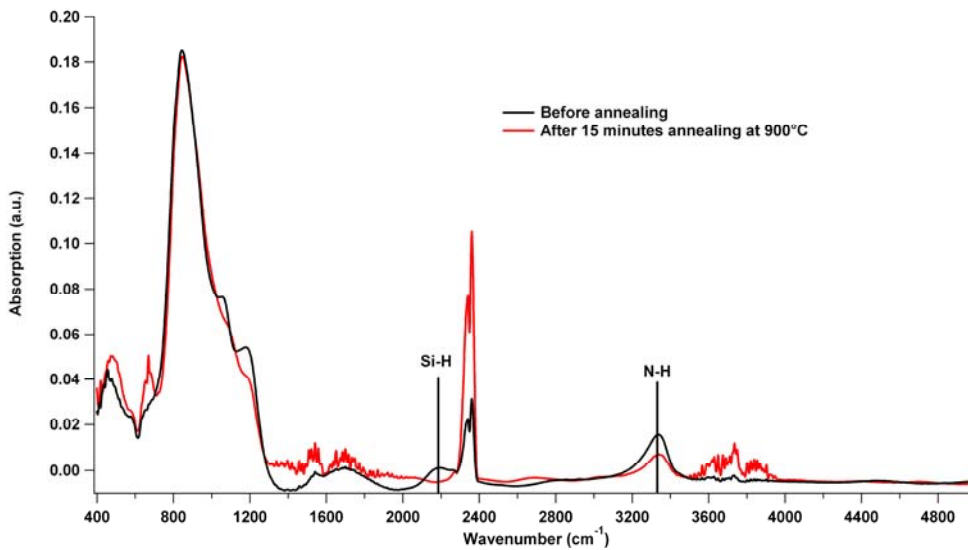
Fig. 70: IRFT spectra of a SiN$_x$ coating on crystalline silicon. The black curve is the spectrum of a sample deposit with R=0.16 before the annealing. The red curve is the same sample after 15 minutes annealing at 900°C.

The FTIR measurement shows that the Si-H bonds have completely disappeared and the number of N-H bonds decreased. The N-H bonds start to break around 800°C, they are more stable than the Si-H one. Two processes could play a role in the destruction of the electrical passivation effect. On the one hand an increase of the defect density could occur. On the other hand we could have a diminution of the field effect due to a reorganization of the states inside the SiN$_x$ changing the fixed charge.

Another remarkable effect is the decrease of the thickness of the layer. The samples, prepared under standard conditions were first measured by ellipsometry in order to determine the refractive index and the thickness.

The ellipsometry measurements show that the layers lost about 10 nm (for different "start" thickness) (Fig.71 and Fig.72). This reduction can be attributed to the loss of the hydrogen. But no differences are visible concerning the refractive index. This is remarkable because it means that the density is the same, or if the hydrogen diffused out, the density will normally have to change. This was already observed for refractive indices lower than 2.1 (it is the case for this sample n=1.86), a stronger increase was founded for SiN$_x$ with a refractive index higher than 2.1 [IV.32, 16]
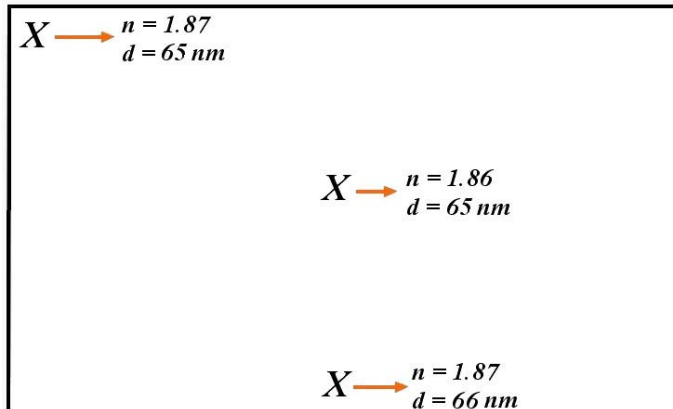
95

Fig. 71: Ellipsometry measurement made on the sample n080805 at three different points (X on the scheme) before the annealing. The refractive index is about 1.86 and the thickness 65 nm.

X → $n = 1.87$ $d = 65\,nm$

X → $n = 1.86$ $d = 65\,nm$
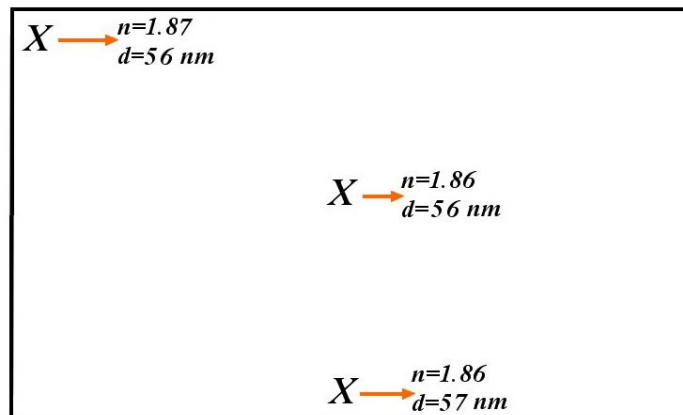
X → $n = 1.87$ $d = 66\,nm$

Fig. 72: The same sample after the annealing at 900°C during 15 minutes. The same points were measured. The refractive index is stayed at 1.86 but the thickness decreased about 10 nm.

X → $n=1.87$ $d=56\,nm$

X → $n=1.86$ $d=56\,nm$

X → $n=1.86$ $d=57\,nm$

To have a better overview of this phenomenon, an annealing at 900°C under N_2 flux during 15 minutes was performed on three other samples with different ration R.

	SiH4	NH3	N2	Temperature	Time of deposition
Sample A	32 sccm	200 sccm	54 sccm	350°C	31 min 05 s
Sample B	100 sccm	200 sccm	54 sccm	350°C	20 min 35 s
Sample C	100 sccm	50 sccm	54 sccm	350°C	27 min 24 s

Tab. 4: Condition of deposition of the three samples used to the high temperature annealing.

The samples were deposited with different concentration of silicon inside the SiN_x layer to see if the influence of the annealing depends also on the silicon / nitrogen ratio. The XPS measures give the following ratio:

Sample A: [Si]/[N] = 1.81

Sample B: [Si]/[N] = 1.91

Sample C: [Si]/[N] = 3.3

And the ellipsometric measurements of those three samples:

Sample A: d = 252 nm; n = 1.86

Sample B: d = 240 nm; n = 1.95

Sample C: d = 240 nm; n = 2.55

An annealing of 15 minutes at 900°C was done. The first remark is that the morphology of the samples B and C changed. Spots and cracks appeared on the surface. An analysis at the optic microscope was performed for the three samples and shows clearly a modification of the surface. Those modifications are different following the quantity of silicon inside the SiN_x layer. For the sample with a low SiH_4/NH_3 ratio (R=0.16) only cracks appeared at the surface. (Fig.73)

Fig. 73: Image of the surface of the sample A after the annealing obtained with an optical microscope (X100). The black lines are cracks.

The effect is different with a stronger Si/N ratio (R=0.5). In this case some spots appeared with the cracks, like shown in Fig.74 and Fig.75.

97
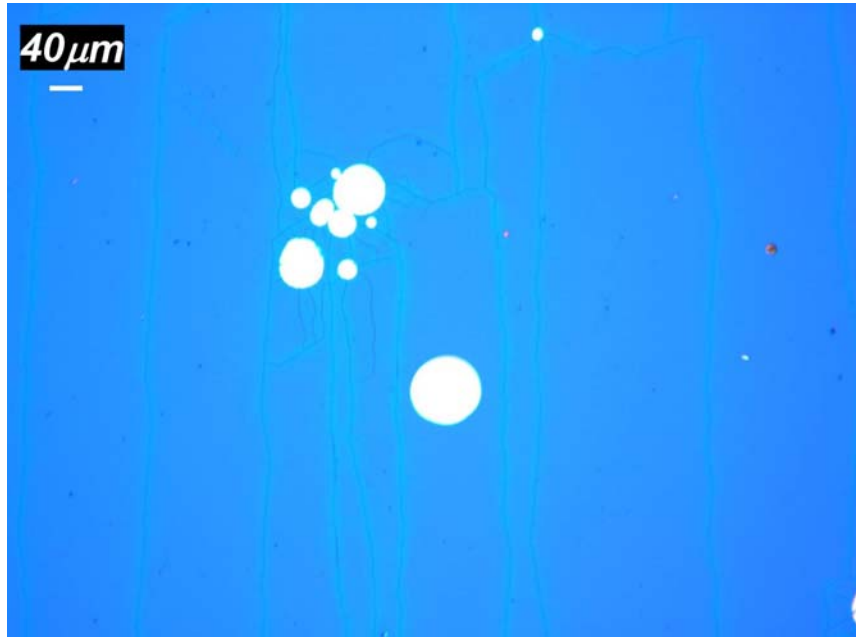
Fig. 74: Image of the surface of the sample B after the annealing obtained with an optical microscope (X100). The black lines are cracks and white spots appeared.
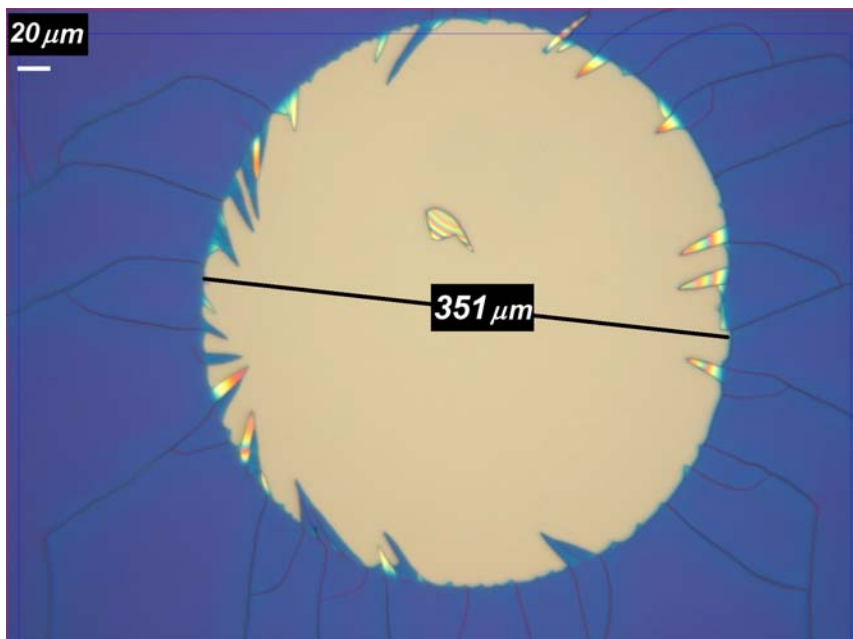
Fig. 75: Magnification of a spot on the surface of the sample B (X200). The cracks can be recognized around the spot.

The sample C with the higher ratio R (R=5) shows another modification. In this case there are no more cracks anymore and only spots appeared plus particles related evidently with the spots like shown on Fig.76.
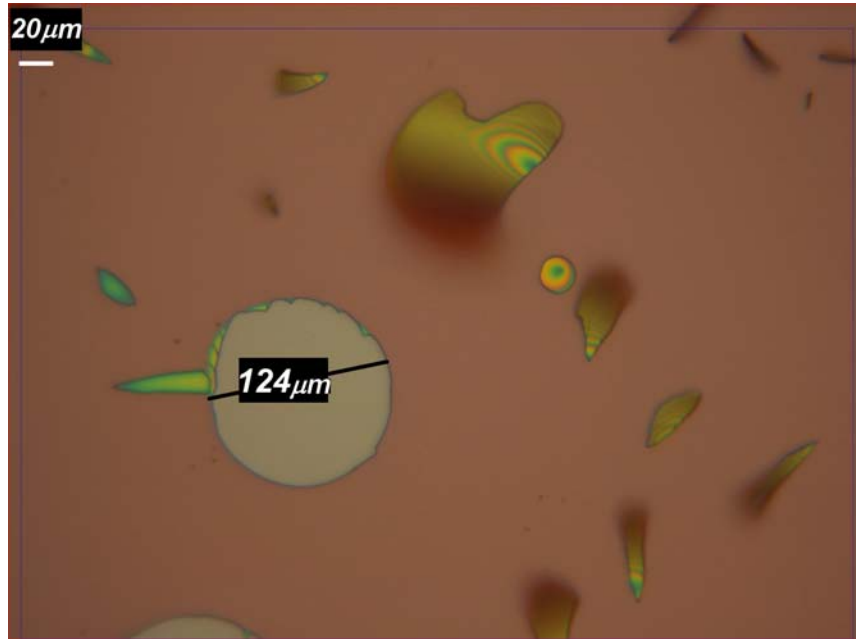
Fig. 76: Image of the surface of the sample C after the annealing obtained with an optical microscope (X200). The cracks disappeared and spots appeared.

A better view of the particles, their quantity and the general morphology of the surface can be observed on the Fig.77.
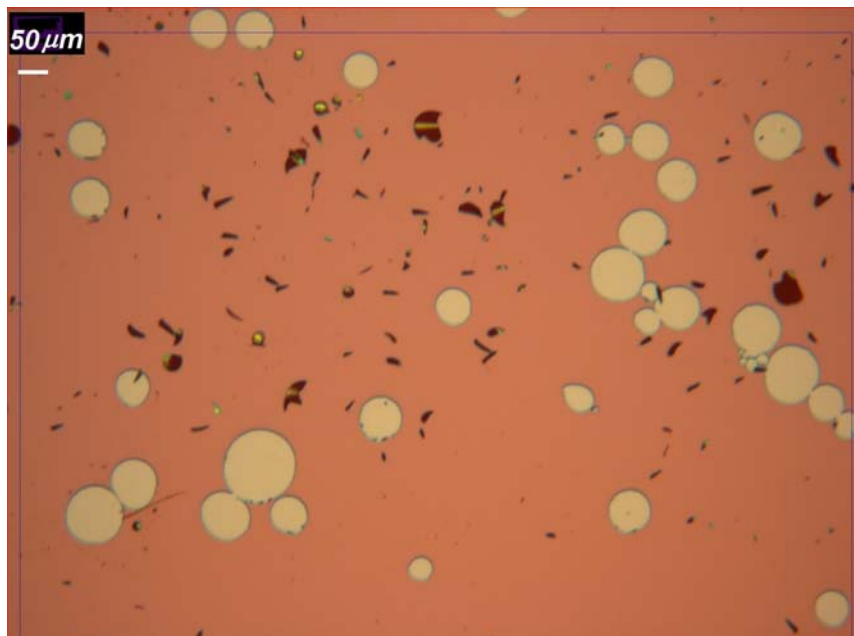
Fig. 77: Image of the surface of the sample C after the annealing obtained with an optical microscope (X500). A big quantity of particles related with the spots appears.

Analyse of the samples A, B and C with a profilometer shows us that the spots are in fact "well-like holes". Measurements were performed on the spots of the samples B (Fig.78) and C (Fig.79, Fig.80). As it can be seen on the Fig.79 and Fig.80, the well-like holes are homogeneous in depth.
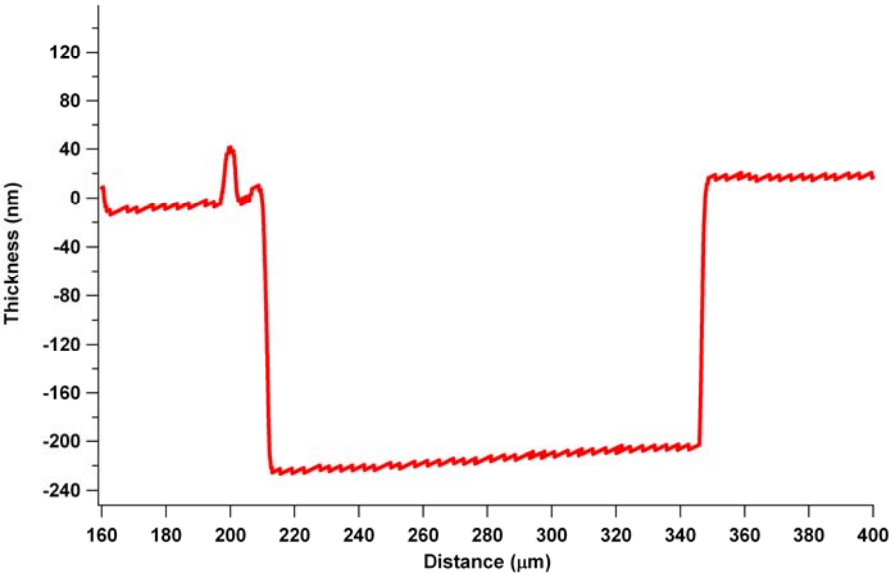

Fig. 78: Measure with a dektak profilometer of a spot at the surface of the sample B. The spots are in fact well-like holes.
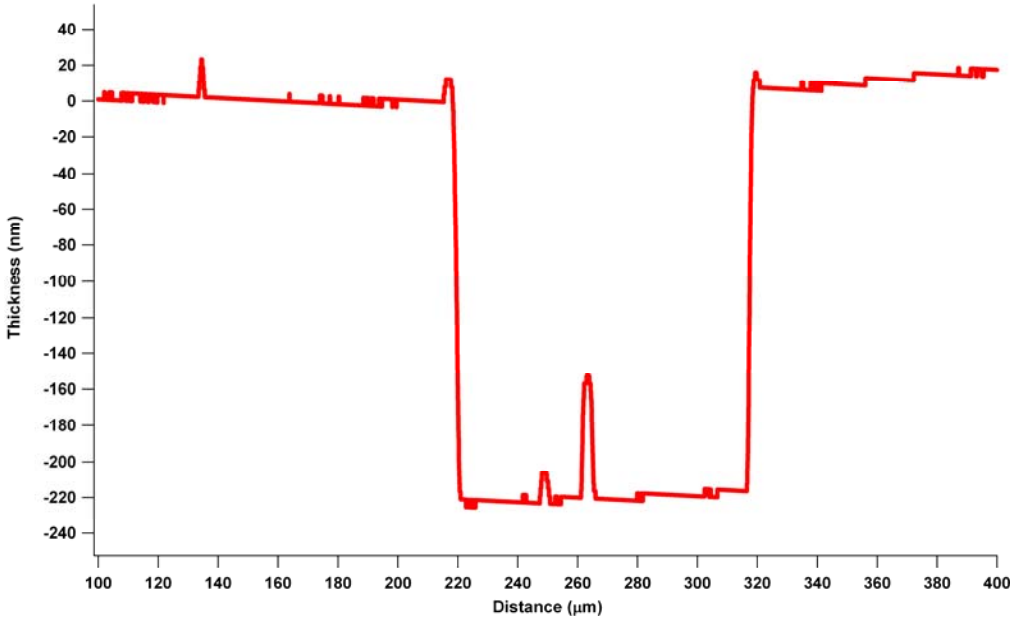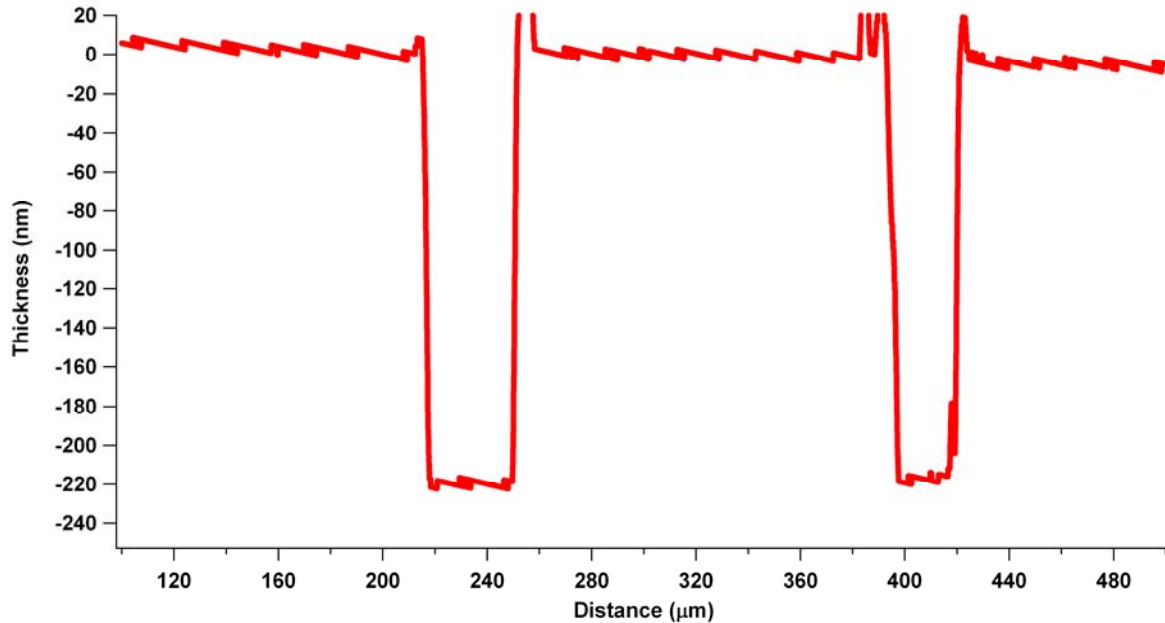

Fig. 79: Measure with a dektak profilometer of a spot at the surface of the sample C.

Fig. 80: Two consecutives spots (or wells) measured with a dektak profilometer at the surface of the sample C. The wells seem to be constant in depth.

The samples were then measured by FTIR and ellipsometry again. (The samples are now named Sample X_a).

Sample A_a: d = 241 nm; n = 1.84

Sample B_a: d = 225 nm; n = 1.95

Due to the highly damaged surface the determination of the thickness and the refractive index of the sample C_a was impossible with the monochromatic ellipsometer. However, the change of the colour indicates a modification of the thickness. The thickness of the sample C_a can still be estimated. If we look on the profile and the ellipsometric measurement of the sample B_a we can remark that the well-like holes are as deep as the SiN_x layer. And if we refer to the reduction of the thickness induced on the two other samples then the thickness of the SiN_x layer of the sample $SampleC_a$ must be around 220 nm thick which corresponds to a loss of 20 nm in the thickness after annealing.

We can also observe that the refractive index stays constant. The refractive index is related to the density of the layer [IV.17], a diminution of the thickness may induce an increase of the density which is not visible with the measurements of the refractive index. The reason of this behaviour is not clear, two processes can occur: The hydrogen can diffuse out of the layer and the components of the layer can at the same time rearrange themselves.

In order to confirm the results of the first sample concerning the evolution of the bonding in the film, FTIR measurements were performed on the samples $SampleA_a$,

SampleB$_a$ and SampleC$_a$ too. The same kinds of processes were observed. On the Fig.81, 82 and 83 we can observe a decrease of the N-H bonds and Si-H one.

The formation of the well-like holes is not that clear. These wells did not appear for a low ratio R and an explanation can be the evacuation of the hydrogen through path initialized by precursors such as silicon cluster. However, an annealing at 900°C leads to a drastic reduction of the hydrogen content inside the layer and to a destruction of the electrical passivation effect of the silicon nitride.
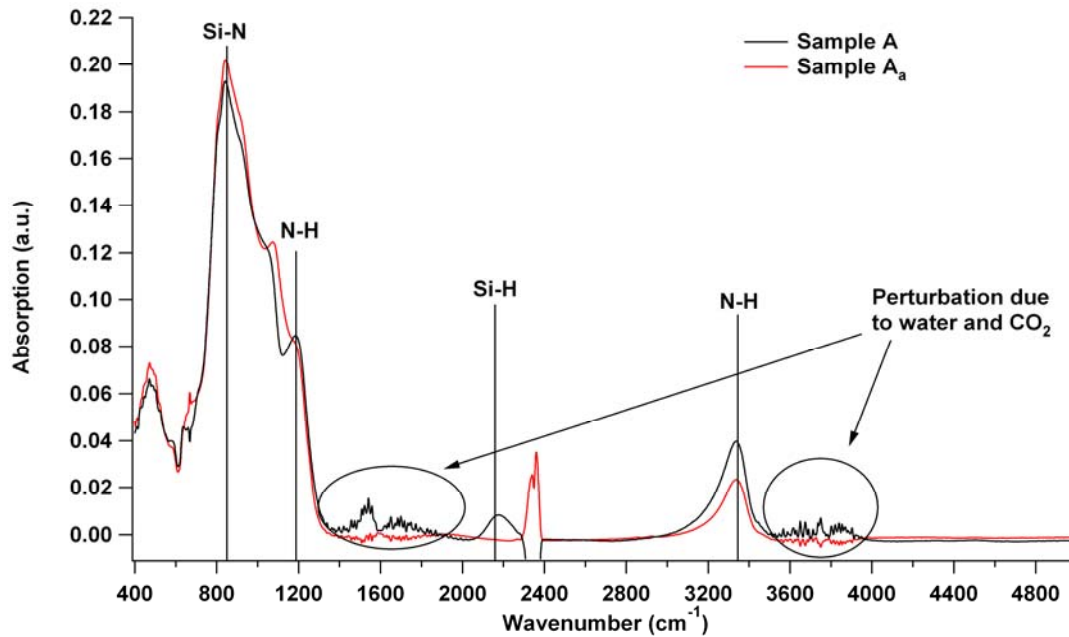

Fig. 81: Spectra of the sample A (with the lower ratio R (=0.16)) before the annealing at 900 °C and after (sample A$_a$). The diminution of the N-H and especially Si-H bonds are visible.
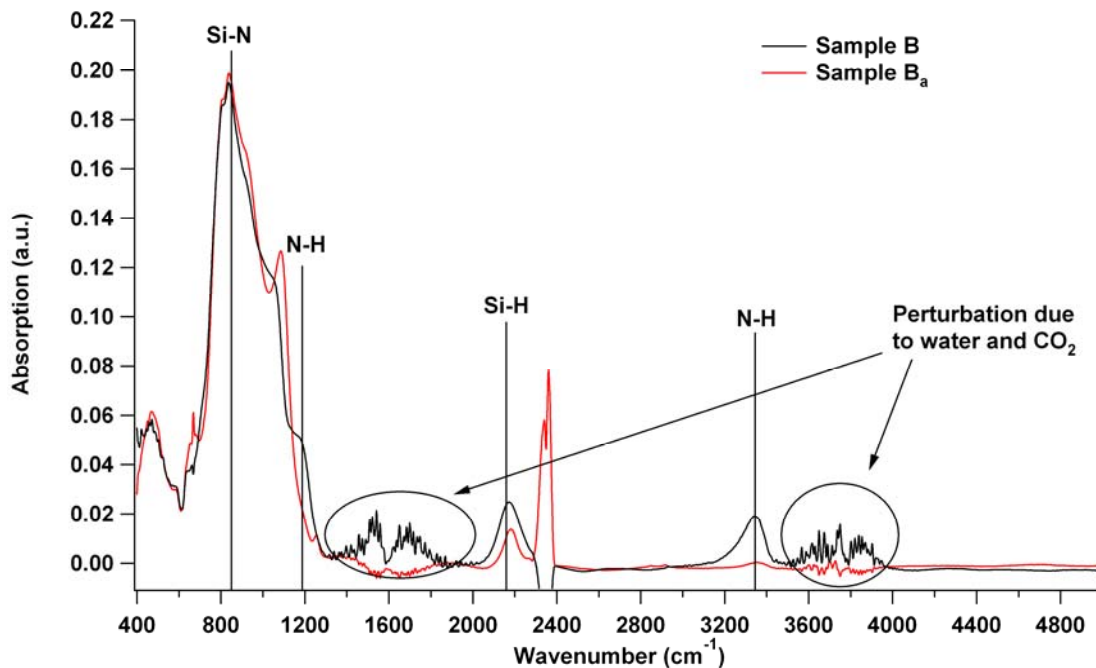

Fig. 82: Spectra of the sample B (with a ratio R (=0.5)) before the annealing at 900 °C and after (sample Aa).
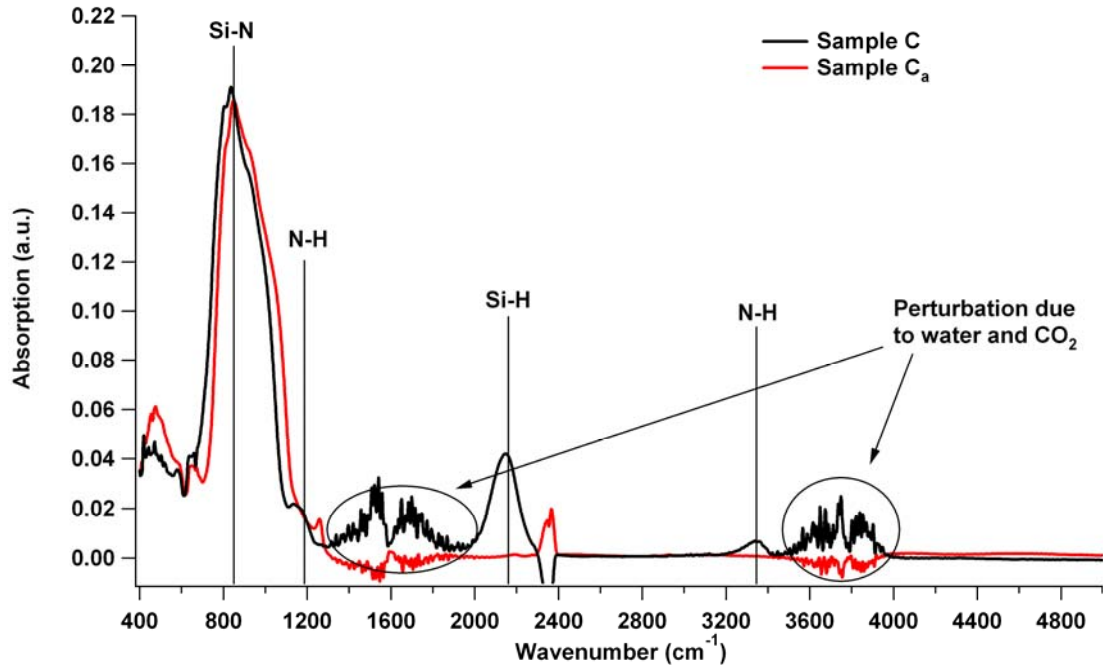
Fig. 83: Spectra of the sample B (with a ratio R (=0.5)) before the annealing at 900 °C and after (sample Aa). The Si-H and N-H bonds disappeared completely.

4.2.8 _Double layers_

The possibilities offered by the PECVD deposition allow us to deposit systems composed by more than one layer. The different layers can be deposited under different conditions. A small overview of the possibilities offered by a double layer system will be done. The two SiN_x layers were deposited with a high difference in the ratio R in order to see the effect on the electrical passivation but also on the anti-reflection (the two main properties relevant for our needs). The difference of the electrical passivation induced by the variation of the ratio R was fairly small as seen in the chapter *4.2.4. Electrical passivation on n-type silicon*. But a reduction of the passivation takes place for high R (Fig.84). The first system is composed firstly by a thin layer with a high R onto which a thicker layer with a low R is deposited.
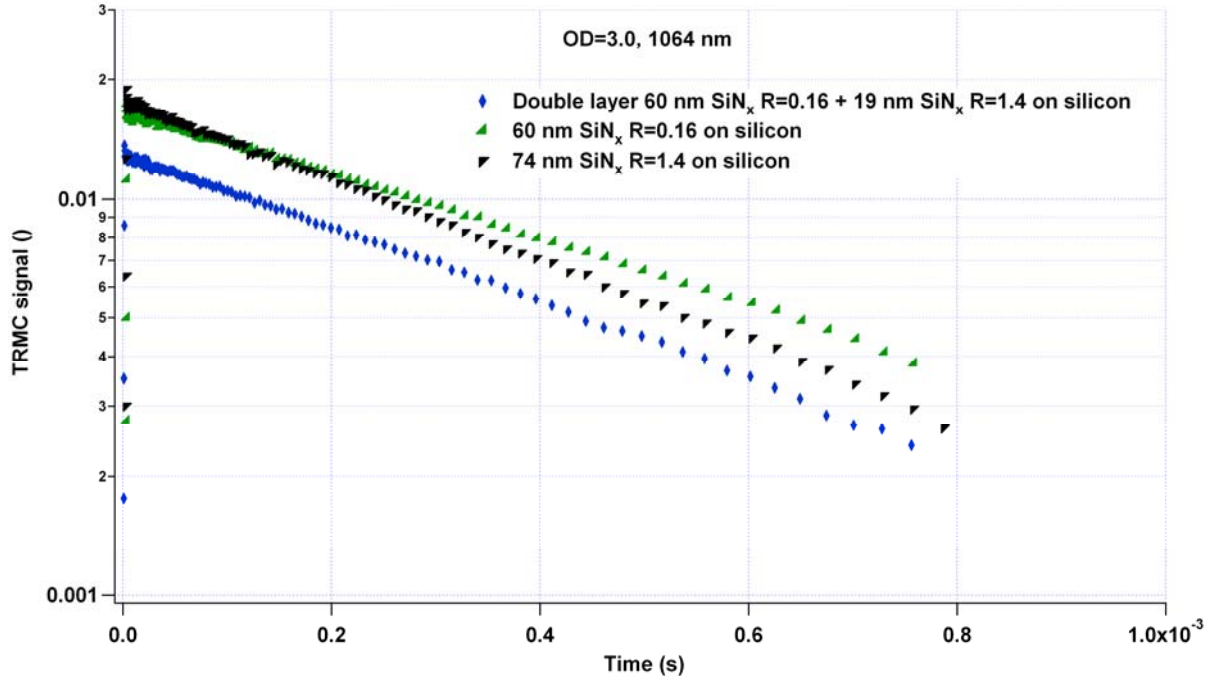
Fig.84: TRMC measurement of three samples. The black and the green curves are measurements corresponding to a high R SiNx single layer system and a low R one. The Blue curve is the double layer system.

In this case the surface recombination velocities are:

$$S_{SingleR=0.16}^{max} = 20 \ \text{cm.s}^{-1}$$

$$S_{SingleR=1.4}^{max} = 25 \ \text{cm.s}^{-1}$$
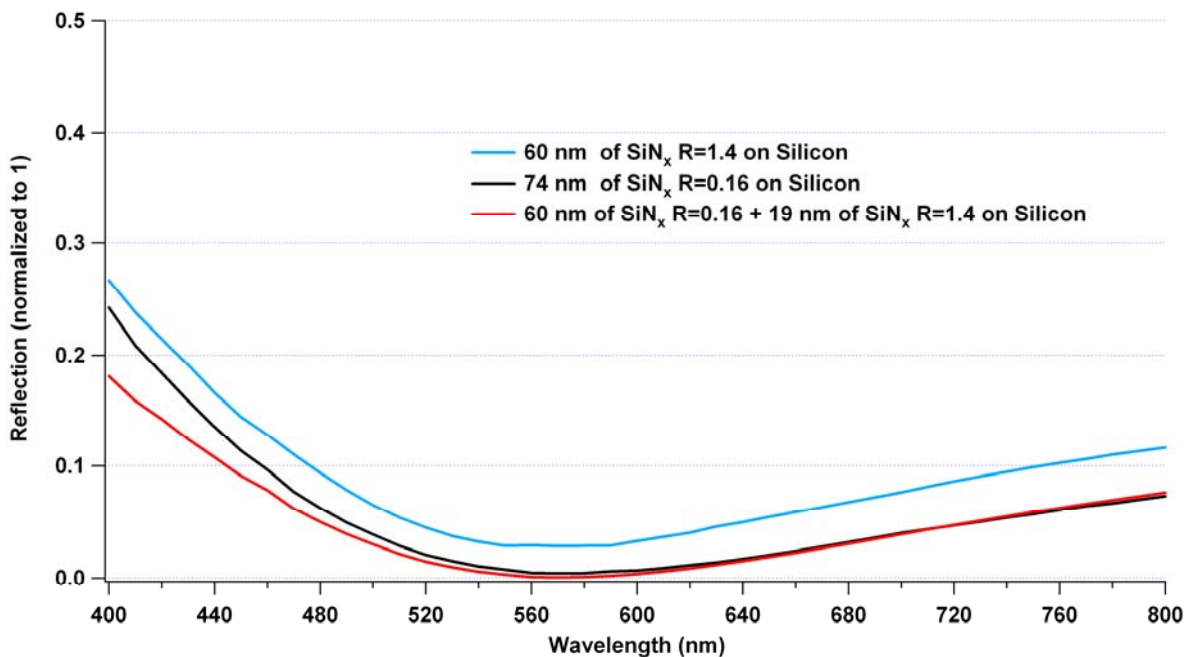
$$S_{Double}^{max} = 23 \ \text{cm.s}^{-1}$$

Fig. 85: Simulation of the double and single layer system used above. The thicknesses were taken to determine the minimum of reflection for the three samples.

Concerning the electrical passivation effect, the double layers system seems to bring a small enhancement. However the layer deposited directly onto the silicon substrate must be thin, otherwise the effect of the second layer will not be perceptible.

For the anti-reflection, a simulation of the three kinds of layers shows a small enhancement of this effect with the double layer system (Fig.85). That is an effect of the increase from air (n=1) to silicon (n=4.32) of the refractive indices.

The improvement of the passivation effect of a bad electric passivating layer but with very low absorption due to a thin good passivating but more absorbing layer was tried. On a silicon crystalline substrate, a thin layer (25 nm thick) of SiN_x with R=1.2 was deposited. This layer was then covered with a SiN_x deposited without N_2 in the precursor gas (40 nm). This layer was found to have a low absorption but a bad passivation compared to the one deposited with N_2 and R=1.2. On the Fig.86 the results of the TRMC measurements are shown.
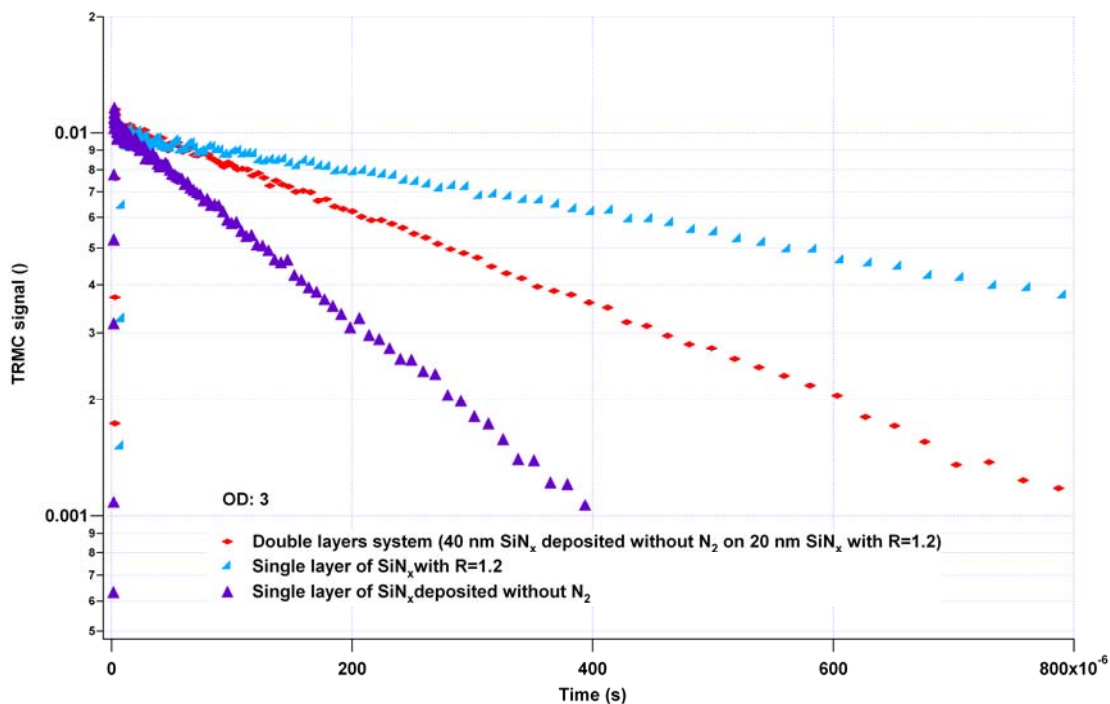
Fig. 86: The red curve represents the measurements of a silicon crystalline substrate covered with a thin layer (25 nm thick) of SiN_x with R=1.2. This layer was then covered with a SiN_x deposited without N_2 in the precursor gas (40 nm). The blue and the purple curves show the TRMC measurements of respectively the single layer of SiN_x with R=1.2 and SiNx deposited without N_2.

The electrical passivation effect of the SiN_x deposited without N2 in the precursor gases is clearly enhanced by the addition of the thin good passivating layer between the coating and the substrate.

$$S_{Single\_withoutN_2}^{max} = 62 \ cm.s^{-1}$$

$$S_{SingleR=1.2}^{max} = 13 \ cm.s^{-1}$$

$$S_{Double}^{max} = 24 \, cm.s^{-1}$$

The fact that the electrical passivation induced by double layers system is not as good as the one performed by the single layer system (blue curve on the Fig.86) can have two explanations. The first is that the layer is not thick enough to have the maximum concentration of fixed charges necessary to have the optimum passivation. The second reason could be that the deposition of the second layer induces a reorganisation in the first one.

In this case an improvement of the anti-reflection properties can be observed. As show on the Fig.87, the double layers reflect less light over the range of interest than the two single systems.

The double layer system allows an increase of the electrical passivation property of a coating but also its optic properties such as the anti-reflection and the transmission (Fig.88). Nevertheless, further studies or simulations are necessary to enhance the anti-reflection for example.
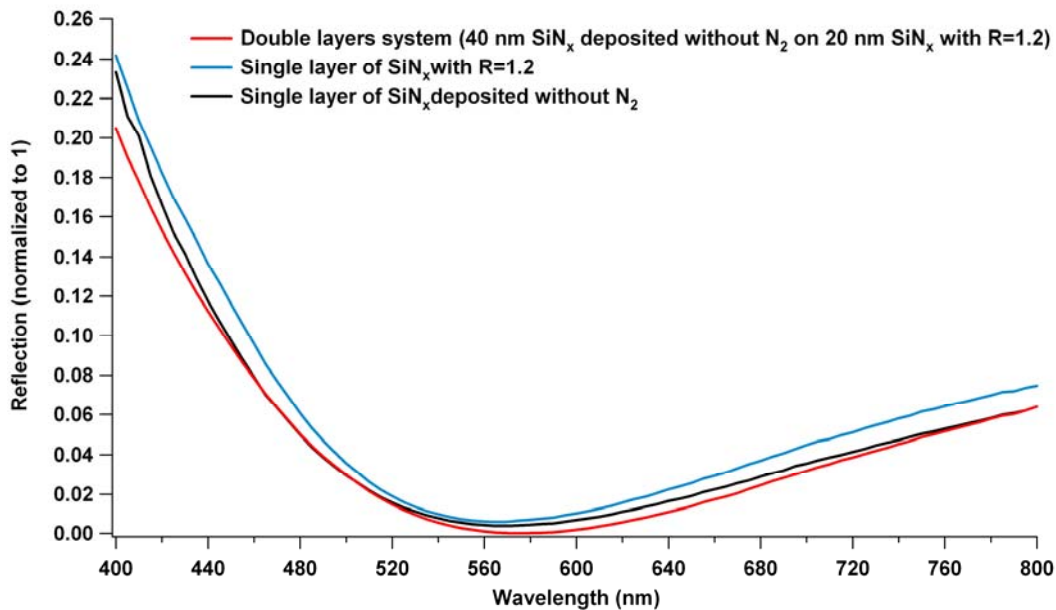
Fig. 87: Comparison between the measured reflection of the double layers system (red line) and the two other single layer systems (blue and black line). The thickness of each layer was first simulated to have the minimum of the reflection at the same wavelength.
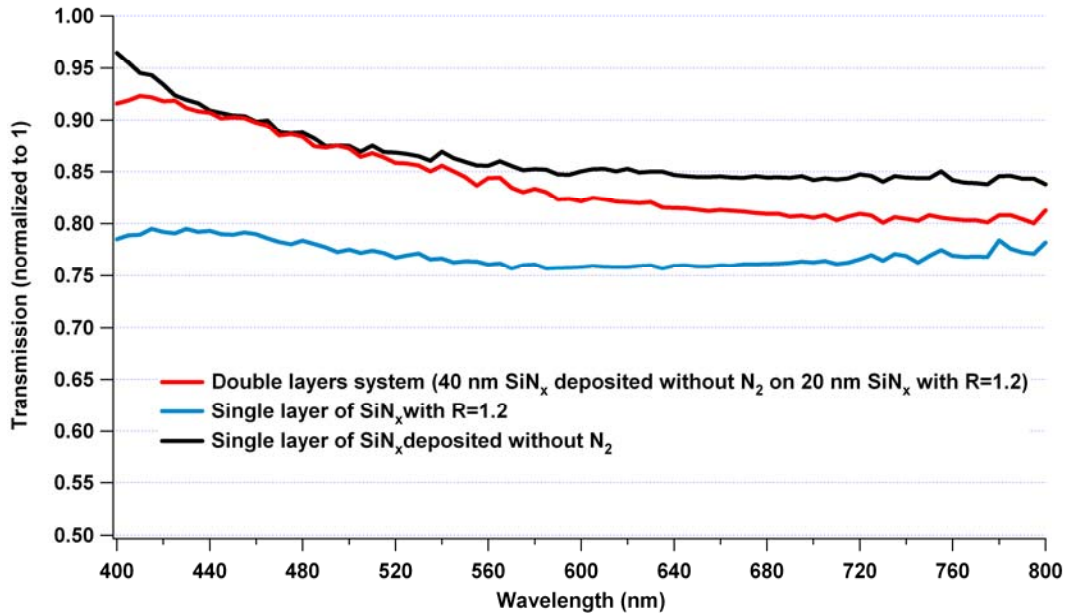
Fig. 88: Comparison between the measured transmission of the light through the double layers system (red line) and the two other single layer systems (blue and black line). For the transmission the depositions were made on quartz.

4.2.9 Electrical passivation on p-type silicon

Fig. 89: Representation of the depletion zone induced by a SiN$_x$ coating on p-type silicon. With: E$_c$ the conduction band, E$_f$ the Fermi energy, E$_v$ the valence band, Q$_f$ the fixed charge in the SiN$_x$, W the width of the space charge.

107

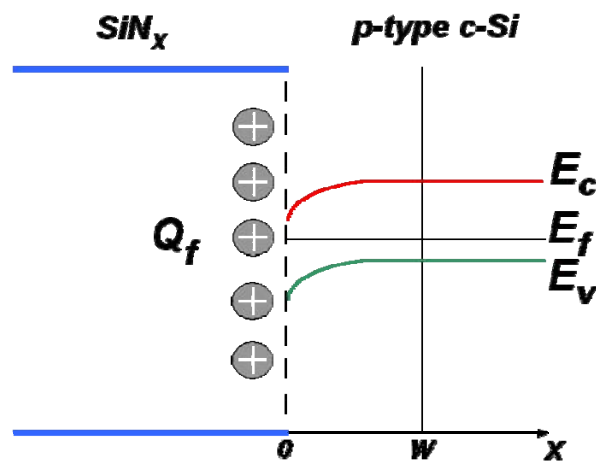In the following experiments, p-type crystalline silicon was used as substrate instead of n-type crystalline silicon. In the case of n-type silicon the deposition of SiN_x at the surface will create an accumulation (of majority charge-carriers) layer at the interface. With p-type, silicon nitride will generate a depletion (of the majority charge-carriers) layer at the interface (Fig.89).

Fig.90 shows the TRMC signal of a p-type silicon substrate covered on both sides with SiN_x. Four different intensities, from a low one (OD 5) to a high one (OD 2.3) were used. Two phenomena can be observed with these measurements. In the first 10 µs the signal decreases more strongly at low intensities (and did not decrease at high intensities). This phenomenon is due to the reduction of the mobility of electrons at the interface c-Si/SiN_x. Indeed, at the interface, a separation of the charge-carriers takes place. The electrons (minority charge-carriers) will go to the interface where their mobility falls from 1500 cm²/(Vs) to 300 cm²/(Vs). The TRMC signal, related to the mobility of the charge-carriers, will decrease. This phenomenon will be dependent on the intensity because at higher intensities the bands become flatter and flatter. The electrons and holes are no longer separated and thus the electrons will not be collected anymore by the surfacial space charge layer and then only a small part of them reduce their mobility at the surface. For high intensity a second phenomenon occurs after around 100 µs. The charge-carriers start to recombine at the interface. This is also due to the non-separation induced by the flat bands. The final decay (around 500 µs) is due to the recombination in the space charge region.
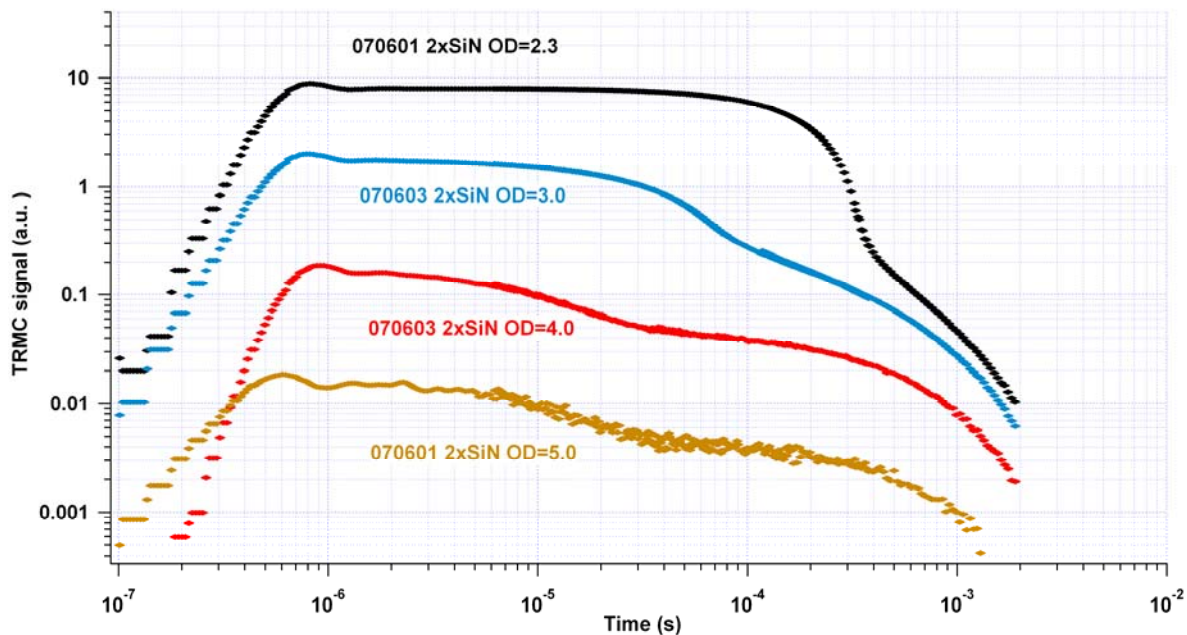
Fig. 90: TRMC signal induced by a 1064 nm laser pulse on a p-type crystalline silicon substrate (100 Ω.cm, 0.530 mm thick) covered on both side with SiNx (standard conditions, R=0.16) for 4 different intensities.

The processes are decomposed on the Fig.91 and Fig.92. The first shows the decrease of the TRMC signal due to the reduction of the mobility of the electrons at the interface p-type c-Si/SiN$_x$. The effect at low intensities is clear. The weak decrease at high intensities is due to the start of the recombination process via interface states.

Fig. 91: TRMC signal induced by a 1064 nm laser pulse on a p-type crystalline silicon substrate (100 Ω.cm, 0.530 mm thick) covered on both side with SiNx (standard conditions, R=0.16) for 4 different intensities. The scale is semi logarithmic and shows only the first decay process (reduction of the mobility of the electrons)

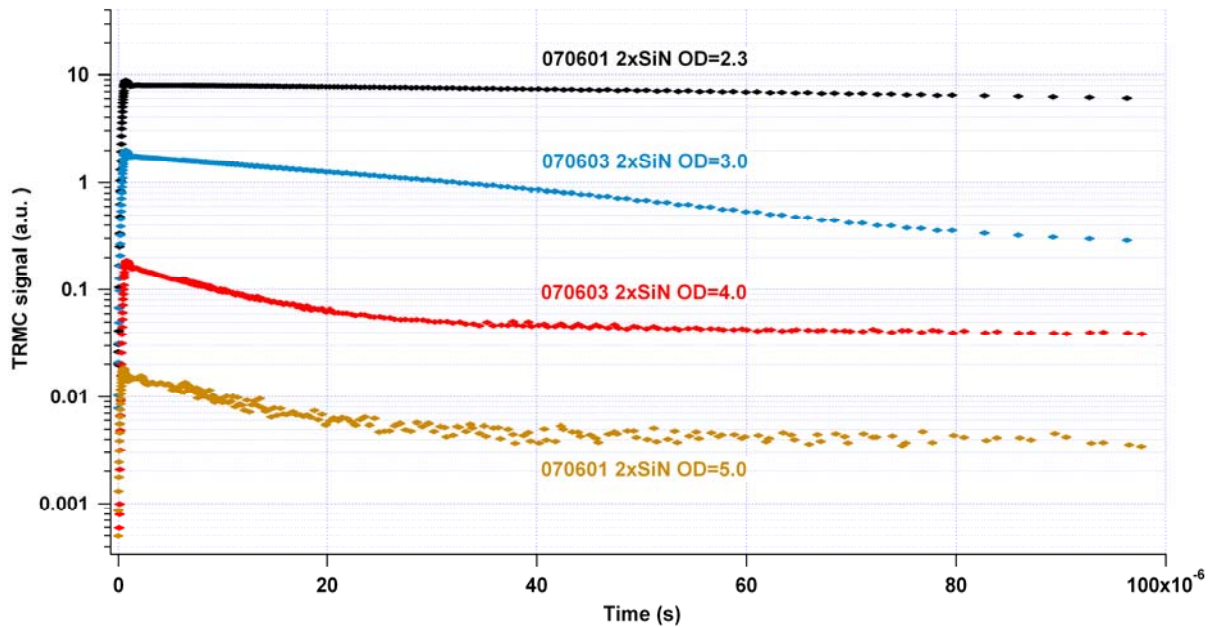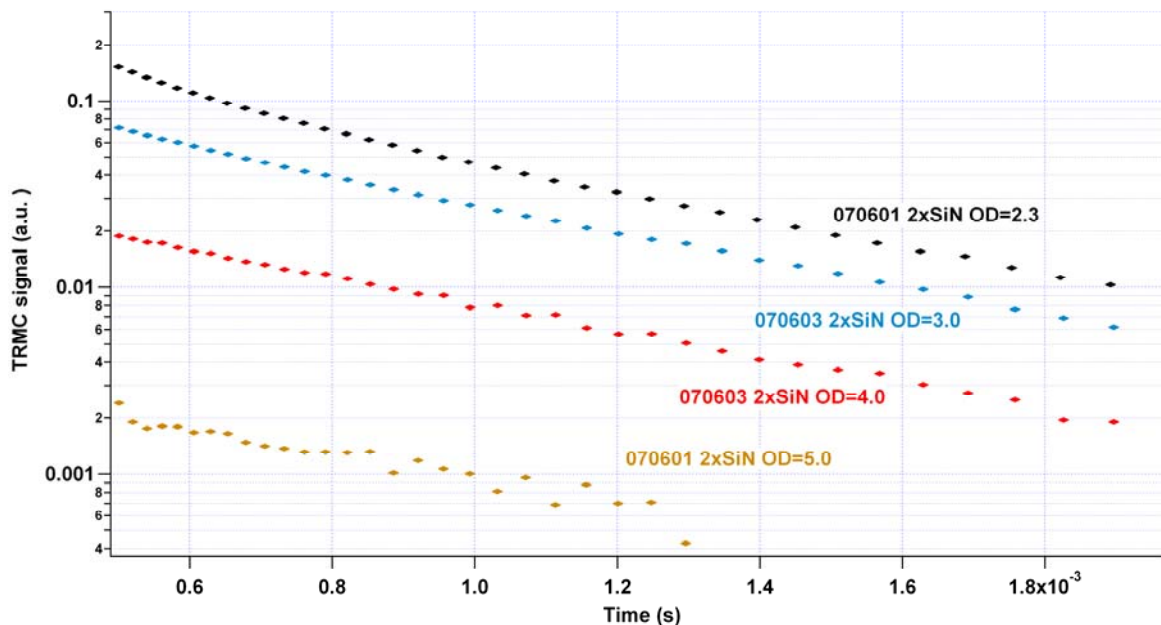On the next picture (Fig.92), the final decay, i.e. the recombination in the space charge region is shown.

Fig. 92: TRMC signal induced by a 1064 nm laser pulse on a p-type crystalline silicon substrate (100 Ω.cm, 0.530 mm thick) covered on both side with SiNx (standard conditions, R=0.16) for 4 different intensities. The scale is semi logarithmic and shows the final decay process due to the recombination in the space charge region.

On Fig.93, the difference of the TRMC signal between a substrate of p-type c-Si covered on both sides and a sample covered only on one side is shown. The generation of the excess charge-carriers is done by a 1064 nm laser pulse (bulk generation). In the case of the sample covered on one side we have two extreme cases, on one side a maximal recombinative surface and on the other one a non-recombinative surface.
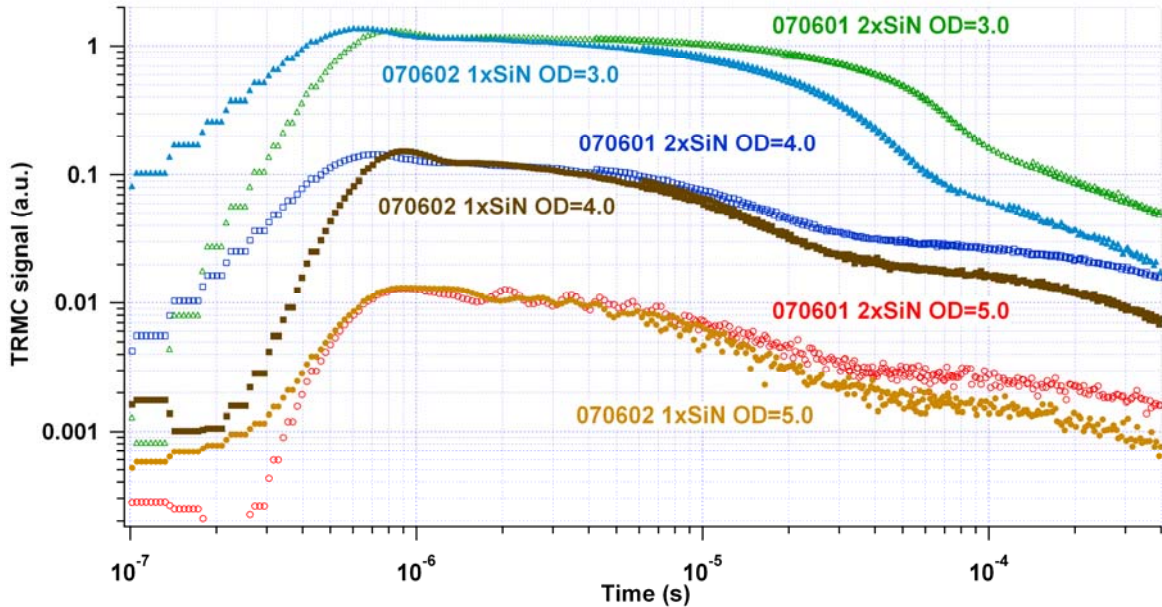
Fig. 93: Comparison between the TRMC signal induced by a 1064 nm laser pulse in a p c-Si substrate covered on both sides with SiNx and a p c-Si substrate covered only on one side with the same SiN$_x$.

The phenomena are the same as in the case seen before. The difference of the signal between the one side covered and the both sides covered is that in the one side covered sample, the excess charge-carriers will recombine quickly because of the presence of an additional decay channel (the bare side). There the mobilities will fall to zero (recombination). This is totally independent of the intensity.

In contrast to homogeneous excitation for 532 nm radiation the pulse- intensity plays a role. With this wavelength the excess charge-carriers are generated at the surface. If the sample is illuminated at the covered side (this is the case in Fig.94) the charge-carriers will be stored by the space charge region. If the intensity is low, i.e. not many excess charge-carriers are generated, it is clear that nearly all electron-hole pairs will be separated at the illuminated p Si/SiN$_x$ interface. When the intensity increases, and thus the number of excess charge-carriers, the space charge can not store efficiently all charge-carriers and so a part of them will attain the other face and recombine.
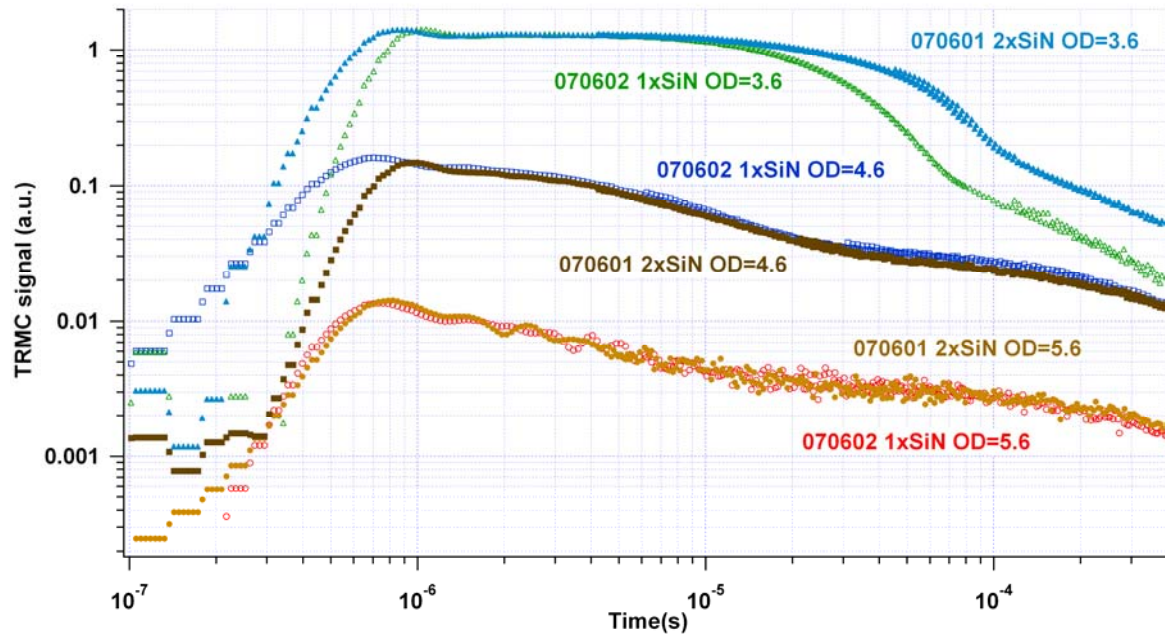
Fig. 94: Comparison between the TRMC signal induced by a 532 nm laser pulse on a p c-Si substrate covered on both sides with SiNx and a p c-Si substrate covered only on one side with the same SiNx.

Thus at low intensities there is no difference between the sample covered on both faces with SiN_x and the sample covered only on one face. At higher intensities there is an additional fast (surface) decay channel at the uncovered face in the latter sample.

4.3. Comparison between different coatings

This section will look at the effect of a silicon oxide layer and amorphous silicon. The silicon oxide layer (100 nm thick) was thermally grown on both sides of a p-type silicon (100 Ω.cm, 0.530 mm thick) in order to compare it with the SiN_x and the measurement made in the section *4.2.8. Electrical passivation on p-type silicon*. The amorphous silicon was p-doped (p a-Si:H) and 12 nm were deposited on n-type crystalline silicon (1.5 Ω.cm, 0.243 mm thick) by PECVD to give an overview of the system used in the a-Si:H/c-Si heterocontact solar cell of invert geometry.

On the Fig.95, the same experiment done with SiN_x on p-type silicon (*4.2.8. Electrical passivation on p-type silicon*) is compared with a silicon oxide layer instead of SiN_x. The oxide like the silicon nitride creates an inversion at the surface of p-type silicon. The silicon oxide was also grown on p-type crystalline silicon. At low intensity (OD 5) the decay due to the reduction of the mobility of the electrons at the interface in the SiN_x covered samples is absent in the SiO_2 covered samples. This means that contrary to the c-Si/SiN_x interface, there is no reduction of the electron mobility at the interface c-Si/SiO_2. The decrease of the signal, due to recombination at the interface appears earlier with the silicon oxide, this means that this phenomenon is stronger with oxide. However, the final decay is much slower with oxide, which indicates that the recombination in the space charge is weaker in the Si/SiO_2 interface.
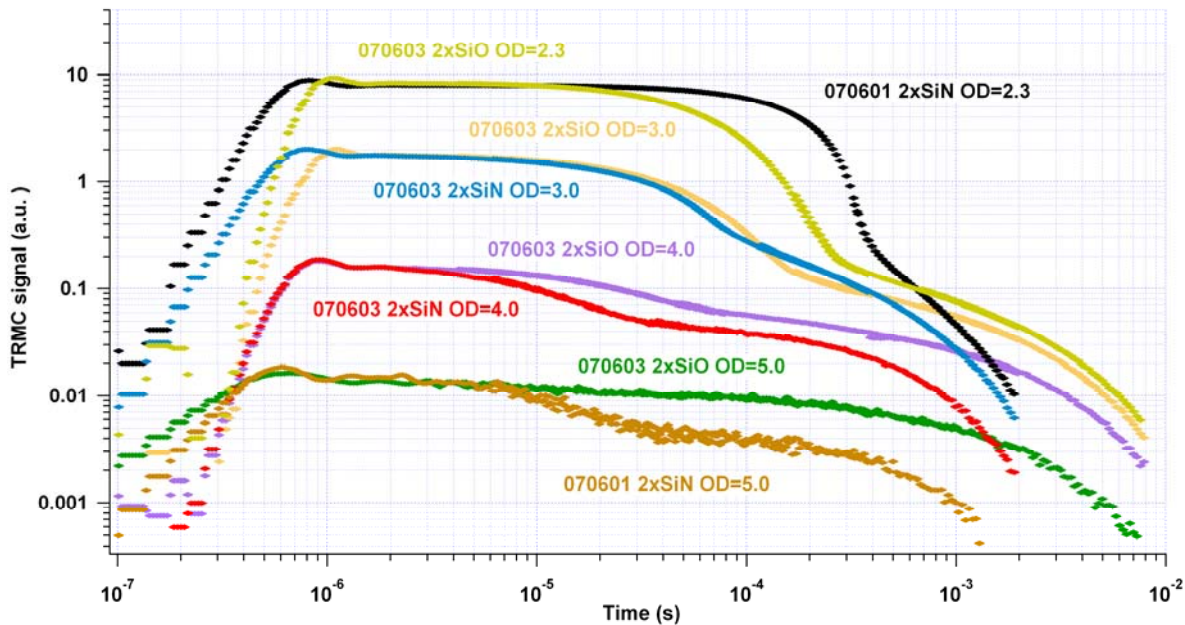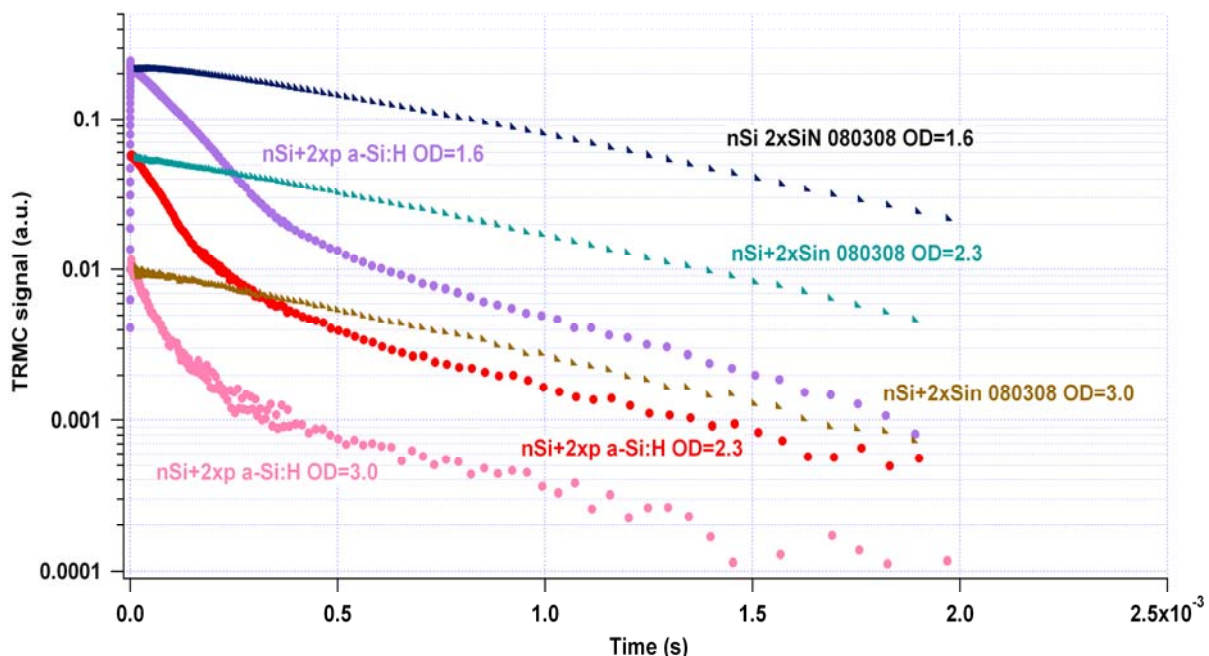

Fig. 95: TRMC signal induced by a 1064 nm laser pulse on a p-type crystalline silicon substrate (100 Ω.cm, 530 μm thick) covered on both sides with SiNx (standard conditions, R=0.16) and the same p-type c Si substrate covered on both sides with SiO2 for 4 different intensities.

The p a-Si:H was deposited on n-type crystalline silicon. Fig.96, shows the TRMC signals induced by a 1064 nm laser pulse on two sample, one normal n-type crystalline silicon covered on both sides with SiN_x (standard deposition, R=0,16) the other is n-type crystalline silicon covered with p a-Si:H silicon on both sides. The amorphous silicon will be used to separate the generated charge-carriers. As in the case of SiN_x on p-type crystalline silicon, the deposition of p a-Si:H on n c-Si will create a space charge, but this space charge region extends in both materials, it is a p-n junction. The holes will be injected in the p a-Si:H region where their mobility decreases (380 cm²/(Vs) to 1 cm²/(Vs)). Contrary to SiN_x, the amorphous silicon will be used to extract the generated charges carriers. But the mechanisms are the same:

- Separation of the excess charge-carriers due to the space charge.

- Reduction of the mobility of the hole in the p region.

In the case of p-type a-Si:H/ n-type c-Si, the recombination is mostly due to the recombination at the a-Si:H/c-Si interface. The TRMC measurements can then give a good overview of the quality of the interface. It can be noticed that the separation of charge-carriers in p-type c-Si/SiN_x can also be used for excess charge-carrier separation in a solar cell.

Fig. 96: TRMC signals induced by a 1064 nm laser pulse on two kinds of sample: a n-type crystalline silicon substrate (1 Ω.cm, 0.243 mm thick) covered on both sides with p a-Si:H and a n-type crystalline silicon substrate (1 Ω.cm, 0.243 mm thick) covered on both side with SiN_x (standard conditions, R=0.16).

5. Solar cells

This work was done within the framework of the inverted a-Si:H/c-Si heterocontact solar cell. The motivation and explanation are given in *2.6.3 Motivation for the inverted geometry silicon solar cell.* The first results are available.
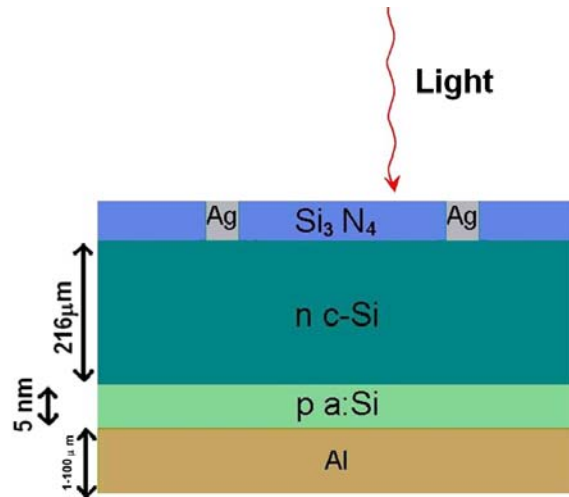
Fig. 97: Scheme of an inverted silicon solar cell. The bulk is a n-type piece of silicon. The junction is made by deposition of a p-type amorphous silicon. Silicon nitride is used as electrical passivation and anti-reflection layer

The cell is based on an n-type c-Si crystalline wafer with a resistiviy of 3 Ω.cm. The wafer is cleaned following the process given in the chapter *4.1. Deposition method.* The wafer is coated on one side with SiN_x (standard deposition parameters, R=0.16, 70 nm thick) then a layer of p-type a-Si:H is deposit on the opposite side. Back and front contacting is performed [V.1].
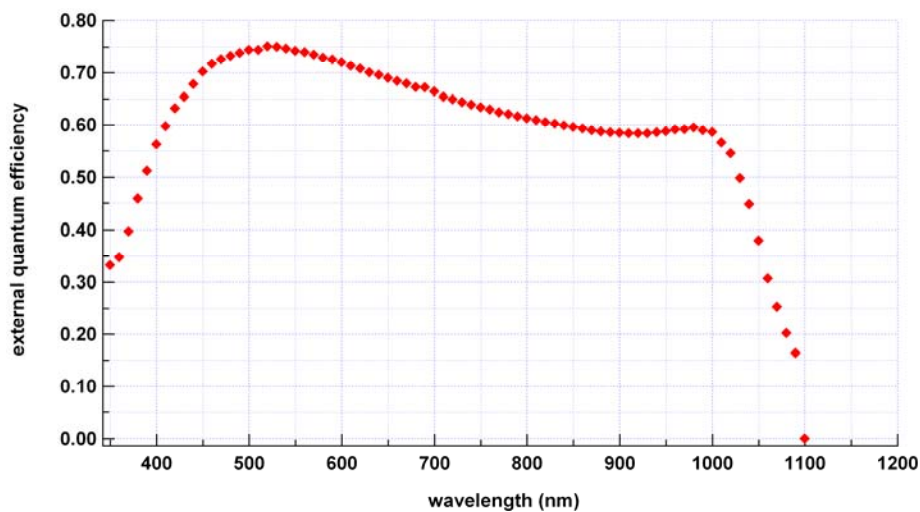
Fig. 98: Spectrum of the external quantum efficiency of the inverted a-Si:H/c-Si heterocontact solar cell. The illuminating light-spot was placed between two contact fingers.
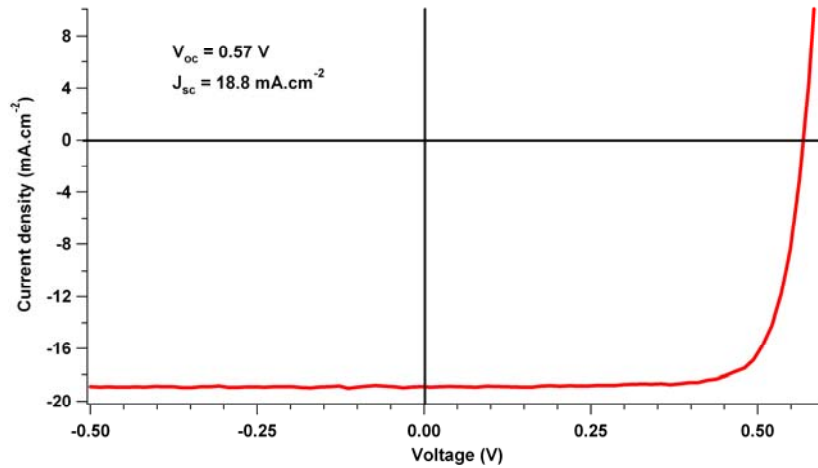
Fig. 99: I-V of our first inverted a-Si:H/c-Si heterocontact solar cell. The cell surface is 3.8 cm² under an irradiance of 100 mW/cm². The fill factor is 78.2 %

The first measurements are not very impressive but the process can be enhanced to obtain better results. As shown on the Fig.98, the external quantum efficiency is reasonably good in the blue part of the spectrum (between 450 and 500 nm), which was one of the aims. The I-V curve shown in Fig.99 gives an open circuit voltage of 0.57 V and a short circuit current of 18.8 mA.cm^{-2}. Even if these values are acceptable they are too low, the open circuit voltage is nowadays around 0.7 V and the short circuit current density around 40 mA.cm^{-2} [V.2]. The fill factor is 78.2% which is close to the best value of 80% reached nowadays [V.2]. The efficiency of the first cell is 9.3%, this is far away from the best efficiency obtained with mono-crystalline silicon solar cells (24.7%) [V.2] but not that bad for the first try

Now the process has to be enhanced, especially the front contact through the SiN$_x$ which is not that easy to obtain without damaging the interface silicon nitride/c-Si. Another point is the adaptation of the SiN$_x$ layer for the cell, to find the best relation between the passivation, the absorption and the anti-reflection.

6. Conclusions

Silicon nitride is a polyvalent coating for silicon solar cells: Electrical passivation, chemical passivation and anti-reflection properties on silicon. In addition to the low temperature budget of the Plasma Enhanced Chemical Vapour Deposition it is a method which allows us to tune very easily the parameters of deposition and thus the parameters of the layers deposited. The study of the modifications of every parameter of deposition is long and tedious work. In this work, in order to investigate two important properties of the SiN_x (optical and electrical passivation properties), only the modifications induced by variation of the ratio of the precursor gases and the temperature of deposition were studied. Comparison with silicon oxide and amorphous silicon were performed to investigate the charge-carrier kinetics at the different interfaces in the case of the inverted a-Si:H/c-Si heterocontact solar cell.

Concerning the deposition parameters, the ratio of the silicon and nitrogen content inside the layers was found to be proportional to the ratio R of the precursor gases in the plasma (SiH_4/NH_3). The depositions are homogeneous in the plane of the layer concerning the refractive index and the thickness. The increase of the ratio R was studied. It had the effect of an increased deposition rate, an increased refractive index and a higher number of Si-H bonds in the layers. On the other hand, the increase in the temperature of deposition decreases the deposition rate but increases the refractive index. Structural characterizations performed with ERDA show that the hydrogen content stays the same independently of the ratio R.

The optical properties of silicon nitride were confirmed to be appropriate for an anti-reflection front coating for the solar spectrums maximum. The SiN_x has a really low absorption for a large range of the ratio of SiH_4/NH_3 of the precursor gases {0.16 until 1}. For a ratio R lower than 1 the absorption at 520 nm is lower than 0.7%. However, for high R (R=5), a formation of clusters of silicon in the amorphous SiN_x matrix was found. These clusters lead to a strong increase of the absorption of the light.

The possibility to adapt the anti-reflection to our needs is also a great advantage. With an appropriate thickness and refractive index the reflection at 560 nm can be reduced to

0.03%. This value is very small but now further work has to be performed in order to reduce the overall reflection, with multiple layer systems. These two optical properties show the advantage of using a SiN_x layer as front coating to maximize the light coupling.

The electrical passivation induced at the surface by a coating of silicon nitride was also observed to be excellent and appropriate for silicon solar cells. This effect is especially efficient when the SiN_x is deposited on n-type silicon because of the accumulation layer created at the silicon surface. On p-type silicon it was found that the mobility of the electrons at the interface c-Si/SiN_x is reduced. This effect does not appear with silicon oxide. The electrical passivation is not strongly influenced by the silicon content in the SiNx, the best result was found for low silicon content (R=0.16 at 350°C). Very low surface recombination velocities (< 20 cm.s^{-1}) were obtained showing the excellent electrical passivation. The temperature of deposition has more influence on the passivation effect. The surface recombination velocity increases to 60 cm.s^{-1} for deposition at 300°C. This electrical passivation effect will increase the excess charge-carriers lifetime and will therefore increase the photocurrent (and thus the efficiency of a solar cell).

During this work a problem appeared. The possibility to reproduce a layer with the same electrical passivation properties was found to be very difficult. A variation of $\pm 47\%$ for the lifetime was observed for samples deposited under the same conditions. The reasons for this variation were not clearly determinable. However, it was observed that a reduction of this variation is possible by the use of a thin silicon oxide layer between the silicon substrate and the SiN_x coating. The variation of the lifetime for samples with the thin oxide layer is reduced to $\pm 15\%$.

Some remarkable effects were also observed. The formation of silicon clusters at high silicon content was observed with ellipsometrical measurements. This effect can be reasonably attributed to the increase of the silicon contents inside the layer. Such observations have been reported in the past but the mechanisms [VI.1] of formation need to be clarified. Another phenomenon observed was the formation of well-like holes with a diameter between 30 μm and 400 μm in the silicon nitride layer during strong annealing. Even if this process

was proven to destroy the passivation effect of the layer, it would be interesting to understand and explain the formation of these wells (maybe for other applications)

The properties of the silicon nitride as a front coating were proven to be appropriate for silicon solar cells. This work has also shown that these properties are sensitive to the deposition parameters and further studies of the effect of the deposition parameters are needed for two reasons:

- The mechanisms behind these effects must be understood more clearly.

- The properties of the SiN_x layer have to be optimized in order to fit as best as possible with our needs and optimize the efficiency of our cells.

7. References

1. Introduction

[I.1] http://www.energywatchgroup.org/Publications.23+M5d637b1e38d.0.html

[I.2] **A. G. Aberle**, (2001) Solar Energy Materials and Solar Cells **65**, Issues 1-4, pp239-248.

2. Theory

[II.1] **D. E. Aspnes**, (1983). "Dielectric functions and optical parameters of Si, Ge, GaP, GaAs, GaSb, InP, InAs, and InSb from 1.5 to 6.0 eV." Phys. Rev. B **27**(2): 985 - 1009.

[II.2] **F. Bernoux**, (2003). "Ellipsométrie. Instrumentation et applications." Techniques de l'ingénieur. Mesure et contrôle RD3. 2003, vol. RD3, n°R6491, p. R6491.1-R6491.12

[II.3] **AZZAM (R.M.A.) and BASHARA (N.M.).** – Ellipsometry and polarized light. North Holland (1977).

[II.4] **R.A. Sinton and A. Cuevas**, Appl.Phys.Lett. **69** (1996) p.457

[II.5] **R. Schieck and M. Kunst**, Solid-State Electron. **41** (1997) p.1755

[II.6] **W. van Roosbroeck**, Bell Syst. J. **29** (1950) p.560

[II.7] **H. Nagel, C. Berge and A.C. Aberle**, J.Appl.Phys. **86** (1999) p.6218

[II.8] **R. Schieck**, Ph.D. thesis, Technical University Berlin, Germany (1998)

[II.9] **J. Schmidt**, IEEE Transactions on Electr. Devices **46** (1999) p.2018

[II.10] **S. Dauwe**, PhD thesis Hannover, Germany (2004)

[II.11] **P.P. Altermatt, J. Schmidt, G. Heiser and A.G. Aberle**, J.Appl.Phys. **82** (1997) p.4938

[II.12] **J. Schmidt, M. Kerr and P.P. Altermatt**, J.Appl.Phys. **88** (2000) p.1494

[II.13] **R.N. Hall**, Phys.Rev. **87** (1952) p.387

[II.14] **W. Shockley and W.T. Read**, Phys.Rev. **87** (1952) p.387

[II.15] **O. Hahneiser and M. Kunst**, J.Appl.Phys. **85** (1999) p.7741

[II.16] **O. Hahneiser**, Ph.D. Thesis, Free University Berlin, Germany (1998)

[II.17] **J.-N. Chazalviel**, Coulomb screening by mobiles charges, Birkhäuser ,Boston (1998) p.201-238

[II.18] **H. Mathieu**, Physique des semiconducteurs et des composants electroniques, Masson, Paris (1987) p.433-442

[II.19] **B. Sapoval and C. Hermann**, Physique des semi-conducteurs, Ellipses, Paris (1990) p.167-172

[II.20] **M. Kunst, G. Müller, R. Schmidt and H. Wetzel**, Appl.Phys.A:Solid Surf. **46** (1988) p.77

[II.21]   **K.L. Luke and L.J. Cheng**, J.Appl.Phys. **61** (1987)p.2282

[II.22]   **A. Sanders and M. Kunst**, Solid-State Electronics **34** (1991) p.1007

[II.23]   **M. Kunst and A. Sanders**, Semicond. Sci .Technol. **7** (1992) p. 51

[II.24]   **A. G. Aberle**, Overview on SiN surface passivation of crystalline silicon solar cells, Solar Energy Materials & Solar Cells **65** (2001), p. 239-248

[II.25]   **S. R. Wenham** *et al*., Solar Energy Materials & Solar Cells **65** (2001), p. 377-384

[II.26]   **J-F. Lelievre**, Ph.D. thesis, Institut National des Sciences Appliquées Lyon, France (2007)

[II.27]   **Martin A. Green, K. Emery, Y. Hishikawa, W. Warta**, Research and Applications **16**(5) (2008). P. 435-440.

[II.28]   **A. Rohatgi and Ji-Weon Jeong**, Applied Physics Letters, **82** (2) (2003) p224

[II.29]   http://www.csr.utexas.edu/projects/rs/hrs/process.html

[II.30]   **F. Wunsch, G. Citarella, O. Abdallah and M. Kunst**, Journal of Non-Crystalline Solids **352**, Issues 9-20, (2006), p. 1962-1966.

3. methods

[III.1]   **A.En Naciri, L. Broch, L. Johann and R. Kleim**, Thin Solid Films **406** (2002) p.103–112

[III.2]   **M. Mansour**, Ph-D thesis, Université de Metz, France. (2006)

[III.3]   **O. S. Heavens**, Ph-D Optical properties of thin solid films, London (1955)

[III.4]   **M. Kunst and G. Beck**, J. Appl. Phys. **60** (1986) p. 3558

[III.5]   **B. Harbecke**, Appl. Phys. B **39** (1986) p.165

[III.6]   **H. C. Neitzert and M. Kunst**, J. Vac. Sci. Technol. A **13**(6) (1995) p. 2753

[III.7]   **D.K. Schroder** Semiconductor material and device characterization, Wiley Interscience, New York (1990) p.359-447

[III.8]   **G. Citarella, O. Abdallah and M. Kunst**, Materials Science and Engineering B **91–92** (2002) p. 229–233

[III.9]   **S. Grigull, U. Kreissig, H. Huber and W. Assmann**, Element-dependent ERDA probing depths using different detection systems, Nucl. Instr. Meth. B **132** (1997) p. 709-717

[III.10]   http://www.hmi.de/isl/ana/erda-1.html

[III.11]   **U. Kreissig, S. Grigull, K. Lange, P. Nitzsche and B. Schmidt**, Nucl. Instr. Meth. B**136-138** (1998) p. 674

[III.12]   **S. Hüfner**, "Photoelectron Spectroscopy Principles and Applications", Third Edition, Springer, (2003)

[III.13]   **D.Briggs and M.P. Seah**, "Practical Surface Analysis", SECOND EDITION, Volume 1 - Auger and X - ray Photoelectron Spectroscopy, Wiley (2000)

[III.14]   http://www.biophyresearch.com/pdf/ftir.pdf

[III.15]   **F.N. Dultsev and A.P. Solowjev**, (2005), Surface & Coatings Technology **195**, pp 102–106

[III.16]   **A. Aydinli** *et al*, Solid State Communications **98**, No. 4 (1996) p.273-277

[III.17]   http://en.wikipedia.org/wiki/Infra-red_spectroscopy

4. Coatings on silicon substrate

[IV.1]   **Asuha, T. Kobayashi,** *et al*. Applied Physics Letters **81**(18) (2002) p. 3410-3412.

[IV.2]   **Asuha, S. Imai,** *et al*. Applied Physics Letters **85**(17) (2004) p. 3783-3785.

[IV.3]   **H. Caquineau, G. Dupont, J. P. Couderc and B. Despax**, J. Vac. Sci. Technol. A **14**(4) (1996) p. 2071

[IV.4]   **A. Dollet, J. P. Couderc and B. Despax**, Plasma Sources Sci. Technol. **4** (1995) p. 94-106.

[IV.5]   **B. Stannowski, J. K. Rath,** *et al*. Journal of Applied Physics **93**(5) (2003) p.2618-2625.

[IV.6]   **S. Fujita and A. Sasaki**, J. Electrochem. Soc.132(2) (1985) p.398-402

[IV.7]   **G. Santana, A. Morales-Acevedo**, Solar Energy Materials & Solar Cells **60** (2000) p.135-142

[IV.8]   **AG. Aberle**, Solar Energy Materials & Solar Cells **65** (2001) p. 239-248

[IV.9]   **J. Schmidt and AG. Aberle**, Journal of Applied Physics **85** (1999) p. 3626

[IV.10]   **S. Winderbaum, F. Yun and O. Reinhold**, Journal of Vacuum Science & Technology A 15 (1997) p. 1020-1025

[IV.11]   **B. Swatowska and T. Stapinski**, Vacuum **82**(10) (2008) p. 942-946

[IV.12]   **J. Yoo, S.K. Dhungel and J. Yi**, Thin Solid Films 515(12) (2007) p. 5000-5003

[IV.13]   **L Zhong and F. Shimura,** Applied Physics Letters **62**(6) (1993) p. 615-617.

[IV.14]   **W. L. Warren** *et al*., J. Electrochem. Soc. 139(3) (1992) p.880

[IV.15]   **G. Morello**, Journal of Non-Crystalline Solids **187** (1995) p. 308-312.

[IV.16]   **J-F.Lelievre**, Ph.D. thesis, Institut National des Sciences Appliquées Lyon, France (2007)

[IV.17]   **C.J.F. Böttcher and P. Bordewijk**, « theory of electric polarization » volume II, Elsevier scientific publishing company, Amsterdam (1978).

[IV.18]   **K. R. Lee, K. B. Sundaram and D. C. Malocha**, Journal of Materials Science: Materials in Electronics **5** (5) (1994) p. 255-259

[IV.19]   **S.Dauwe**, PhD thesis Hannover, Germany (2004)

[IV.20]   **R. Ludemann**, Materials Science and Engineering B,**58**, Issues 1-2, (1999) p.86-90.

[IV.21]   **R.E.I. Schropp *et al*,**. Thin Solid Films **516**, Issue 5 (2008) p. 496-499.

[IV.22]   **Hui Yan *et al*.,** J. Appl. Phys. **32**. (1993) p. 876-886

[IV.23]   **W. L. Warren *et al*.,** Appl. Phys. Lett. **63**(19) (1993) p. 2685

[IV.24]   **W. L. Warren *et al*.,** J. Electrochem. Soc. **143**, No. 11 (1996) p. 3685

[IV.25]   **Becharia Nadji**, Journal of Materials Processing Technology **181**, Issues 1-3 (2007) p. 230-234.

[IV.26]   **C. Leguijt *et al*.,** Solar Energy Materials and Solar Cells **40** (1996) p. 297-345

[IV.27]   **J. R. Elmiger, and M. Kunst**, Applied Physics Letters **69**(4) (1996) p.517-519.

[IV.28]   **C. Swiatkowski, A. Sanders, *et al*.,** Journal of Applied Physics **78** (3) (1995) p.1763-1775.

[IV.29]   **A. Cuevas *et al*.** 4th world conference on photovoltaic energy conversion, Hawai, 8-12 May 2006, pp 1148-1151

[IV.30]   **H. F. W. Dekkers, G. Beaucarne, *et al*.**. Applied Physics Letters **89**(21) (2006) 211914.

[IV.31]   **M. Molinari *et al*.,**, J. Appl. Phys. **101** (2007)123532

[IV.32]   **L. Cai, A. Rohatgi, *et al*.**. Journal of Applied Physics **80** (9) (1996) p.5384-5388.

5. Solar cell

[V.1]   **F. Wunsch, G. Citarella, O. Abdallah and M. Kunst**, Journal of Non-Crystalline Solids **352**, Issues 9-20 (2006) p. 1962-1966.

[V.2]   **Martin A. Green, K. Emery, Y. Hishikawa, W. Warta**, Research and Applications **16**(5) (2008). P. 435-440.

6. Conclusion

[VI.1]   **J-F. Lelievre**, Ph.D. thesis, Institut National des Sciences Appliquées Lyon, France (2007)

The source of the simulation program shown below was written in basic. The entire source code cannot be written because of its length. The parts used to manage the different applications such as the graphics generation or the handling of the windows are useless. Only the part concerning the management of the equations is given.

```
Main()
Call ptig
'gammamax, gamint and gama are defined in the sub function
Call gammamax((nbcouches))    'nbcouches is the number of layers
        For M = nbcouches To 1 Step -1
                Call gamint((M))
                Call gama(False, (M - 1))
          Next M
          ref = (gamma(0).real ^ 2) + (gamma(0).Imag ^ 2)  'ref is the reflection
          'Store the reflection for the wavelength lambda in coord(y,x)
           coord(1, P) = lambda * 10000000#
           coord(2, P) = ref
        Next K

End


Sub ptig()
        petitgamma(0).real = 0
        petitgamma(0).Imag = 2 * pi / lambda
        For I = 1 To nbcouches
        petitgamma(I).real = couches(I).alpha / 2
        petitgamma(I).Imag = 2 * pi * couches(I).indicen / lambda
        Next I
End Sub

Sub gamint(G As Integer)
        Dim den As complex
        Dim num As complex
        den.Imag = (petitgamma(G - 1).Imag) - (petitgamma(G).Imag)
        den.real = (petitgamma(G - 1).real) - (petitgamma(G).real)
        num.Imag = (petitgamma(G - 1).Imag) + (petitgamma(G).Imag)
        num.real = (petitgamma(G - 1).real) + (petitgamma(G).real)
        gammaint(G).real = ((den.real) * (num.real) + (den.Imag) * (num.Imag))
        gammaint(G).real = (gammaint(G).real) / (((num.real) ^ 2) + ((num.Imag) ^ 2))
        gammaint(G).Imag = ((den.Imag) * (num.real) - (den.real) * (num.Imag))
        gammaint(G).Imag = (gammaint(G).Imag) / (((num.real) ^ 2) + ((num.Imag) ^ 2))
End Sub


Sub gammamax(G As Integer)
        Dim den As complex
        Dim num As complex
        den.Imag = (petitgamma(G).Imag) - (petitgamma(0).Imag)
        den.real = (petitgamma(G).real) - (petitgamma(0).real)
        num.Imag = (petitgamma(G).Imag) + (petitgamma(0).Imag)
        num.real = (petitgamma(G).real) + (petitgamma(0).real)
        gamma(G).real = ((den.real) * (num.real) + (den.Imag) * (num.Imag))
        gamma(G).real = (gamma(G).real) / (((num.real) ^ 2) + ((num.Imag) ^ 2))
        gamma(G).Imag = ((den.Imag) * (num.real) - (den.real) * (num.Imag))
        gamma(G).Imag = (gamma(G).Imag) / (((num.real) ^ 2) + ((num.Imag) ^ 2))
End Sub
```

```
Sub gama(last As Boolean, G As Integer)
        Dim den As complex
        Dim num As complex
        ' complex is a user defined type of variable composed by two double part
        For the real part (.real) of the number and the imaginary part (.imag)

        Dim X As Double
        Dim expo As Double

        expo = Exp(-(couches(G + 1).alpha * couches(G + 1).epaisseur))
        'decarts = couches(G).indiceN * Sin(phi) / couches(G + 1).indiceN
        'phi = Atn(decarts / Sqr(-decarts * decarts + 1))
        jki = Cos(phicouche(G + 1))
        'Cos(Atn(decarts / Sqr(-decarts * decarts + 1)))
        X = ((4 * pi * couches(G + 1).epaisseur * couches(G + 1).indicen) *
        Cos(phicouche(G + 1))) / lambda

        If last = False Then

        den.real = (gammaint(G + 1).real)
        den.real = den.real + Cos(X) * (gamma(G + 1).real) * expo
        den.real = den.real + Sin(X) * (gamma(G + 1).Imag) * expo

        den.Imag = (gammaint(G + 1).Imag)
        den.Imag = den.Imag - Sin(X) * (gamma(G + 1).real) * expo
        den.Imag = den.Imag + Cos(X) * (gamma(G + 1).Imag) * expo

        num.real = 1 + (gammaint(G + 1).real) * (gamma(G + 1).real) * Cos(X) * expo
        num.real = num.real + (gammaint(G + 1).real) * (gamma(G + 1).Imag) * Sin(X) * expo
        num.real = num.real + (gammaint(G + 1).Imag) * (gamma(G + 1).real) * Sin(X) * expo
        num.real = num.real - (gammaint(G + 1).Imag) * (gamma(G + 1).Imag) * Cos(X) * expo

        num.Imag = (gammaint(G + 1).real) * (gamma(G + 1).Imag) * Cos(X) * expo
        num.Imag = num.Imag + (gammaint(G + 1).Imag) * (gamma(G + 1).real) * Cos(X) * expo
        num.Imag = num.Imag - (gammaint(G + 1).real) * (gamma(G + 1).real) * Sin(X) * expo
        num.Imag = num.Imag + (gammaint(G + 1).Imag) * (gamma(G + 1).Imag) * Sin(X) * expo

        Else

        den.real = (gammaint(G + 1).real)
        den.real = den.real - Cos(X) * (gamma(G + 1).real) * expo
        den.real = den.real - Sin(X) * (gamma(G + 1).Imag) * expo

        den.Imag = (gammaint(G + 1).Imag)
        den.Imag = den.Imag + Sin(X) * (gamma(G + 1).real) * expo
        den.Imag = den.Imag - Cos(X) * (gamma(G + 1).Imag) * expo

        num.real = 1 - (gammaint(G + 1).real) * (gamma(G + 1).real) * Cos(X) * expo
        num.real = num.real - (gammaint(G + 1).real) * (gamma(G + 1).Imag) * Sin(X) * expo
        num.real = num.real - (gammaint(G + 1).Imag) * (gamma(G + 1).real) * Sin(X) * expo
        num.real = num.real + (gammaint(G + 1).Imag) * (gamma(G + 1).Imag) * Cos(X) * expo

        num.Imag = (gammaint(G + 1).real) * (gamma(G + 1).real) * Sin(X) * expo
        num.Imag = num.Imag - (gammaint(G + 1).real) * (gamma(G + 1).Imag) * Cos(X) * expo
        num.Imag = num.Imag - (gammaint(G + 1).Imag) * (gamma(G + 1).real) * Cos(X) * expo
        num.Imag = num.Imag - (gammaint(G + 1).Imag) * (gamma(G + 1).Imag) * Sin(X) * expo
        End If

        gamma(G).real = ((den.real) * (num.real) + (den.Imag) * (num.Imag))
        gamma(G).real = (gamma(G).real) / (((num.real) ^ 2) + ((num.Imag) ^ 2))
        gamma(G).Imag = ((den.Imag) * (num.real) - (den.real) * (num.Imag))
        gamma(G).Imag = (gamma(G).Imag) / (((num.real) ^ 2) + ((num.Imag) ^ 2))

End Sub
```

Appendix II : Physical properties

Silicon

Chemical series :	Metalloids
Classification (Groupe, Peroid, Block) :	14, 3, p
Atomic weight :	28.0855 g.mol^{-1}
Electron configuration :	[Ne] 3s^2 3p^2
Electron per shell :	2, 8, 4
Effective mobility of the electrons :	1400 cm^2/Vs
Effective mobility of the holes :	380 cm^2/Vs
Crystal structure :	Diamond cubic
Electro negativity (Pauling scale) :	1.90
Permittivity :	11.9
Band gap :	1.12 eV
Refractive index (at 530 nm) :	4.15
Density :	2.328 g.cm^{-3}
Atomic volume :	12.1 cm^3/mol
Melting point :	1414 °C
Bowling point :	2355 °C
Mohs hardness :	7
Speed of sound (20 °C) :	8433 m/s

Silicon nitride   (data for the standard form Si$_4$N$_3$)

Molecular formula :	Si$_3$N$_4$
Molar mass :	140.28 g.mol^{-1}
Density :	3.44 g.cm^{-3}
Melting point :	1900 °C
Refractive index (at 530 nm) :	1.9
Band gap :	5.1 eV
Conduction band offset with silicon :	2.2 eV
Valence band offset with silicon :	1.8 eV
Relative static dielectric constant :	7.4

List of abbreviations

SiN_x:	Silicon nitride Si_3N_4 in its amorphous form
c-Si:	mono-crystalline silicon
a-Si:H	Amorphous silicon
ARC:	Anti-Reflective Coating
PRPSE:	Polarizer Rotating Polarizer Spectroscopic Ellipsometer.
ERDA:	Elastic Recoil Detection Analysis
TRMC:	Time Resolved Microwaves Conductivity
XPS:	X-ray Photoemission Spectroscopy
FTIR:	Fourier Transform InfraRed spectroscopy
r:	Ration of the silicon and nitrogen content in the silicon nitride layer =[Si]/[N]
R (in chapter 4):	Ration of the Silane and the Ammoniac in the plasma = $[SiH_4]/[NH_3]$
S:	Surface recombination velocity

Curriculum vitae

David Klein

Date of Birth: 10th of March 1982

2000:	Baccalauréat série S (scientifique)	
2000-2002:	DEUG Science et vie de la matière	(University of Metz)
2002-2003:	License de physique	(University of Metz)
2003-2004:	Maitrise de physique	(University of Metz)
2004-2005:	DEA science de la matière et des interfaces	(University of Metz)
2005-2008:	Preparation of a Ph-D at the Hahn-Meitner-Institut in Berlin Wansee	